FACULTY OF MATHEMATICS AND PHYSICS, CHARLES UNIVERSITY, PRAGUE

AND

ASTRONOMICAL INSTITUTE OF ACADEMY OF SCIENCES OF CZECH REPUBLIC

Drahomíra Pecinová

Study of physical characteristics of meteor showers based on Ondřejov radar observations

DOCTORAL THESIS

Supervisor: RNDr. Jiří Borovička, CSc.

Ondřejov, 2005

Acknowledgements:

This doctoral thesis originated during the doctoral study at the branch F1 - Theoretical Physics, Astronomy and Astrophysics at the Astronomical Institute of Academy of Sciences of the Czech Republic in Ondřejov and at the Faculty of Mathematics and Physics of Charles University in Prague within the years 2001-2005. The work was also supported by grant GA ČR 205/03/1405. I would like to express my gratitude to supervisor Dr. J. Borovička for his valuable comments and suggestions. I also want to thank my beloved husband who has been my informal consultee for stimulating discussions and his patience.

Ondřejov, December 2005

Contents

Chapter 1

Introduction

Meteor astronomy has been developing from the middle of the 19th century. The first task concerned the relation of meteor streams to comets, namely the origin of streams due to breaks of comets as represented by Andromedids and their parent body, the Biela comet. Later also other tasks became important, namely those connected with the physical properties of meteoroids forming the streams. To be able to answer those questions the methods enabling determination of atmospheric trajectories had to be applied. These methods originated at the end of 18th century when Benzenberg and Brandes observed meteors simultaneously from two observing points separated by several tens kilometres. After the photography was sufficiently developed, it became the method capable of yielding data on physical properties of meteoroids. Since meteoroids are subject to drag force during their atmospheric motion it was necessary to determine the meteoroid velocity at each points of its trajectory. This was achieved by using rotating shutter. It enabled the study of velocity variability and consequently of the physical properties of meteor bodies. The photographic studies of meteor event are the most precise from all that are being in use at present. They can cover individual event and are able to study it in a great detail. However, they are confined to relatively bright meteors.

After the end of the Second World War the photographic observations were completed by radar technique. Since that time radars, originally radars of war, have been used to study meteors. The radar method has both advantages and drawbacks when comparing it with the photographic one. One of its advantage lies in the fact that it can be used in periods when the bad weather prevents the photography to be employed. Moreover, it can be used also during a day when a photography cannot be used at all. The daytime showers (e.g. β Taurids) were discovered namely by means of radars. On the other hand, radar can be affected by outer interference due to storms or commercial transmitters. The next advantage is that radars are able to register much fainter meteors than photography. Furthermore, although radars can provide us with data on individual meteors, their precision is lower than of photographic data. The classical meteor radars work at wavelengths from about 5 m up to 11 m. This wavelength span is given on the one hand by the demand that the

radar signal should be sufficiently strong. Since the strength of the signal is directly proportional to the 3rd power of the wavelength of used equipment it means that the higher the wavelength the greater number of faint meteors could be observed. On the other hand, the greater the wavelength the greater possibility that the radar wave could be reflected by ionospheric irregularity. Thus, some compromise had to be accepted and this is the interval mentioned above. Besides, number of observed meteors can be increased, among others, by using a radar that transmits higher power, which is expensive, however. To sum up, the way of development of classical radar astronomy was to construct radars transmitting power from approximately 10 kW up to several hundreds kW at meter wavelengths. In nineties radars working at much higher frequencies than classical radars, formerly used in military service or in studies of upper ionosphere, started to be employed also for exploration of meteor events. These equipments transmit pulses that are a few MW strong. Their field of view is usually wide only a fraction of one degree so that they cannot be used for monitoring of activity of meteor showers. They are used for physical studies of processes inside the meteor trails, instead.

Obviously, if we are interested in velocities and atmospheric trajectories of individual meteoroids together with connected physical quantities such as shape-density coefficient and ablation parameter, we need to add other side receivers (at least 2) to the radar. Because in the case of the Ondřejov meteor radar we have at our disposal only single-station observation we concentrate mainly on observations of activity curves of selected meteor showers and on determination of their mass distribution indices and fluxes. However, we were looking for a statistical method that would allow us to connect our observations with physical properties of meteoroids. This work describes the method like this that enables us to compute several important quantities typical for a particular meteor shower and also its application to our long-term series of data which we have been collecting since 1958. Among others, we have at our disposal range of each individual observed echo from the radar. The principle of our method is based on knowledge of range distributions of radar echoes. These range distributions mirror the fact that ionized meteor trails associated with a particular meteor shower occur inside a restricted height interval. The interval depends on the radiant position, on the masses and speeds of meteoroids contributing to the range distribution and on the other physical quantities, which we can describe by means of the ablation parameter σ and the shape-density coefficient K. Since during the observations of meteor showers we register simultaneously a lot of meteors with various masses, their mass distribution described by the mass distribution index s together with the shower flux density Θ_{m_0} form the shape of their range distribution curve. We have developed the model reflecting all these facts and we have managed to applied it to 127 range distributions of seven meteor showers. However the method requires the sufficiently quality of data as discussed in the relevant section so that its practical application has some restrictions.

This doctoral thesis consists of 6 chapters. The second and third ones are devoted to the physical theory the range distribution model is based on. After that we describe a few basic facts about

radar observations, namely about the Ondřejov meteor radar and the used data. The derivation of the model is given in chapter 5 together with mathematical methods of getting desired parameters. Next part deals with our results which we comment and summarize in the last chapter.

We have developed the method in the hope it will be useful in field of meteor astronomy at least a bit.

Chapter 2

Simple physical theory of meteors

This chapter includes the simple physical theory of meteors we need to put to use in our model of the range distribution. The theory in question connects instant mass of a meteoroid m and its velocity v with initial values of these quantities regarding the fact that the meteoroid (characterized by its physical quantities) moves within the Earth's atmosphere, which puts up resistance to its movement. The interaction of a single-body meteoroid with the air is described by means of a few fundamental equations underlying the ground of the theory of meteors. In this chapter, we assume the meteoroid body to be non-fragmenting and non-rotating. Moreover, we accept the meteoroid body as the sphere to simplify our model. Let us denote the initial values (before entering the Earth's atmosphere, at time $t \to -\infty$) by symbols v_∞ and m_∞.

Hereafter we often use (mainly in different expressions of mass and velocity of a meteoroid as a function of its atmospheric height) the exponential dependence of the air density ϱ on the height h in the widely used form

$$\varrho(h) = \varrho_o \exp\left(-\frac{h}{H}\right). \tag{2.1}$$

The constants ρ_o and H result from the least-square fit of this dependence to the reference atmosphere given by CIRA [17], within the height interval 80-120 km.

We need to use in our computations a following relationship defining a geometric dependence of the height of the meteoroid flight h on time t:

$$\frac{dh}{dt} = -v \cos z_R, \tag{2.2}$$

where z_R is the zenith distance of the radiant. We usually suppose this $\cos z_R$ to be independent of height h because variability in values of z_R can prove to be significant only in cases of very long bright meteors the trajectory of which extends over the large part of the Earth's surface. Thus, this relation does not take into account the curvature of the Earth's surface. The length of the meteoroid flight l relates to time t by the relation $dl = vdt$.

2.1 Deceleration and mass-loss equations

The first fundamental equation, **the deceleration equation** (e.g. Bronshten [9]), is based on the assumption that the momentum mdv lost by a non-rotating meteoroid is proportional to the momentum of the oncoming air flow. The air mass impinging upon the cross-sectional area S of the meteoroid at velocity v during time dt is $S\varrho v dt$. Thus, we arrive at the deceleration equation

$$m\frac{dv}{dt} = -\Gamma S\varrho v^2, \tag{2.3}$$

where Γ is the drag coefficient expressing the portion of the momentum of the oncoming air flow converted into deceleration of the meteoroid body. Coefficient Γ may be either less than unity or greater than unity. The first case corresponds to an incomplete transfer of momentum to the meteoroid (e.g. if some of the impinging molecules flow around it), the second one can occur when the reactive momentum of the molecules rebounding from the meteoroid surface or of the molecules evaporating from the meteoroid itself become appreciable. Certainly, the value of Γ also depends on the shape of the meteoroid body.

The second fundamental equation, called either **the mass-loss equation** or **the ablation equation**, deals with the process of ablation. Ablation is defined as any removal of meteoroid mass via its passage through the Earth's atmosphere in the form of gas, droplets or solid fragments. The derivation of the equation follows from the assumption that a certain portion Λ of the kinetic energy $\frac{1}{2}S\varrho v^3$ of the oncoming stream of molecules is expanded on the ablation (vaporization or fusion and spraying) of the meteoroid mass dm at the time dt. After denoting Q as latent heat of vaporization or fusion of the meteoroid material in units of energy (including the energy that needs to be delivered to mass dm in order to heat it up from its initial temperature T_o to its evaporation or melting temperature), the mass-loss equation takes the form (e.g. Bronshten [9])

$$\frac{dm}{dt} = -\frac{\Lambda}{2Q}S\varrho v^3. \tag{2.4}$$

Here Λ is called the heat-transfer coefficient. Since the energy expanded on ablation cannot evidently exceed the total kinetic energy of the oncoming stream of molecules, this coefficient is less or equal unity. Apart from the energy used for heating and ablation of the meteoroid mass dm, some part of the energy of the impinging molecules is consumed by heating up of the meteoroid itself, another part is converted into radiation and ionization of atoms and molecules of both the meteoroid and the air and also a significant portion of energy is dissipated by reflected air molecules and vapor molecules and atoms. Introducing a very important parameter σ, known as **the ablation parameter**, by the relation

$$\sigma = \frac{\Lambda}{2Q\Gamma} \qquad \left([\sigma] = s^2.m^{-2}\right),$$

we can rewrite equation (2.4) into the well-known form

$$\frac{dm}{dt} = -\sigma\Gamma S\varrho v^3. \tag{2.5}$$

To proceed further, in accordance with generally adopted procedure in the meteor physics, we connect the cross-sectional area S of the meteoroid with its instant mass m in the following way

$$S = A\left(\frac{m}{\delta}\right)^{\frac{2}{3}}, \tag{2.6}$$

where δ is bulk density of the meteoroid, and symbol A stands for a numerical constant, which is related to a supposed shape of the meteoroid body. As mentioned, we consider it to be the sphere. Thus, in this case

$$A = \pi\left(\frac{3}{4\pi}\right)^{\frac{2}{3}} \doteq 1.21$$

(for example, $A = 1.0$ for a cube).

To simplify notations, we introduce another familiar parameter, **the shape density parameter** K, by the definition

$$K = \frac{A\Gamma}{\delta^{2/3}} \qquad \left([K] = m^2 kg^{-2/3}\right) v. \tag{2.7}$$

Trying to solve the system of two equations (2.3) and (2.5), we usually make use of some simplifications. Let us now highlight four interesting cases. We assume coefficients of the meteoroid describing its physical features $(\sigma, K, \delta, \Lambda, \Gamma)$ to be constant during the meteoroid's flight in all subsequent cases.

1. **Constant velocity of meteoroid**

   In this special case the meteoroid's body preserves its velocity during whole flight. Kashcheev et al. [26] having investigated question of the deceleration of meteors have arrived at the conclusion that from the most severe deceleration suffer meteoroids having low velocity of 15 km s^{-1} for which the velocity at the point of maximum ionization drops from the above value to 14.2 km s^{-1}. This difference is even lower for faster meteoroids. According to these authors the difference between v_∞ and the meteoroid velocity at the point of maximum evaporation (coinciding with the point of maximum ionization), v_m, can be expressed as

   $$v_\infty - v_m = 1.22/(\sigma v_\infty).$$

   They have used $\sigma = 0.1\,s^2\,km^{-2}$ for meteors of velocity 15 km s^{-1}. However, this value is (with the exception of cometary material of the Giacobini-Zinner type with $\sigma \simeq 0.21$) the upper limit of values listed in Ceplecha et al. [15]. We will deal with meteors of showers possessing velocities at least 30 km s^{-1} and lower values of σ so that we can estimate the upper limit of the velocity difference of order of 1 km s^{-1} for them. The velocity of a meteor can substantially drop only at the end of ionization curve. This view is also supported by Voloshchuk et al. [60] who have concluded that most of observed meteors do not show any observable deceleration. The standard deviations of velocities of known showers are usually greater than the above differences published by Kashcheev et al. [26]. It implies that we cannot introduce substantial error when assuming constant velocity of meteoroids of showers

KNIHOVNA MAT.-FYZ. FAKULTY
Knihovna Fr. Zavišky (fyz. odd.)
Ke Karlovu 3
121 16 Praha 2

we will deal with. Moreover, this point is also in accordance with results of simultaneous TV-radar observations performed at Ondřejov in 2000 - 2002. Only one of 76 meteors common to both techniques had real deceleration (Pecina [42]). Thus, the assumption of constant velocity of meteors is fully plausible and will be employed when constructing the radar distribution model.

Hence, we write $v = v_\infty$ at any time of a meteoroid passage through the Earth's atmosphere. It is enough to take into consideration only the equation of ablation (2.5). Inserting (2.6) into (2.5) regarding the definition K provide us with

$$\frac{dm}{dt} = -\sigma K m^{2/3} \varrho(h) v_\infty^3. \tag{2.8}$$

While there is time t on the left-hand side of (2.8) as an independent variable, there is height h in the same role on the right hand side. It is necessary to unite the independent variables. It seems to be the most advantageous to switch from time t to height h. Transition can be carried out by means of the commonly valid equation (2.2). After rearranging terms we get

$$m^{-2/3}\frac{dm}{dh} = \sigma K \varrho(h) v_\infty^2 / \cos z_R. \tag{2.9}$$

The integration provides us with the following solution:

$$m = m_\infty \left(1 - \frac{\sigma K v_\infty^2}{3 m_\infty^{1/3} \cos z_R} \int_h^\infty \varrho(\bar{h}) d\bar{h}\right)^3 \tag{2.10}$$

From this result it is possible to calculate the height, at which the meteoroid's mass is totally ablated. A relevant condition is

$$\frac{\sigma K v_\infty^2}{3 m_\infty^{1/3} \cos z_R} \int_h^\infty \varrho(\bar{h}) d\bar{h} = 1. \tag{2.11}$$

Employing the atmosphere profile (2.1), we end up with the density and the height of the end point h_e as a function of $v_\infty, m_\infty, \sigma, K$ and $\cos z_R$:

$$\varrho_e = \frac{3 m_\infty^{1/3} \cos z_R}{\sigma K H v_\infty^2} \tag{2.12}$$

$$h_e = -H \ln\left(\frac{3 m_\infty^{1/3} \cos z_R}{\varrho_o \sigma K H v_\infty^2}\right). \tag{2.13}$$

The following three Graphs (2.1), (2.2) and (2.3) show dependencies of height h_e of the end point on m_∞, σ and v_∞. Evidently, the lower the velocity of a meteoroid and the smaller value of σ the deeper penetration into the Earth's atmosphere we can expect. On the contrary, the ending height of the penetration of the meteoroid of constant velocity v_∞ increases due to decreasing initial mass m_∞. All curves were delineated for $z_R = 45°$, $H = 5.409$ km and $\varrho_o = 56.803$ kg m^{-3}.

2. **Constant mass of meteoroid**

The situation in question happens mainly in the case of micrometeoroids (i. e. particles of

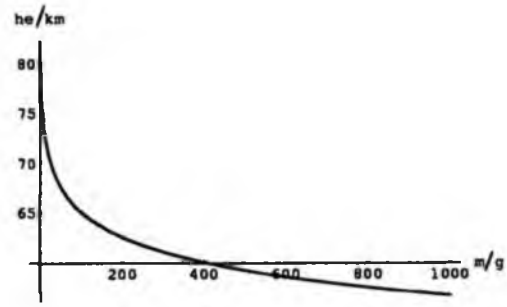

Figure 2.1: Height h_e as a function of m_∞. The curve was depicted for mass m_∞ within the interval $(1, 1000)$ g and for $v_\infty = 50$ km s^{-1}, $\sigma = 0.01$ s^2 km^{-2}.

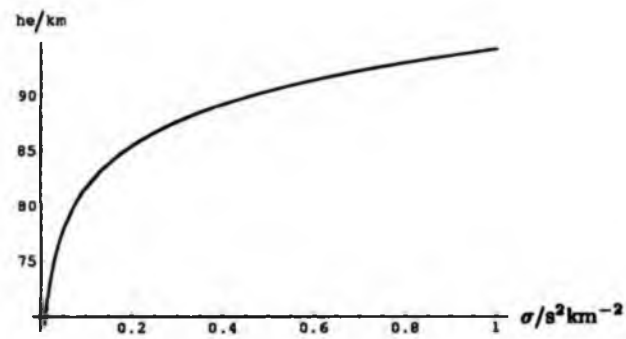

Figure 2.2: Height h_e as a function of σ. The curve was depicted for the ablation parameter within the interval $(0.01, 1)$ s^2 km^{-2} and for $v_\infty = 50$ km s^{-1}, $m_\infty = 1$ g.

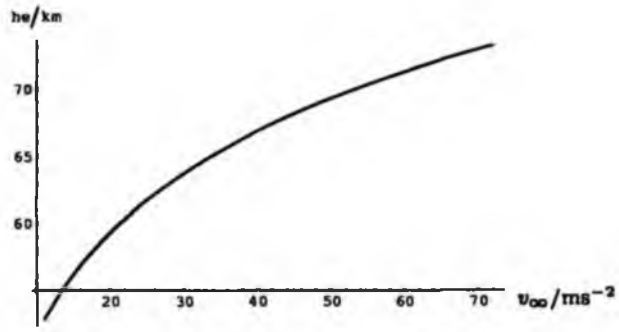

Figure 2.3: Height h_e as a function of v_∞. The curve was depicted for the initial velocity within the interval $(11, 72)$ km s^{-1} and for $m_\infty = 1$ g, $\sigma = 0.1$ s^2 km^{-2}.

micron sizes). They are strongly decelerated so that they cease earlier than they are able to begin to lose mass. Hence, it is enough to consider only the equation of deceleration (2.3). Similarly to the first case, after switching to height h regarding the formula (2.6) and the definition of K, we can easily perform the integration. It enables us to write

$$v = v_\infty \exp\left[-\frac{K}{m_\infty^{1/3}\cos z_R}\int_h^\infty \varrho(\bar{h})\,d\bar{h}\right]. \tag{2.14}$$

The dependence of height h on time t can be computed after (2.2). In the case of the atmospheric profile (2.1) the equation (2.14) takes the simpler form

$$v = v_\infty \exp\left[-\frac{KH}{m_\infty^{1/3}\cos z_R}\varrho(h)\right]. \tag{2.15}$$

It is worth noting that in this case the ratio $\frac{v}{v_\infty}$ depends only on the shape-density coefficient K, not on the ablation parameter σ.

3. Quasi-modeling of "slowly" decelerating meteoroids

Both cases of non zero deceleration and of constant mass of meteoroid are highly idealistic. In practice the meteoroid loses mass as well as velocity during its atmospheric flight. The former case is often considered in computations regarding TV meteors since a majority of these observed meteors do not significantly change their velocity in a considerable way as we have recognized from our simultaneous TV-radar observations (Pecina [43]). On the other hand, because meteoroids move in resistant medium of the Earth's atmosphere they should slow down due to the drag force even in case when they do not lose any mass. That was analysed in the second case. Now, in our third case, we make a compromise between two previous special cases.

When we try to estimate the value of a velocity loss only due to the drag force according to (2.15) for three different masses of meteoroids we get Figure 2.4. The constants used in computations were following: $K = 1$ cm^2 g$^{-2/3}$, $z_R = 45°$, H= 5.409 km and $\varrho_o = 56.803$ kg m^{-3}.

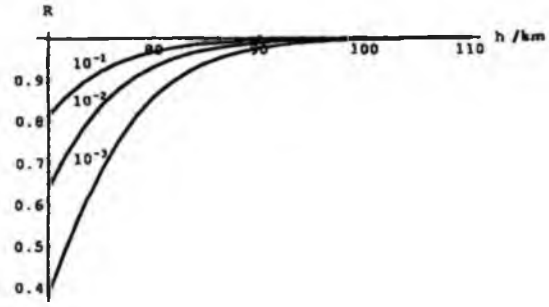

Figure 2.4: The ratio $R = \frac{v}{v_\infty}$ computed for three different masses of meteoroids: 10^{-3}, 10^{-2} and 10^{-1} g. The relevant curves are marked with the corresponding value of m_∞.

Evidently, the greater mass of a meteoroid the less progressive change of velocity. Hence, let us now assume a very small change in velocity value expressed by the equation (2.14). Our subsequent step forward in integrating the equations of a meteoroid motion consists in inserting the expression (2.14) into the ablation equation (2.5) together with relation (2.6). Replacement of the independent variable t by the height h and subsequent integration results in

$$m = m_\infty \left\{ 1 - \frac{K\sigma v_\infty^2}{3 m_\infty^{1/3} \cos z_R} \int_h^\infty \exp\left(- \frac{2K}{m_\infty^{1/3} \cos z_R} \int_x^\infty \varrho(\bar{h})\, d\bar{h} \right) \varrho(x)\, dx \right\}^3 ,$$

which can immediately be further integrated to yield

$$m = m_\infty \left\{ 1 - \frac{\sigma v_\infty^2}{6} \left[1 - \exp\left(- \frac{2K}{m_\infty^{1/3} \cos z_R} \int_h^\infty \varrho(\bar{h})\, d\bar{h} \right) \right] \right\}^3 . \qquad (2.16)$$

The dependence (2.16) describes the mass loss very well namely in the case of slowly decelerating bodies. This is the most general formula valid under the general dependence of $\varrho = \varrho(h)$. In the case of the atmospheric profile (2.1) the integral in the argument of exponential function yields $H\,\varrho$. Then the relevant formula reads

$$m = m_\infty \left\{ 1 - \frac{\sigma v_\infty^2}{6} \left[1 - \exp\left(- \frac{2KH}{m_\infty^{1/3} \cos z_R} \varrho(h) \right) \right] \right\}^3 . \qquad (2.17)$$

This expression could further be simplified when the argument of the exponential were small enough in comparison with unity. It allows us to use the well-known expansion $\exp(-x) \simeq$

$1 - x$. After performing this together with the atmospheric profile (2.1), expressions (2.17) and (2.10) coincide. Furthermore, the expression (2.17) can be written by means of (2.15) in the form

$$m = m_\infty \left\{ 1 - \frac{\sigma v_\infty^2}{6} \left[1 - \left(\frac{v}{v_\infty} \right)^2 \right] \right\}^3 . \tag{2.18}$$

Now, we can guess from the last expression the meteoroid's velocity at the point where its mass equals to zero. We get

$$v = v_\infty \sqrt{1 - \frac{6}{\sigma v_\infty^2}}. \tag{2.19}$$

4. **Both variable velocity and mass of meteoroid**

Let us put once again stress on the fact that the coefficients connected with physical features of meteoroids remain constant. On substituting dependence of S on mass m as expressed by (2.6) into the equations (2.3) and (2.5) we arrive at the following system

$$\frac{dv}{dt} = -Km^{-1/3}\varrho(h)v^2, \tag{2.20}$$

$$\frac{dm}{dt} = -\sigma K m^{2/3}\varrho(h)v^3. \tag{2.21}$$

After dividing the second equation by the first one we get the following differential expression:

$$\frac{dm}{m} = \sigma v dv. \tag{2.22}$$

Granting that σ remains constant or depends on velocity, we immediately get the first integral of the system:

$$m = m_\infty \exp\left(- \int_v^{v_\infty} \sigma(v) v dv \right). \tag{2.23}$$

As long as σ is invariable, (2.23) transforms into a very known expression (e.g. Bronshten [9])

$$m = m_\infty \exp\left[\frac{\sigma}{2}(v^2 - v_\infty^2) \right]. \tag{2.24}$$

After inserting this first integral into the deceleration equation (2.3) together with (2.6), we get

$$\frac{e^{\sigma v^2/6}}{v^2} dv = -K m_\infty^{-\frac{1}{3}} e^{\sigma v_\infty^2/6} \varrho dt, \tag{2.25}$$

and after the integration (taking height h as independent variable we arrive at

$$\mathrm{Ei}\left(\sigma v_\infty^2/6\right) - \mathrm{Ei}\left(\sigma v^2/6\right) = \left(2K/m_\infty^{1/3} \cos z_R \right) \exp\left(\sigma v_\infty^2/6\right) \int_h^\infty \varrho(\bar{h}) d\bar{h}. \tag{2.26}$$

Function Ei, which is called the integral exponential function, is defined by the integral

$$p.v. \int_{-\infty}^{x} \frac{e^\xi}{\xi} d\xi. \tag{2.27}$$

The symbol $p.v.$ (principal value) stands for the main value of the integral. When we use an inverse function to $\mathrm{Ei}(x)$, $\mathrm{Ei}^{-1}(x)$, it is possible to rewrite (2.26) in the form

$$v(h) = \sqrt{\frac{6}{\sigma} \mathrm{Ei}^{-1} \left[\mathrm{Ei}\left(\sigma v_\infty^2\right) - \left(\frac{2K e^{\sigma v_\infty^2/6}}{m_\infty^{1/3} \cos z_R} \right) \int_h^\infty \varrho(\bar{h}) d\bar{h} \right]} \tag{2.28}$$

At this stage, we have a relationship $v = v(h)$ "in attendance" of the other parameters $v_\infty, m_\infty, \sigma, K$ and $\cos z_R$. We easily obtain the dependence of meteoroid's mass m on height h by substituting (2.28) into (2.24).

The expression (2.26) allows us to derive velocity v_{md} at the maximum deceleration point. Let us now take the atmospheric profile (2.1). We are now able to rewrite (2.20) by means of the first integral (2.24) and (2.26) as:

$$\dot{v} = -\frac{\cos z_R}{2H} v^2 \exp\left(-\sigma v^2/6\right) \left[\mathrm{Ei}(\sigma v_\infty^2/6) - \mathrm{Ei}(\sigma v^2/6)\right]. \tag{2.29}$$

After taking derivation of (2.29) with respect to time we obtain the condition

$$\left(\frac{1}{6}\sigma v_{md}^2 - 1\right) \exp\left(-\sigma v_{md}^2/6\right) \left[\mathrm{Ei}(\sigma v_\infty^2/6) - \mathrm{Ei}(\sigma v_{md}^2/6)\right] + 1 = 0, \tag{2.30}$$

from which we can calculate the velocity at the maximum deceleration point, v_{md}, denoted as md. The deceleration itself is given by the expression

$$\left(\frac{dv}{dt}\right)_{md} = -\frac{\cos z_R}{2H} \frac{v_{md}^2}{1 - \sigma v_{md}^2/6}. \tag{2.31}$$

This equation has one solution inside the interval $0 < \frac{1}{6}\sigma v_{md}^2 < 1$ provided that the inequality $v_\infty / v_{md} \geq \sqrt{e}$ holds true (e is the Euler's number). The complete discussion of solution of (2.30) can be found in Pecina [44]. If we know the geometry of the flight, the profile of the Earth's atmosphere and values of deceleration and velocity at the point of maximum deceleration, we are able to estimate the ablation parameter σ. This is one of many ways of its determination. The other methods can be listed in Ceplecha [12]. Unfortunately, these ways are not applicable for our purposes because all of them are tightly bounded to some significant point on the meteoroid's trajectory. As there is only one point on the ionization curve at our disposal in the case of a single-station radar observation, we are not able to make use of them.

5. **Variable physical parameters of meteors**

   The fifth case takes into consideration the fact that physical coefficients describing physical properties of meteoroids can vary during their flights via Earth's atmosphere. As we are not concerned with this case in our work we can warmly recommend the paper Pecina [41] to avid reader.

6. **Use of Levin's proposition**

   We will now consider the process of ablation of a meteoroid which begins not at the instant when the meteoroid enters the Earth's atmosphere but at some height h_B. It is height at which the meteoroid's body is heated up enough to get started the process of ablation. ϱ_B denotes the air density corresponding to h_B. Generally, ϱ_B can be a function of m_∞: $\varrho_B = \varrho_B(m_\infty)$. For our purpose we will focus only on the non-deceleration case. In accordance with Levin [29] we consider not only the initial shape of the meteoroid (sphere in our case)

but also the law governing its variation during ablation. We define this law in terms of the parameter μ:

$$S = S_\infty \left(\frac{m}{m_\infty}\right)^\mu . \tag{2.32}$$

Obviously, if the ablating body remains self-similar, then $\mu = 2/3$. In the case of a cylinder or parallelepiped evaporating from its end, $\mu = 0$. For a wedge losing mass from its lateral faces, $\mu = 1/2$. In principle, however, μ may also be negative, e.g. if the body is deformed and flattened under the pressure of the oncoming flow, so that its midsection increases despite the mass loss. Most often (unless otherwise stipulated) it is assumed that $\mu = 2/3$, i.e. the body is self-similar. Levin's parameter μ can partially stand for fragmentation due to the cross-sectional change given by (2.32). As we will see later, the usage of μ can improve the fitting of theoretical range distribution to the observed one.

We take the deceleration equation in the form (2.3). But there is necessity of modification of the mass-loss equation due to μ. This statement we will now prove. Because we take the atmosphere profile in the form (2.1), it also means

$$dh = -\frac{H}{\varrho} d\varrho. \tag{2.33}$$

By combination of equations (2.2) and (2.33) we get another important relation:

$$dt = \frac{H}{\varrho v \cos z_R} d\varrho. \tag{2.34}$$

Let us now substitute the cross-section (2.32) and (2.34) into the ablation equation (2.5). After making necessary adjustments we arrive at the term

$$\left(\frac{m}{m_\infty}\right)^{-\mu} d\left(\frac{m}{m_\infty}\right) = -\frac{HK\sigma v_\infty^2}{m_\infty^{1/3} \cos z_R} d\varrho. \tag{2.35}$$

Then integration in (2.35) provides us with

$$\begin{aligned} m &= m_\infty \{1 - (1-\mu) \frac{HK\sigma v_\infty^2}{m_\infty^{1/3} \cos z_R} [\varrho - \varrho_B]\}^{\frac{1}{1-\mu}}, \quad \varrho \geq \varrho_B \\ m &= m_\infty, \qquad\qquad \varrho < \varrho_B. \end{aligned} \tag{2.36}$$

When we substitute this result into (2.5), we have

$$\begin{aligned} \dot{m} &= -Km_\infty^{2/3} \sigma v_\infty^3 \varrho \{1 - (1-\mu) \frac{HK\sigma v_\infty^2}{m_\infty^{1/3} \cos z_R} [\varrho - \varrho_B]\}^{\frac{\mu}{1-\mu}}, \quad \varrho \geq \varrho_B \\ \dot{m} &= -Km_\infty^{2/3} \sigma v_\infty^3 \varrho, \qquad\qquad \varrho < \varrho_B. \end{aligned} \tag{2.37}$$

We can see that in the case of $\varrho < \varrho_B$ the relation $m = m_\infty$ holds true in accord with (2.36) but also $\dot{m} \neq 0$ is valid in compliance with (2.37). These two facts are in diametric contradiction! There is only one way how to avoid this discrepancy. We have to take the ablation equation (2.5) in the form

$$\dot{m} = -\sigma \Gamma S (\varrho - \varrho_B) v_\infty^3 He(\varrho - \varrho_B), \tag{2.38}$$

where $He(x) = 1$ for $x \geq 0$ and $He(x) = 0$ for $x < 0$ is known as Heaviside function. So, the necessity to modify the mass-loss equation is proved. At this stage we can proceed to derivation of terms expressing loss of mass of meteoroids during their passage through the Earth's atmosphere. We will concentrate on the non-deceleration case that is employed in our model and we will take the equation (2.38) as principal. After its integration regarding (2.32), (2.34) and $v = v_\infty$ we arrive at the dependencies $m = m(\varrho)$ and $\dot{m} = \dot{m}(\varrho)$:

$$m = m_\infty \left\{1-(1-\mu)\frac{HK\sigma v_\infty^2}{m_\infty^{1/3}\cos z_R}\left[\varrho-\varrho_B-\varrho_B \ln\left(\frac{\varrho}{\varrho_B}\right)\right] He(\varrho-\varrho_B)\right\}^{\frac{1}{1-\mu}}, \tag{2.39}$$

$$\dot{m} = -K m_\infty^{2/3}\sigma v_\infty^3(\varrho-\varrho_B)\left\{1-(1-\mu)\frac{HK\sigma v_\infty^2}{m_\infty^{1/3}\cos z_R}\left[\varrho-\varrho_B-\varrho_B \ln\left(\frac{\varrho}{\varrho_B}\right)\right] He(\varrho-\varrho_B)\right\}^{\frac{\mu}{1-\mu}} He(\varrho-\varrho_B). \tag{2.40}$$

It can be easily seen from (2.40) that $\dot{m} = 0$ for $\varrho < \varrho_B$ is valid, which is correct.

2.2 Light

The luminosity equation belongs to the fundamental equations of the theory of meteors. It is derived on the basis of the fact, established by the analysis of meteor spectra, that the major contribution to the radiation of the meteor comes from the emission of its atoms evaporating from meteoroid surface. Atmospheric lines and bands are usually of secondary significance while the luminosity of the meteoroid's surface itself (i. e. the blackbody radiation) may be neglected. It is usually assumed that the radiation intensity I of the meteor is proportional to the kinetic energy of the mass dm evaporated in time dt:

$$I = -\tau(v)\frac{dm}{dt}\frac{v^2}{2}. \tag{2.41}$$

The symbol τ stands for the luminosity coefficient (often designated also as luminous efficiency). It generally depends on the velocity v, mass m and composition of the meteoroid.

It would be possible to assume more generally that $I \propto dE_k/dt$, where dE_k is kinetic energy of a meteoroid and that both parts of it have their own luminosity coefficients. Then

$$I = -\tau_1(v)\left(\frac{dm}{dt}\right)\frac{v^2}{2} - \tau_2(v)\left(\frac{dv}{dt}\right) m\, v. \tag{2.42}$$

But when we substitute dv/dt from (2.22) into (2.42), we gradually get:

$$\begin{aligned} I &= -\tau_1(v)\frac{dm}{dt}\frac{v^2}{2} - \tau_2(v)\frac{dv}{dt} m\, v = -\tau_1(v)\frac{dm}{dt}\frac{v^2}{2} - \tau_2(v)\frac{dm}{dt}\frac{1}{\sigma} = \\ &= -\{\tau_1(v) + \tau_2(v)\frac{2}{\sigma v^2}\}\frac{v^2}{2}\frac{dm}{dt} = -\tau_(v)\frac{dm}{dt}\frac{v^2}{2}. \end{aligned}$$

Thus, the general assumption can be included into classical formula (2.41) provided we modify the luminosity coefficient in an appropriate way (see e. g. Pecina and Ceplecha [44]). Thus we use the original equation (2.41) hereinafter. τ as a general function of velocity is frequently substituted by the relation $\tau = \tau_o v^n$ (e.g. Bronshten [9]).

Provided we are interested in expression of a value of meteor velocity at the point of maximum of radiation intensity v_{mI}, we have to take derivative of the luminosity equation with respect

to time t. Firstly, we modify the equation (2.41) by substituting for dm/dt from the ablation equation (2.21) and then we replace the term $m^{2/3}$ by means of the equation (2.24):

$$I = \frac{1}{2}\sigma K\tau(v)m_\infty^{2/3}\exp\left(\frac{-\sigma v_\infty^2}{3}\right)\exp\left(\frac{\sigma v^2}{3}\right)v^5\varrho(h). \tag{2.43}$$

This expression is called **the light curve** and expresses the dependence of I on height h or time t respectively. Secondly, we perform logarithmical derivation of (2.43) with respect to time t. Let's take a notice of function $\varrho(h(t))$ in the process (see relation (2.2)) and the fact that we take σ as independent of v. The result evidently has to equate to zero. We arrive at the following expression giving the velocity v_{mI} at the maximum light (Ceplecha [11])

$$\left[\frac{2}{3}\sigma v_{mI}^2 + \frac{v_{mI}}{\tau}\left(\frac{d\tau}{dv}\right)_{v_{mI}} + 5\right]\cdot\left[\mathrm{Ei}(\sigma v_\infty^2/6) - \mathrm{Ei}(\sigma v_{mI}^2/6)\right] - 2\exp\left(\frac{\sigma v_{mI}^2}{2}\right) = 0, \tag{2.44}$$

regarding the equation (2.29) and the atmospheric profile (2.1). The equation gives us a chance to compute the value of σ provided we know the dependence of $\tau = \tau(v)$ and v_{mI} (Pecina and Ceplecha [44]).

2.3 Meteor ionization

The fact that meteoroids during their passage through the Earth's atmosphere leave the ionized conducting path provides us with possibility of studying them by means of the radar. The formation of an ion-electron trail is a consequence of inelastic collisions between the evaporating atoms of a meteoroid and air molecules and atoms. The trail is supposed to be a quasi-neutral as a whole. One of the most important feature of the trail we work with is the electron line density α_e (a number of electrons per a unit length). This quantity follows from the ionization equation (e.g. Bronshten [9])

$$\alpha_e = -\frac{\beta}{\mu_a v}\left(\frac{dm}{dt}\right), \tag{2.45}$$

where the symbol μ_a stands for the average mass of a meteor atom. We usually adopt after Ceplecha et al. (1998) the value $\mu_a = 40\times\mu_H$ ($\mu_H = 0.1673534056\times10^{-26}$kg is the mass of hydrogen). The symbol β is called the ionization coefficient or the ionization probability (dimensionless quantity) and equals to the average number of free electrons formed during collisions of one evaporated meteor atoms with other particles. The notation of the equation expresses the fact that ionization comes from meteor atoms but not from the atmosphere particles.

The quantity β depends on meteor velocity in an unknown way. There have been a lot of attempts to describe that relationship between meteoroid's velocity and ionization probability. Several of them are listed in Table 23 in Bronshten [9]. Although it is possible to use whatever ionization theory in our model, we prefer three of them, which seem to be the most plausible. They are undermentioned below.

1. Verniani and Hawkins [59] have developed a theory based on observations with

$$\beta = \beta_c v^m, \tag{2.46}$$

where the constants $\beta_c = 0.1 \cdot 10^{-7}$ and $m = 4$.

2. Kashcheev B.L. et.al [26] evolved semiempirical model

$$\beta = \beta_k v^n, \tag{2.47}$$

with constants $\beta_k = 0.12649 \cdot 10^{-6}$ and $n = 3.5$ ($[v]$ =km s^{-1}).

3. Jones W. [23] described the dependence in question in the following way:

$$\beta = \beta_o v^{n_1} (v - v_n)^{n_2}, \tag{2.48}$$

where $\beta_o = 0.94 \cdot 10^{-5}, n_1 = 0.8, n_2 = 2$ and $v_n = 10$ km s^{-1}. He developed a theoretical model valid for velocities up to 35 km s^{-1}.

We get the very important dependence of the electron line density α_e on height h, **the ionization curve**, by substituting $\frac{dm}{dt}$ from the ablation equation (2.21) into (2.45):

$$\alpha_e(h) = \frac{\beta(v)}{\mu_a} \sigma K \rho(h) m^{2/3} v^2. \tag{2.49}$$

This expression expresses obvious fact that α_e depends except for height h also on parameters σ and K and initial values m_∞, v_∞. Let us now gradually analyse above mentioned case.

1. **Constant velocity of meteoroid**

We get the desired expression for the ionization curve by substituting (2.10) and (2.1) into (2.49):

$$\alpha_e(h) = \frac{\beta(v_\infty)}{\mu_a} \sigma K \rho(h) v_\infty^2 m_\infty^{2/3} \left(1 - \frac{\sigma K v_\infty^2 H}{m_\infty^{1/3} \cos z_R} \varrho(h)\right)^2. \tag{2.50}$$

To find the expression of α_e at the point of the maximum ionization, we calculate the derivative of (2.50) by height h and put the result zero. When using the atmosphere profile (2.2) we reach the density and the height of the point of the maximum ionization

$$\varrho_{\max} = \frac{m_\infty^{1/3} \cos z_R}{K H \sigma v_\infty^2}, \tag{2.51}$$

$$h_{\max} = -H \ln \left(\frac{m_\infty^{1/3} \cos z_R}{\varrho_o K H \sigma v_\infty^2} \right). \tag{2.52}$$

As a matter of interest we can compare the equations (2.12) and (2.50), i.e. two densities at two important points on the meteor path. The meteoroid with constant velocity reaches its maximum ionization at the point with three times smaller density of the air then density at its end point is. The electron line density $\alpha_{\max}$ at the point in question is

$$\alpha_{\max} = \frac{4}{9} \frac{\beta(v_\infty)}{\mu_a H} m_\infty \cos z_R. \tag{2.53}$$

We can see very interesting result valid only in the case when a meteoroid has constant velocity: there is a direct proportion between $\alpha_{\max}$ and m_∞. We apply this result in subsection (4.5.1). The ionization curves depicted for various values of $m_\infty, v_\infty, \sigma$ and K are drawn

in Figs. 2.5 - 2.8. All curves were delineated for $z_R = 45°$, $H = 5.409$ km, $\varrho_o = 56.803$ kg m^{-3} and $\mu = 6.69414 \times 10^{-26}$ kg. The used model of ionization probability β was in accord with (2.47).

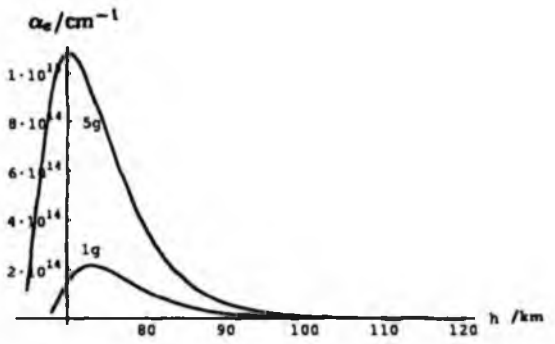

Figure 2.5: The course of the ionization curve for two values of m_∞, 1 and 5 g. The bigger initial mass the deeper in atmosphere the ionization curves begin and cease. Obviously, the bigger mass the greater value of α_{max} at the maximum ionization point. All curves were computed for $v_\infty = 36$ km s^{-1}, $\sigma = 0.01$ s^2 km^{-2} and $K = 1$ cm^2 g$^{-2/3}$.

2. **Constant mass of meteoroid**

   Obviously, there is no sense in derivation of the ionization curve for non-ablating meteoroids.

3. **Quasi-modeling of "slowly" decelerating meteoroids**

   To obtain desired expression for α_e, we have to substitute (2.15) and (2.17) into (2.49):

$$\alpha_e(h) = \frac{\beta(v_\infty)}{\mu_a}\sigma K \rho(h) m_\infty^{2/3}\left\{1 - \frac{\sigma v_\infty^2}{6}\left[1 - \exp\left(-\frac{2KH}{m_\infty^{1/3}\cos z_R}\varrho\right)\right]\right\}^2 \cdot$$
$$\cdot\ v_\infty^2 \exp\left(-\frac{2KH}{m_\infty^{1/3}\cos z_R}\varrho\right). \qquad (2.54)$$

4. **Both variable velocity and mass of meteoroid**

   Let us to substitute (2.24) into (2.49). Finally, we arrive at very complicated relation

$$\alpha_e(h) = \frac{\beta(v_\infty)}{\mu_a}\sigma K \rho(h) v^2 m_\infty^{2/3} \exp\left[\frac{\sigma}{3}(v^2 - v_\infty^2)\right], \qquad (2.55)$$

   in which $v(h)$ is given by the expression (2.28). The computation of the maximum point of the ionization curve is in Pecina and Ceplecha [44].

5. **Use of Levin's case** After substituting (2.40) into (2.45) we arrive at the dependence of $\alpha = \alpha(h)$:

$$\alpha_e = \frac{K m_\infty^{2/3}}{\mu_a}\sigma v_\infty^2 \beta(v_\infty)(\varrho(h) - \varrho_B)\left\{1 - (1-\mu)\frac{HK\sigma v_\infty^2}{m_\infty^{1/3}\cos z_R}\left[\varrho(h) - \varrho_B - \varrho_B \ln\left(\frac{\varrho(h)}{\varrho_B}\right)\right]\right\}^{\frac{\mu}{1-\mu}} He(\varrho(h) - \varrho_B). \qquad (2.56)$$

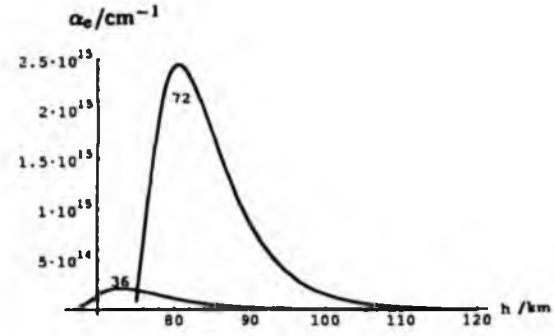

Figure 2.6: The course of the ionization curve for two values of v_∞, 36 and 72 km s^{-1}. The smaller initial velocity is the deeper in atmosphere the ionization curves begin and cease. Obviously, the greater value of v_∞ the greater value of α_{max} at the point of maximum ionization. All curves were computed for $m_\infty = 1$ g, $\sigma = 0.01$ s^2 km^{-2} and $K = 1$ cm^2 $g^{-2/3}$.

The courses of the ionization curve for different values of μ are drawn in Fig. 2.9. All of them were delineated for the following constants and quantities: $z_R = 45°$, $H = 5.409$ km, $\varrho_o = 56.803$ kg m^{-3} and $\mu_a = 6.69414 \times 10^{-26}$ kg. The used model of ionization probability β was in accord with (2.47) and ϱ_B corresponds to 150 km.

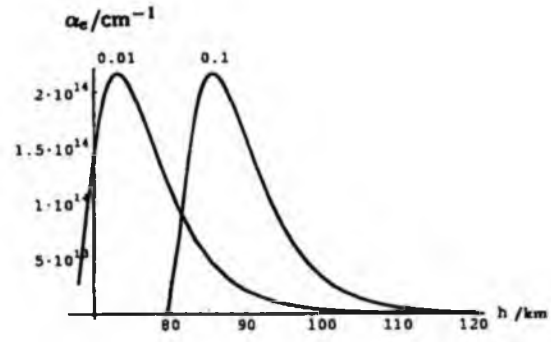

Figure 2.7: The course of the ionization curve for two values of σ, 0.01 and 0.1 $s^2\ m^{-2}$. There is no change in massiveness of α_{max} for various values of the ablation coefficient. But the smaller value of σ is the deeper in atmosphere the ionization curves is situated. All curves were computed for $m_\infty = 1$ g, $v_\infty = 36$ km s^{-1} and $K = 1$ $cm^2\ g^{-2/3}$.

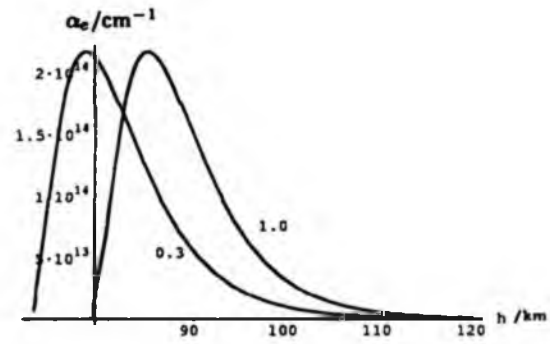

Figure 2.8: The course of the ionization curve for three values of K, 0.2 m, 2/3 and 0.8 $cm^2\ g^{-2/3}$. Again, there is no change in massiveness of α_{max} for various values of the shape-density parameter and also the smaller value of σ is the deeper in atmosphere the ionization curves are situated. All curves were computed for $m_\infty = 1$ g, $v_\infty = 36$ km s^{-1} and $\sigma = 0.1$ s^2 km^{-2}.

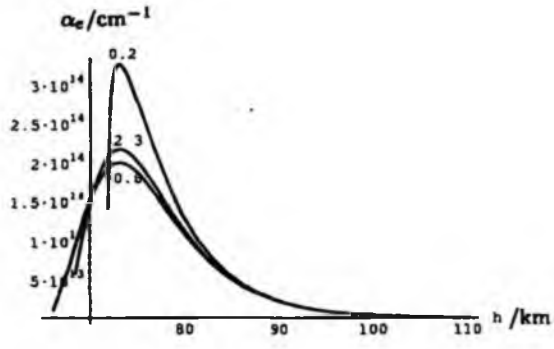

Figure 2.9: The course of the ionization curve for three values of μ, 0.2, 2/3 and 0.8. The smaller value of μ the bigger value of α_{max} at the maximum ionization point and the higher the ending point of the ionization curve is. The value 2/3 of Levin's parameter is valid for the classical theory (see also (2.50)). All three curves were computed for $m_\infty = 1$ g, $v_\infty = 36$ km s^{-1}, $\sigma = 0.1$ s^2 km^{-2} and $K = 1$ cm^2 g$^{-2/3}$.

Chapter 3

Radar echo theory

When we study meteors by means of the radar we make use of the fact that after passage of a meteoroid through the Earth's atmosphere a ionized electrically conducted path is created. Let us stress that our work deals only with the back-scatter echo phenomena and we mainly restrict ourselves to study the overdense echoes for reasons we will mention in section (5.1).

3.1 Permitivity of meteor train

We need the expression for the echo duration T_D as a function of the electron line density α_e inside the train in our model of the range distribution. To derive that, we firstly have to express the permitivity ε of a meteor train as a function of number density of free electrons N_e. For our purpose we are only interested in the electrical part of the electromagnetic wave with frequency ω transmitted by the radar. The electric intensity $\vec{E}$ depends on time in a harmonic way

$$\vec{E} = \vec{E}_o \exp(-i\omega t).$$

After a passage of a meteoroid, free electrons and ions are created and they move under influence of the electromagnetic wave falling on them. The full position vector of a charge, $\vec{r}_f$, consists of two components. The first one, $\vec{r}_{eq}$, gives the equilibrium position of a charge it would possess in case if no external electrical field were applied. External periodical field forces the charge to fluctuate around its equilibrium position. The deviation from this position is characterized by $\vec{r}$. As a consequence, the full position vector is $\vec{r}_f = \vec{r}_{eq} + \vec{r}$. Only variability of $\vec{r}$ contributes to polarization inside the train. The motion equation of the charged particle with charge q and mass m in the external electrical field of intensity $\vec{E}$ reads

$$m\ddot{\vec{r}} = q\vec{E}_o \exp(-i\omega t) \tag{3.1}$$

and has the following solution:

$$\vec{r} = -\frac{q}{m\omega^2}\vec{E}. \tag{3.2}$$

In further considerations, subscripts e and i denote electrons and positive ions. Since the ratio of mass of an electron to positive ion in the simplest case is $\frac{m_e}{m_i} \ll 1$, the deviation vector $\vec{r}_i$ is much smaller than $\vec{r}_e$. Thus, it is enough to take into account only electrons.

The electric displacement $\vec{D}$ within the meteoric path can be expressed by means of the polarization vector $\vec{P}$ (the Gauss system of units) as

$$\vec{D} = \vec{E} + 4\pi\vec{P}. \tag{3.3}$$

$\vec{P}$ stands for the dipole moment of volume unit of a medium. The following relation is generally valid:

$$\vec{P} = -e\vec{r}_e N_e + e\vec{r}_i N_i \tag{3.4}$$

We remind here our gentle reader, the symbol e designates the absolute value of charge of electron. We assume plasma is quasineutral as a whole. It means the relation $N_e \simeq N_i$ between the number densities of electrons and the one of positive ions holds true. Let us make a note that plasma is weakly ionized, its degree of ionization is about 10^{-5} in meteor region and for the critical value of electron line density α_{crit} (see section (3.3)). Then the logical implication of the fact $|\vec{r}_i| \ll |\vec{r}_e|$ is that (3.4) takes the form

$$\vec{P} = eN_e(\vec{r}_i - \vec{r}_e) \simeq -eN_e\vec{r}_e. \tag{3.5}$$

To proceed further, we get by means of (3.2) (since for electrons $q = -e$) and (3.3) the useful expression:

$$\vec{D} = \left[1 - \frac{4\pi e^2}{m_e\omega^2} N_e\right] \vec{E}. \tag{3.6}$$

After realizing $\vec{D} = \varepsilon\vec{E}$, we arrive at the desired expression for permitivity ε:

$$\varepsilon(\omega, \vec{r}, t) = 1 - \frac{4\pi e^2}{m_e\omega^2} N_e(\vec{r}, t). \tag{3.7}$$

We can see that ε depends not only on the wavelength of transmitted electromagnetic wave but also on distance r from the meteor axis and time t. The value of permitivity is a matter of prime importance when we solve the set of the Maxwell equations of electromagnetic field inside the meteor train. The curious reader can find more details e.g. in Landau [28]. Furthermore, according to its sign the radar echoes are divided into two basic categories as we will see in section (3.3).

3.2 Number density of electrons

Once the thermalization stage has been finished and the trail of the initial radius r_o has been produced (see the section (3.4)), the sufficiently longer stage of balancing of concentrations goes after. The gradual decay of number density of electrons N_e is a result mainly of three effects: ambipolar diffusion, recombination and attachment of free electrons to neutral particles.

As we will see, the most important phenomenon of reducing of the echo strength is ambipolar diffusion. We do not urge to take the magnetic field into consideration because of its weakness

and due to small velocity of meteors in comparison with speed of light. So, ambipolar diffusion should be isotropic. Since the transversal dimension of a meteor train is much smaller than the corresponding lateral one, we can consider the decay of N_e only in a direction perpendicular to an axis of a meteoric train. We also assume the whole region of the initial radius r_o is created at time $t = 0$s. The Gaussian distribution for the radial density of electrons is adopted throughout this work as the most reasonable model. The standard form of the radial diffusion equation is (McKinley [35])

$$\frac{\partial N_e(r,t)}{\partial t} = \frac{D(h)}{r}\frac{\partial}{\partial r}\left(r\frac{\partial N_e(r,t)}{\partial r}\right), \tag{3.8}$$

where $N_e(r,t)$ is the number density of electrons at time t and distance r from the axis of the train and $D = D(h)$ is the ambipolar diffusion coefficient ($[D]$=m^2 s^{-1}). The initial condition of (3.8) is

$$N_e(r,0) = \frac{\alpha_e}{\pi r_o^2} e^{-\frac{r^2}{r_o^2}}. \tag{3.9}$$

The problem is solvable by means of the integral Hankel transformation (e.g. Bateman [5]). The volume density may then be expressed as

$$N_e(r,t) = \frac{\alpha_e}{\pi(r_o^2 + 4Dt)} \exp\left[-r^2/(r_o^2 + 4Dt)\right], \tag{3.10}$$

The relation (3.10) means the fact that the ionized cylinder expands due to ambipolar diffusion and for this purpose there is a decay of number density of electrons N_e. When we consider a meteoric train as a part of ionized medium confined inside the domain with boundary defined as the distance at which N_e drops to the value of $N_e\, e^{-1}$, we get an expression for the radius r of the meteor cylinder

$$r^2 = r_o^2 + 4\,D\,t. \tag{3.11}$$

The diffusion coefficient D increases with height in the meteor region. It may depend significantly on local atmospheric conditions and shows daily and seasonal variations. In regions of occurrence of meteor trains it is widely used the following approximation found out from observations (Greenhow [18]):

$$D \doteq 4.9\,10^4\, p^{-1}. \tag{3.12}$$

Here p is the atmospheric pressure (the Gauss system of units). The relation (3.12) is not handy in practical computations and it is frequently rewritten according to the rules of thermodynamics as

$$D\,\varrho = D_r\,\varrho_r. \tag{3.13}$$

Subscripts r mean the values at the reference height. We have chosen $D_r = 4.2$m^2 s^{-1} valid for height of 93 km (e.g. Belkovich [6]). In practice we use (3.13) with (2.1) and CIRA [17]. Our gentle reader can get more information about D e.g. in Chen [16]).

Electrons can also recombine with the positive ions to form neutral molecules or atoms. This effect can be expected to contribute to an eventual dissipation of the meteor train. When ion collide with electron, they have non-zero probability (mainly in the case of slow relative speed) that they

will recombine and neutral molecule or atom will be created. We take loss of plasma caused by recombination into consideration in (3.8) by a negative source term, which is proportional to the product of number densities of positive ions and electrons, $N_i N_e$. In our quasineutral plasma $N_i N_e \doteq N_e^2$ holds true. Thus, we modify the differential diffusion equation by adding $-a_e N_e^2$ to the right-hand side of (3.8)

$$\frac{\partial N_e}{\partial t} = \frac{D}{r}\frac{\partial}{\partial r}\left(r\frac{\partial N_e}{\partial r}\right) - a_e N_e^2. \tag{3.14}$$

Here a_e is the electron recombination coefficient ($[a_e]$ =m^3 s^{-1}). The approximate solution to (3.14) is

$$N_e(r,t) = \frac{\alpha_e}{(t-t_o)(4\pi D + \frac{1}{2}\alpha_e a_e \ln\frac{t}{t_o}) + \pi r_o^2}\exp\left[-r^2/(4D(t-t_o)+r_o^2)\right], \tag{3.15}$$

where (unlike (3.10)) α_e is the electron line density at an initial time $t = t_o$. Thus, provided the value of $4\pi D$ compares with the value of $\frac{1}{2}\alpha_e a_e \ln\frac{t}{t_o}$, recombination would be able to play the role of the same importance as ambipolar diffusion. However, according to Bronshten [9] the most effective process of recombination, the dissociative one, has $a_e \simeq (2 \div 4.5) \times 10^{-13}$ m^3 s^{-1} and, as a consequence, it terminates during 10^{-4} s after the trail formation. This fact implies that the recombination can hardly be a significant factor in comparison with ambipolar diffusion. Hence, in order the recombination could play significant role the a_e should be greater more than 10^4 times in comparison with its present value.

Some electrons may attach themselves to neutral molecules to create negative ions. In considering attachment effects, we subtract a term $b_e N_e N_m$ from the right-hand side of (3.8) where N_m is the number density of neutral molecules capable of forming negative ions and b_e is the coefficient of attachment:

$$\frac{\partial N_e}{\partial t} = \frac{D}{r}\frac{\partial}{\partial r}\left(r\frac{\partial N_e}{\partial r}\right) - b_e N_e N_m. \tag{3.16}$$

The exact solution to (3.16) is

$$N_e(r,t) = \frac{\alpha_e}{\pi(r_o^2 + 4Dt)}\exp\left[-b_e N_m t - r^2/(r_o^2 + 4Dt)\right]. \tag{3.17}$$

In the case $b_e N_m t \ll 1$, attachment will not have an important effect on a behaviour of N_e. The quantity N_m is a function of height (as h falls the number density of neutral molecules rises). In the past molecular oxygen was suspected as one of the most probable molecule involved in the creation of negative ions (McKinley [35]). The coefficient b_e was not well determined but one can find in literature (Bronshten [9]) that in meteoric heights around 100 km (the heights in question in our model) the values of N_m and b_e are so small that attachment has not noticeable influence upon the decay of N_e. Attachment may assert oneself in heights bellow 75 km. On the other hand, Bibarsov [8] has proposed the attachment of electrons to neutral particles of meteor origin, i.e. particles ablated from the meteoroid's surface, happens rather than to oxygen. His view was not accepted by scientific community. Recently ozone has been taken into account (e.g. Jones J. et.al. [21]). However, because of $b_e \simeq 10^{-18}$ cm^3 s^{-1} in that case (Baggaley [4]) and that $N_m \simeq 10^{15}$ m^{-3} at its maximum at 85 km, even ozone cannot play significant role in our observations comprising echoes with durations not exceeding 30 s.

Both last mentioned effects can be expected to contribute to the eventual dissipation of the meteor ionization, but the rates at which they operate should be examined to what extent they are significant in comparison with ambipolar diffusion and turbulence. We consider only ambipolar diffusion in our model due to our detailed analyses of data we have at our disposal. Our careful examination of the long-term series of observations of selected meteor showers revealed that the activity of the overdense echoes longer than about 30s is mostly on the zero level. For example no activity of ζ Perseids and β Taurids in the echo duration category exceeding 10s was observed, the corresponding limit for autumn Taurids was 5s. Certainly there are exceptions, e.g. Leonids (Pecina and Pecinová, [45]) when we have recorded echoes with durations of order of minutes. But it is rather rare. For this reason we compute exclusively with the echoes that have durations from 0.4s up to 30s and we are not compelled to deal with the effects of recombination and attachment. Besides, both phenomena should occur at rather lower heights while our echoes originate at grater ones.

At the end of this section we would like to stress the fact that ambipolar diffusion occurs without affecting the line electron density α_e that remains independent of time t. Let us evaluate α_e to support this statement. Obviously (in the cylindrical coordinates):

$$\alpha_e = \int_0^\infty N_e dS, \tag{3.18}$$

where $dS = r\,dr\,d\phi$. After substituting the relevant solution for N_e and performing the integration we have the following results.

1. The integration in the case of the pure ambipolar diffusion gives us:

$$\begin{aligned} \alpha_e &= \int_{r=0}^{+\infty}\int_{\phi=0}^{2\pi} \frac{\alpha_e}{\pi(r_o^2+4Dt)} \exp\left[-r^2/(r_o^2+4Dt)\right] r\,dr\,d\phi = \\ &= \alpha_e = \text{const.} \end{aligned} \tag{3.19}$$

2. When we think of ambipolar diffusion and recombination as effects affecting the dissipation of a meteor train the integration provides us with:

$$\begin{aligned} \alpha_e &= \int_{r=0}^{+\infty}\int_{\phi=0}^{2\pi} \frac{\alpha_e}{(t-t_o)(4\pi D + \frac{1}{2}\alpha_e a_e \ln\frac{t}{t_o}) + \pi r_o^2} \exp\left[-r^2/(4D(t-t_o)+r_o^2)\right] r\,dr\,d\phi = \\ &= \frac{\pi\alpha_e\left[4D(t-t_o)+r_o^2\right]}{(t-t_o)(4\pi D + \frac{1}{2}\alpha_e a_e \ln\frac{t}{t_o}) + \pi r_o^2} = \alpha_e(t). \end{aligned} \tag{3.20}$$

3. The surface integral of N_e in the case of ambipolar diffusion together with attachment to neutral particles has the solution:

$$\begin{aligned} \alpha_e &= \int_{r=0}^{+\infty}\int_{\phi=0}^{2\pi} \frac{\alpha_e}{\pi(r_o^2+4Dt)} \exp\left[-r^2/(r_o^2+4Dt) - b_e N_m t\right] r\,dr\,d\phi = \\ &= \alpha_e e^{-b_e N_m t} = \alpha_e(t). \end{aligned} \tag{3.21}$$

To sum up, we confirm the generally widespread claim that only in the case we can neglect the other affects except the ambipolar diffusion the electron line density α_e remains constant.

3.3 Types of radar echoes

As we have mentioned above, in section (3.1), the division of meteor trains from point of radar view can be perform due to sign of permitivity ε. This quantity is generally complex and its value has an essential influence on the form of a solution of Maxwell equations inside the meteor train. As long as there is $\varepsilon > 0$ inside the whole ionized trail, the radio wave penetrates the trail and scattering occurs at every electron. Then we talk about **the underdense (unsaturated) echoes**. On the contrary provided the condition $\varepsilon < 0$ is satisfied, inside some part of the the trail there appears a zone where the electron concentration N_e exceeds a certain critical value and the radio wave is reflected from the boundary of this zone. Such trails are referred to as **the overdense (saturated) echoes**.

The boundary value setting the diving line between two basic kinds of echoes is called **the critical linear electron density** α_{crit} and we will now derive its expression. We get the necessary dependence of ε on the electron line density α by substituting (3.10) into (3.7) and by using the relation $\omega = 2\pi c/\lambda$ (λ stands for wavelength of incident wave):

$$\varepsilon(\lambda, r, h, t) = 1 - \frac{\lambda^2 r_e}{\pi} \frac{\alpha_e}{\pi(r_o^2 + 4Dt)} \exp\left[-r^2/(r_o^2 + 4Dt)\right]. \tag{3.22}$$

The constant $r_e = \frac{e^2}{m_e c^2}$ is the classical radius of electron, $r_e = 2.81 \times 10^{-15}$m ($m_e$ is the mass of electron, e absolute value of charge of electron and c is speed of light). We can see that while for lower α_e permitivity ε is affirmative (the second term of (3.7) does not play an important role in comparison to unity), in the case of higher initial linear concentrations of electrons the values of ε fall below zero. Thus, the critical α_{crit} is given by the condition

$$\varepsilon(0, 0) = 0 \tag{3.23}$$

(on the axis, at the initial time $t = 0$ s). By means of (3.22) we arrive at the equation

$$1 = \frac{\lambda^2 r_e \alpha_e}{\pi^2 r_o^2}, \tag{3.24}$$

which implies the expression of α_{crit}

$$\alpha_{\text{crit}} = \frac{1}{r_e} \cdot \left(\frac{r_o \pi}{\lambda}\right)^2, \tag{3.25}$$

or

$$\alpha_{\text{crit}} \simeq 3.5 \times 10^{15} \left(\frac{r_o}{\lambda}\right)^2 \text{m}^{-1}. \tag{3.26}$$

The value of α_{crit} depends on used radar! This finding is very important. In the case of the Ondřejov meteor radar ($\lambda = 8$m, $r_o = 1$m), is: $\alpha_{\text{crit}} \simeq 5.5 \times 10^{13}$ m^{-1}. To summarize, when $\alpha_e \ll \alpha_{\text{crit}}$ we work with underdense echoes and when $\alpha_e \gg \alpha_{\text{crit}}$ is satisfied overdense echoes are employed.

The transition from underdense to overdense is not sharply defined. The axial dielectric constant can be highly negative in the overdense train but this does not mean that total reflection

KNIHOVNA MAT.-FYZ. FAKULTY
Knihovna Fr. Zavišky (fyz. odd.)
Ke Karlovu 3
121 16 Praha 2

necessarily occurs. The wave can still penetrate the narrow underdense column, despite the negative ε, though with some loss of strength. The important difference between metals and low-density ionized gases is that the conductivity (as expressed in the wave equation) is complex for metals and real for ionized gases. Thus, the value of α_{crit} is not a turning point. That was the reason for introducing another kind of radar echoes, **the transitive ones**. They stretch over the rather large area, which corresponds to the span of α_e roughly about four orders.

3.3.1 Underdense echoes

To repeat the basic facts, the name the underdense echoes originates from validity of inequality $\varepsilon > 0$ (or $\alpha_e \ll \alpha_{crit}$). The incident radio wave penetrates the column and is scattered by the individual free electrons which oscillate freely in the applied field without colliding with other particles to any great extent. Each electron behaves as if no other were present - secondary radiative and absorptive effects may be neglected and scattering occurs from electrons throughout the trail. These trails are optically thin. Although we do not employ this kind of echoes in our model we touch on a few basic things of the underdense echoes in this subsection just for our gentle reader's sake to give him the complete overview.

The relation between received P_R and transmitted power, P_T, (under the assumption we have the common antenna for transmission and receiving) after backscattering on the underdense train is given by **the radar equation of the underdense echoes** the derivation of which we can find in (Pecina [40]):

$$P_R = P_T \frac{\mathcal{G}^2}{32\,\pi^2} \left(\frac{\lambda}{R}\right)^3 \left(\frac{e^2}{m_e c^2}\right)^2 {\alpha_e}^2 \exp\left(-\frac{8\pi^2 r_0^2}{\lambda^2}\right) \exp\left(-\frac{32\pi^2 D t}{\lambda^2}.\right) \tag{3.27}$$

R is a range of specular point on meteor train from observational location and $\mathcal{G}$ denotes antenna gain.

When we denote A as the amplitude of received signal we can write $A \sim \sqrt{P_R}$. It immediately follows from (3.27) that A drops with time in accord with

$$A = A_0 \exp\left(-\frac{16\,\pi^2\,D\,t}{\lambda^2}\right). \tag{3.28}$$

(In A_0 there are included all quantities from (3.27) which do not depend on time t.) We define the duration T_U of the underdense echoes in a common way as the time constant of the exponential drop of the received amplitude A. We get

$$T_U = \frac{\lambda^2}{16\,\pi^2\,D(h)}. \tag{3.29}$$

The term (3.29) expresses one important fact: the duration of the underdense echoes depends exclusively on the diffusion coefficient. It means, T_U depends on height h via $D(h)$. Hence, if we knew the height of specular points of underdense echoes it would be possible to determine $D(h)$ by measuring their durations during observations. Unfortunately, in the case of the Ondřejov meteor radar it is not realizable because observations are only single-station. Moreover, there are

not any other quantities connected with the real underdense echo such as σ and K and with the parameters of used radar apart from wavelength λ in (3.29). After substituting the values $\lambda = 8$ m and $D_r = 4.2\ \mathrm{m^2\ s^{-1}}$ we get $T_U \doteq 0.17$s.

3.3.2 Overdense echoes

As was already mentioned above, when the dielectric constant ε is negative throughout an appreciable volume of the trail, secondary scattering from electron to electron becomes important. The electrons are no longer independent scatterers. The ionized cylinder behaves as it would be made of metal. The trail is optically thick and scattering occurs mainly from the near side of the trail. Although the incident wave does not penetrate the column freely, even in matter of high conductivity, there is always a certain "skin depth" of penetration of the incident wave, defined as the depth at which the amplitude of the electric vector has fallen to $1/\varepsilon$ of the surface amplitude. Let us now derive the crucial expression for duration T_D of the overdense echoes. The overdense echoes are characterized by the negative permitivity on their axes. The duration T_D then comply with the time at which permitivity $\varepsilon(r,t)$ raises to zero even on the axis. So, we have the condition:

$$\varepsilon(0, T_D) = 0. \tag{3.30}$$

Let us assume the most important process of dissipation of meteor train, ambipolar diffusion. Hence, (3.22) together with the condition (3.30) gives

$$1 - \frac{\lambda^2 r_e \alpha_e}{\pi^2 (r_o^2 + 4DT_D)} = 0. \tag{3.31}$$

The expression of T_D we want is:

$$T_D = \left(\frac{\lambda}{2\pi}\right)^2 r_e \frac{\alpha(h)}{D(h)} - \frac{r_o^2}{4D(h)} \tag{3.32}$$

From expressions (3.29) and (3.32) we can see that both T_U and T_D do not depend on their position within the radar pattern. This fact plays very important role in our model as we will see in chapter (5.1). It is evident from (3.32) that the duration of the radiowave reflection from an overdense meteor trail can be used to determine the electron line density α_e, which depends on the mass and velocity of the meteoroid. Therefore, when a meteor shower (of a known velocity) is observed, or when its velocity can be independently determined in some manner, the mass distribution of the meteoroids, i.e., parameter s in the power law of distribution, can be found from the distribution of durations of overdense trails. We take the bottom line for T_D the value of 0.4s in film records from the Ondřejov meteor radar (see 4.4) to ensure that we work with overdense echoes.

Nothing remains but to mention the radar equation of the overdense echoes (Kaiser [25]):

$$P_R = P_T \frac{\lambda^3}{54\pi^3 R^3} \sqrt{\frac{e^2}{m_e c^2}}\, G^2(\vartheta)\, \sqrt{\alpha(T,h)}. \tag{3.33}$$

3.4 Initial radius of meteor train

Meteor trains typically reach an initial size much greater than the size of the meteoroids which created them in a very short period of time. Since the meteoroid has an initial velocity between roughly 11 and 72 km s^{-1}, atoms ablated from the meteoroid's surface will initially have very high kinetic energies, and take 15 to 20 collisions (Jones [22]) to slow down to thermal velocities. Meteor trails therefore undergo extremely rapid expansion to an initial dimension, at least a meter at 100 km, then diffuse outward. Establishment of thermodynamic equilibrium between air particles and meteoroid's atoms has two phases. The first one, in which energetic balance is being created, has the name **thermalization stage**. The phenomena connected with the second one, in which concentration balance is established, is described in section (3.2). Typical time of thermalization stage is 10^{-4}s (Bronshten [9]) and in the case of the Ondřejov meteor radar cannot be recorded because of its repetition frequency being 500 Hz (thermalization stage finishes sooner than electromagnetic field of transmitted radar wave alters).

There are many models published in scientific literature. For instance (McKinley [35]), (Manning [30]), (Massey and Sida [31]), (Kolmakov [27]) or (Campbel-Brown and Jones [10]). We need to choose a particular one to compute with it. According to Bronshten [9] the size of initial radius depends generally on the velocity of producing meteoroid and on the height at which it is created. The expression describing the dependence on the above mentioned factors reads

$$r_o = C\, v^b(h)\, \rho^{-a}(h),$$

where C is a constant which does not have a simple physical dimension. Since it is necessary to give the velocity as well as height of the reflection point to be able to compute the initial radius, it seems better to rewrite the preceding formula into the form

$$r_o = r_{oo} \left(\frac{\rho_k}{\rho(h)} \right)^a \cdot \left(\frac{v(h)}{v_k} \right)^b, \tag{3.34}$$

where now r_{oo} is the value of initial train radius at some reference height and velocity, having the same dimension as r_o. Bronshten [9] lists a variety of results many authors have arrived at with values of constants they have obtained. In our humble opinion the most reasonable and suitable model following from his observations seems to be the Baggaley's one [3] in which the initial radius is expressed in the form of (3.34) with the following constants:

- $r_{oo} = 1.5$ m (100 km)
- $\rho_k = 0.5306 \cdot 10^{-6}$ kg m^{-3} (100 km)
- $v_k = 40$ km s^{-1}
- $a = 0.45$
- $b = 0.57$

There is the term $\frac{r_o^2}{4D(h)}$ in (3.32). By using (3.13) we gradually get (instead of (3.34)):

$$\frac{r_o^2}{4D(h)} = \frac{r_{oo}^2}{4D_r\rho_r}\rho(h)\left(\frac{\rho_k}{\rho(h)}\right)^{2a}\left(\frac{v}{v_k}\right)^{2b} = c_1\,\rho(h)^{1-2a}\,v(h)^{2b}, \tag{3.35}$$

where $c_1 = \left[\frac{r_{oo}\,\varrho_k^a}{2\,v_k^b}\right]^2 \frac{1}{D_r\,\varrho_r}$ remains constant. The model (3.34) points out that the initial radius depends on height through density of air and velocity of meteoroids. In other words, the initial radius increases as both velocity and height get larger. The attenuation due to the initial radius is directly responsible for the well-known height ceiling effect. Let us look closely at the underdense radar equation (3.27), at its term $\exp\left(-\frac{8\pi^3 r_o^2(h)}{\lambda^2}\right)$. Since atmospheric density decreases with height, the initial radius is expected to increase and that term falls into decline. For a radar at any given wavelength there is a height beyond which no underdense echoes can be recorded because the received power P_R is under sensitivity level (it is drowned by disturbing noise).

Chapter 4

Radar observations

4.1 Basic terms

Observations of a meteor shower can begin at the moment when a stream of meteoroids crosses the Earth's orbit. Meteor phenomena originate as a consequence of an interaction of meteoroids with the atmosphere. By their systematic monitoring of a different kind (visual, photographic, spectroscopic, radar, sound, infrasound, seismic or television and video observations) we can get complete picture about a shower activity i.e. about an activity period, a profile of an activity curve, mass or magnitude distribution and so on. But before we will occupy ourselves with our range distribution model we need to define a few basic terms relating to the radar observation.

- **Flux Θ_{m_0}**
  It is a quantity that quotes a number of meteors crossing the unit surface of the echo plane per time unit having masses in excess of m_o. Mass m_o is an optional constant selected in accordance with the kind of data. Its unit is $\mathrm{m}^{-2}\,\mathrm{s}^{-1}$.

- **Echo plane**
  It is a plane that is perpendicular to the radiant direction and runs through the observational site. So, the position of the echo plane is defined by its normal vector that aims at the radiant. In other words it is a set of all points at which the specular reflection from meteor trails can occur. The definition of the echo plane is bounded up with two another terms. **The local meridian of the echo plane** is the plane defined by the direction to the radiant and the direction to the local zenith. This plane intersects the echo plane in a straight line called **the main straight line of the echo plane** (i.e. the line OB in Fig. 4.1) that is always perpendicular to the straight line of intersection of the echo plane and the horizon (i.e. DE in Fig. 4.1).

- **Collecting area**
  It is a subset of the echo plane. Received power from all its points must exceed the minimal

power P_{min} that the used radar is able to recognize as a signal from a meteor. In the case of the Ondřejov meteor radar $P_{min} = 2.10^{-13}$W (see also Table 4.1).

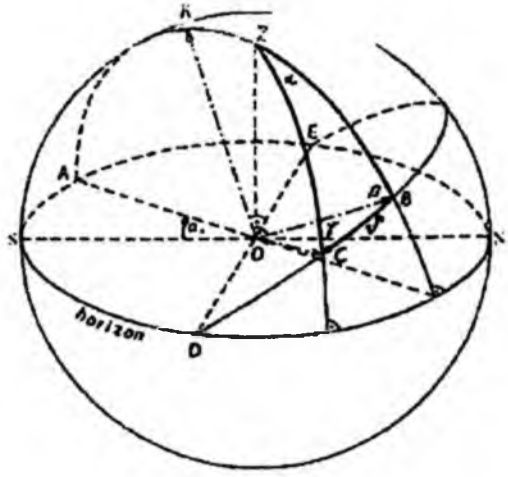

Figure 4.1: The echo plane is determined by points BDE, the observational site O is situated at the origin of the coordinate system. The basic directions are: the radiant direction $\overrightarrow{OR}$, the zenith direction $\overrightarrow{OZ}$, the observational direction $\overrightarrow{OC}$.

Fig 4.1 provides a clear idea about the definitions mentioned above. The origin of the coordinate system is set up at the observational site O. Points BDE establish the echo plane, points ZRA give the position of its local meridian of the echo plane. The direction $\overrightarrow{OR}$ points at the radiant, its horizontal coordinates are (a_R, z_R). The direction $\overrightarrow{OZ}$ is the zenith direction. We observe in the direction $\overrightarrow{OC}$. Points OB define the main straight line. We need to search for relations that allow us to determine horizontal coordinates (a, h) of the specular point C. Let us focus now on the spherical triangle BCZ and express sizes of its sides and angles:

- ZB $= 90° - z_R$
- BC $= \vartheta$ (reckoned from the main straight line $\overrightarrow{OB}$ affirmatively in clockwise sense)
- CZ $= 90° - h$
- $\alpha \;\; = a - a_R - 180°$
- $\beta \;\; = 90°.$

By applying the formulae of spherical trigonometry to the triangle BCZ we get relations:

$$\sin h = +\sin z_R \cos\vartheta \tag{4.1}$$

$$\cos h \cos(a - a_R) = -\cos z_R \cos\vartheta \tag{4.2}$$

$$\cos h \sin(a - a_R) = -\sin\vartheta. \tag{4.3}$$

These relations allow us to determine the desired horizontal coordinates (a, h) of the specular point C when the radiant position and the position within the echo plane given by the angle ϑ are known.

To summarize, after passage of a meteoroid through the Earth's atmosphere a ionized electrically conducted path is created. Its ionization curve stretches within some interval of heights. The specular point can lie at any place on it. Provided we set up a firm direction of an observation within the echo plane (angle ϑ), a mutual relation between linear height h_l and range of the specular point R from the radar is given by means of the cosine theorem of plane trigonometry (R_E is the Earth's radius):

$$(R_E + h_l)^2 = R_E^2 + R^2 - 2R_E R\cos(90° + h). \tag{4.4}$$

By substituting (4.1) into (4.4) ve get

$$h_l = \sqrt{R_E^2 + R^2 + 2\,R_E\,R\sin z_R\cos\vartheta} - R_E. \tag{4.5}$$

And finally we will mention relations we need to know in computations that connect angle ϑ defining position within the echo plane with angles $\bar{\vartheta}$ and $\bar{\varphi}$ describing three-dimensional antenna pattern. The spatial position of the antenna is unambiguously given by two angles: azimuth of the antenna axis a_{axis} and elevation of the direction of maximum transmission ε_m.

$$\begin{aligned}
\cos\bar{\vartheta}\cos\bar{\varphi} &= [\sin\varepsilon_m\sin z_R - \cos\varepsilon_m\cos z_R\cos(a_R - a_{\text{axis}})]\cos\vartheta + \\
&+ [\cos\varepsilon_m\sin(a_R - a_{\text{axis}})]\sin\vartheta, \\
\cos\bar{\vartheta}\sin\bar{\varphi} &= -[\cos z_R\sin(a_R - a_{\text{axis}})]\cos\vartheta - [\cos(a_R - a_{\text{axis}})]\sin\vartheta, \\
\sin\bar{\vartheta} &= [\cos\varepsilon_m\sin z_R + \sin\varepsilon_m\cos z_R\cos(a_R - a_{\text{axis}})]\cos\vartheta - \\
&- [\sin\varepsilon_m\sin(a_R - a_{\text{axis}})]\sin\vartheta.
\end{aligned}$$

We can find the derivation of the preceding formulae in Pecina [38].

4.2 Ondřejov Meteor Radar

The meteor radar is located at the Astronomical Institute of Academy of Sciences of the Czech Republic and has been under operation since 1958. Originally, it was a german military radar ("FREYA") of Air Defence made in 1942. It was rebuilt into today's form during rapid boom of meteor radioastronomy and then it was situated at Ondřejov. Its mechanical construction has been described by Plavcová and Šimek [49]. Fig. 4.2 serves us to get an idea about size of that equipment. The size of an antenna mirror is 6×13.3m, its mid-point is 7.9m above ground surface. The mechanical axis is fixed at the angle of 45° in vertical direction, the cabin of the radar together with the antenna is steerable only in azimuth. A rotation is fully controlled via a punched tape. The system requires human service. Data are recorded on film (see also Fig. 4.5). The antenna is common for transmission and receiving and is made of six half-wave dipoles aligned in two lines.

Behind these dipoles in distance of $\lambda/8$m is located reflecting mirror made of wire cloth. The electrical axis lies about 50.5° above the horizon and coincides with the direction of maximum transmission. The gain in this direction equals to 24, i. e. the transmitted power of our radar exceeds 24× that of omnidirectional transmitter. Vertical section of the antenna pattern shows two lobes from the side one at 17° arises due to interference of direct signal with the signal reflected by the hilly ground surrounding the radar.

Figure 4.2: The Ondřejov meteor radar.

Table 4.1 summarizes in a brief form the technical parameters of the Ondřejov meteor radar. This table is replenished by two Graphs (4.3) and (4.4) that represent the vertical and horizontal section of the antenna pattern.

transmitted power P_T	10 kW
limited receiving power P_R	2.10^{-13} W
efficiency η of antenna as a device	0.95
repetition frequency	500 Hz
pulse length	10 μs
wavelength λ	8 m (37.5M Hz)
maximum antenna gain	24

Table 4.1: The table gives a brief report on technical parameters of the Ondřejov meteor radar

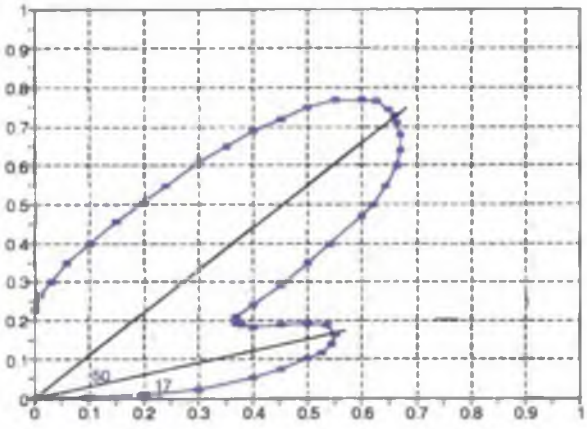

Figure 4.3: The vertical antenna pattern of the Ondřejov meteor radar, normalized to maximum, with its two lobes. The main lobe has maximum at 50.5°, the maximum of the side lobe is at 17°. The beam width between the half-power points is approximately 52°. The x-axis lies in the local horizon.

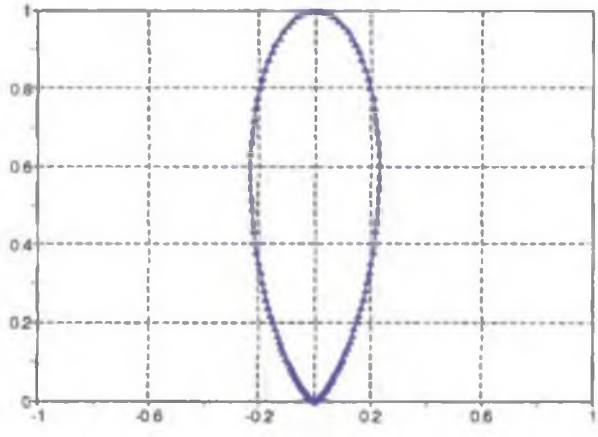

Figure 4.4: The horizontal antenna pattern of the Ondřejov meteor radar, normalized to maximum, has only one lobe. The beam width between the half-power points in the plane orthogonal to that of vertical one is 36°.

4.3 Methods of radar observations

The general principle of meteor observations by back scattering of radio waves off their trails is easy to understand. When a meteor enters the Earth's atmosphere, its ionized trail may scatter or even reflect the radio waves from the transmitter back to the receiver. In the case of the observation by means of the Ondřejov meteor radar the transmitter and the receiver are located at the same observational position. Because the position of the radiant is a function of time it follows that also position of the collecting area of the echo plane from which we can register echoes varies depending on time. Thus, it is necessary to choose the relevant setting of the antenna during an observation. In principle there are two ways how to reach it that we will now show.

Let us denote $\vec{n_r}$ as the unit vector in the direction of a reflecting point of a meteor trail and $\vec{n_R}$ as the unit vector in the direction of the radiant. As usual, we can express both vectors in commonly used spherical coordinates:

$$\vec{n_r} = (\cos a_r \cos h_r, -\sin a_r \cos h_r, \sin h_r)\,,$$

$$\vec{n_R} = (\cos a_R \sin z_R, \sin a_R \sin z_R, -\cos z_R)\,.$$

Symbols correspond to elevation h_r and azimuth a_r of the reflecting point and zenith distance z_R and azimuth a_R of the position of the radiant. Obviously, in order to obtain transmitted radio waves after reflecting or scattering off a meteor trail, the scalar product $\vec{n_r} \cdot \vec{n_R}$ has to be zero. After making a calculation we arrive at the basic observational equation:

$$\cos(a_r - a_R) = -\tan h_r \cdot \cot z_R. \tag{4.6}$$

Apparently, $\tan h_r \cdot \cot z_R \leq 1$ in order the equation (4.6) could be solved. At this stage we distinguish between two cases. We know the motion of the radiant, i.e. z_R, a_R so that the coordinates of the reflecting point are optional.

1. Firstly, we can choose the elevation h_r as known quantity. Clearly, (4.6) has a solution provided $h_r \leq z_R$. We do it in accord with the antenna pattern so as h_r has the same value as the direction of the maximum sensitivity, if possible. We use the set of following almucantars: $50°, 48°, 46°, 44°, 42°, 17°$. Since in this way we get two solutions of (4.6), we usually choose the one with respect to familiarity with the terrain surrounding the meteor radar. The method is called **the almucantar method**. Its advantage lies in the fact that we fix the sensitivity into the radar antenna pattern and this provides us with the observation with constant sensitivity. The disadvantage is the fact that the suitable almucantar does not always exist.

2. Secondly, we can choose the azimuth a_r as known quantity, i.e. we set the radar axis of maximum radiation at this selected azimuth. Due to the definition of the echo plane the difference $(a_r - a_R)$ on the left-hand side of the equation (4.6) has to be equal to $180°$.

Hence it follows the name of the method: **the $A + 180°$ method.** The echo plane cuts the antenna pattern at any observational time in a symmetric way. By means of (4.6) we get the elevation h_r of the reflecting point. In this way of observations the sensitivity (gain) in the direction of the reflecting point varies much more dramatically than in the previous case. Even in some cases we cannot observe due to very high elevation of the radiant (e.g. Quadrantid meteor shower around its culmination) and consequently a low radar sensitivity.

In practice we are usually urged to combine both methods in a suitable way. It is necessary to always keep in mind the way of observations because due to the variable mutual position of the echo plane and the antenna pattern we would get a different signal power from the same echo.

4.4 Data

In the case of the Ondřejov meteor radar each radar echo is characterized by four quantities we have at our disposal. These are:

- ⋆ time instant of echo occurrence
- ⋆ time behaviour of echo amplitude
- ⋆ echo duration of overdense echoes
- ⋆ range of reflecting point on meteor trail from radar

The example of the part of a typical film record is shown in Fig. 4.5. The film record consists of two parts:

1. Record "A" (amplitude record): display of an echo intensity as a function of time, overexposed bottom part is a background noise.
2. Record "D" (range record): display of an echo range as a function of time. Each one of range signs is in the form of a horizontal line. These lines are displayed at a 20-km distance from each other. The record grid begins at 60 km and ends up at 600 km. There is a blocking gap between 300 and 380 km on the film record. This gap arises from an artificial increasing of a range extend from 300 km (given by a radar repetition frequency of 500 Hz) to 600 km and was installed to suppress recording of the ground based reflections. As a consequence all radar echoes are doubled on the film record, their relevant ranges are read in the part which includes their non-doubled image.

There are time marks between parts "A" and "D". A time mark together with following gap means one second, every tenth mark is represented in bold. A sign of Local Time in the form hour:minute (09:21) is recorded on the film after every one minute from a digital clock. The arrow above the time marks points to the direction of increasing time.

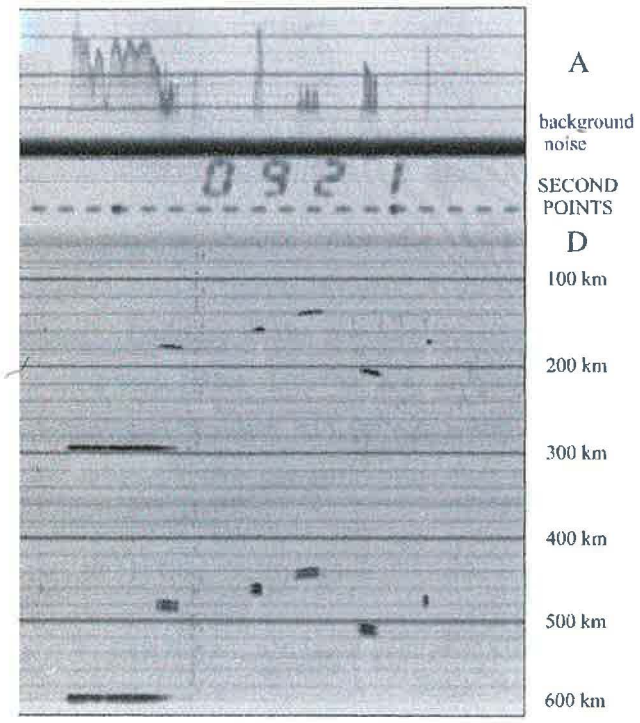

Figure 4.5: The example of a part of a typical film record that includes three underdense and four overdense echoes. This film record represents about 18 seconds of the observations of Leonid meteor shower at 9:21 LT on 18th of November in 2000.

4.5 Mass distribution index

Mass distribution index s is a very important to an inner structure of meteor showers. It is defined by the well-known mass distribution power law expressed by equation

$$dN = c_n\, m^{-s}\, dm, \tag{4.7}$$

giving number of meteors dN having masses within the interval $(m, m+dm)$ (McKInley [35]), c_n is a normalizing factor. Hence, it is obvious that s always has to belong to an restricted range of masses with respect to observation, in which it is usually supposed to be constant. Let us compute the total (cumulative) number of meteors N_c inside the interval from some reference mass m_∞ to $+\infty$:

$$N_c = c_n \int_{m_\infty}^{+\infty} x^{-s}\, dx = c_n\, \frac{m_\infty^{1-s}}{s-1}. \tag{4.8}$$

It is obvious that the mass distribution index s has to be always greater than 1. Failing that, the integral would diverge.

At this point, we concentrate on possible values of s. As it is very often said, when a condition $s < 2$ is fulfilled, a contribution of "fainter meteors" to the total mass of meteor shower is lesser than of "brighter" meteors". Contrary to the previous situation, in the case of $s > 2$, "fainter meteors" determine the total mass rather than "brighter meteors". A derivation given bellow help us to clarify terms "brighter" and "fainter" and the role s plays. To simplify the derivation and make all problem easier we work under the assumption that meteoroids do not decelerate and relate our quantities to the point of maximum light.

Firstly, we substitute into (2.41) from (2.10) taking (2.1) into consideration:

$$I = \frac{1}{2}\sigma K \tau(v_\infty) v_\infty^5 m_\infty^{2/3} \varrho(h) \left(1 - \frac{HK\sigma v_\infty^2}{3 m_\infty^{1/3} \cos z_R}\, \varrho(h)\right)^2. \tag{4.9}$$

Secondly, we calculate the maximum of light curve (4.9) as a function of height h, i.e. the point at which $\frac{dI}{dh} = 0$. Hence

$$\begin{aligned} \frac{dI}{dh} &= \frac{dI}{d\varrho}\frac{d\varrho}{dh} = \\ &= \frac{d\varrho}{dh}\frac{1}{2}\sigma K \tau(v) v_\infty^5 m_\infty^{2/3} \left(1 - \frac{HK\sigma v_\infty^2}{3 m_\infty^{1/3} \cos z_R}\, \varrho(h)\right)\left(1 - \frac{HK\sigma v_\infty^2}{m_\infty^{1/3} \cos z_R}\, \varrho(h)\right). \end{aligned}$$

The height of maximum light occurs at the atmospheric density

$$\varrho_{max} = \frac{m_\infty^{1/3} \cos z_R}{HK\sigma v_\infty^2}, \tag{4.10}$$

coinciding with the density at the height of maximum ionization (2.51), while the maximum light itself reads

$$I_{max} = \underbrace{\frac{2\tau(v_\infty) v_\infty^3 \cos z_R}{9H}}_{c_I} m_\infty = c_I\, m_\infty. \tag{4.11}$$

We have included into c_I the quantities which are constant for meteoroids of particular shower. Thirdly, in the future considerations we rely on the following relation between the light intensity I and corresponding magnitude M (Ceplecha et.al. [15]):

$$M = -2.5 \log I, \quad \text{or} \quad I = 10^{-0.4M}, \tag{4.12}$$

which is valid at any point of the light curve, so that also at its point of maximum.
We know the number of meteors having masses within the interval $(m_\infty, m_\infty + dm_\infty)$ from the distribution power law (4.7):

$$dN_c = c_n \, m_\infty^{-s} \, dm_\infty \tag{4.13}$$

and also the total mass dm_c within the same interval:

$$dm_c = m_\infty \, dN_c = c_n \, m_\infty^{1-s} \, dm_\infty. \tag{4.14}$$

Let us transform this distribution power law into magnitudes. By means of previous relations, we gradually get

$$\begin{aligned} dm_c &= c_n \frac{I_{max}^{1-s}}{c_I^{1-s}} \frac{dI_{max}}{c_I} = \frac{c_n}{c_I^{2-s}} \ln 10^{-0.4} \left(10^{-0.4M_{max}}\right)^{2-s} dM_{max} = \\ &= \gamma_1 \, \kappa^{M_{max}} \, dM_{max}, \end{aligned}$$

$$\begin{aligned} dN_c &= c_n \frac{I_{max}^{-s}}{c_I^{-s}} \frac{dI_{max}}{c_I} = \frac{c_n}{c_I^{1-s}} \ln 10^{-0.4} \left(10^{-0.4M_{max}}\right)^{1-s} dM_{max} = \\ &= \gamma_2 \, \zeta^{M_{max}} \, dM_{max}. \end{aligned}$$

The symbols κ, ζ, γ_1 and γ_2 designate the following:

$$\begin{aligned} \kappa &= 10^{0.4(s-2)}, \\ \zeta &= 10^{0.4(s-1)} = \kappa 10^{0.4} \\ \gamma_1 &= \frac{c_n}{c_I^{2-s}} \ln 10^{-0.4} \\ \gamma_2 &= \frac{c_n}{c_I^{1-s}} \ln 10^{-0.4}. \end{aligned} \tag{4.15}$$

The quantity ζ is called the population index. The connection between s and ζ is obvious: $s = 1 + 2.5 \log \zeta$. Both indices are important parameters for studies of meteoroid streams. As the indices describe the internal structure of individual streams their values are constant only over a limited range of the magnitudes and masses and to a certain degree vary from stream to stream.

On the one hand, mass of a meteor shower in the magnitude range $(M, M+1)$ due to "brighter meteors" and their number equal to

$$m_{c1} = \gamma_1 \int_M^{M+1} \kappa^x \, dx = \gamma_1 \frac{\kappa^{M+1} - \kappa^M}{\ln \kappa}, \tag{4.16}$$

$$N_{c1} = \gamma_2 \int_M^{M+1} \zeta^x \, dx = \gamma_2 \frac{\zeta^{M+1} - \zeta^M}{\ln \zeta}. \tag{4.17}$$

On the other hand, mass of a meteor shower in the magnitude range $(M+1, M+2)$ due to "fainter meteors" and their number equal to

$$dm_{c2} = \gamma_1 \int_{M+1}^{M+2} \kappa^x \, dx = \gamma_1 \frac{\kappa^{M+2} - \kappa^{M+1}}{\ln \kappa}, \tag{4.18}$$

$$N_{c2} = \gamma_1 \int_{M+1}^{M+2} \zeta^x \, dx = \gamma_2 \frac{\zeta^{M+2} - \zeta^{M+1}}{\ln \zeta}. \tag{4.19}$$

Their number ratio $\frac{N_{c1}}{N_{c2}}$ is:

$$\frac{N_{c1}}{N_{c2}} = \frac{\zeta^{M+1} - \zeta^M}{\zeta^{M+2} - \zeta^{M+1}} = \frac{1}{\zeta} = 10^{-0.4(s-1)}. \tag{4.20}$$

Since the condition $s > 1$ is valid, the number N_{c2} of "fainter meteors" is always greater than the number N_{c1} of "brighter meteors". Moreover, let us highlight the sense of the population index as the ratio between the number of meteors with magnitude within the interval $(M+1, M+2)$ and $(M, M+1)$.

We now focus on the ratio $\frac{m_{c1}}{m_{c2}}$:

$$\frac{m_{c1}}{m_{c2}} = \frac{\kappa^{M+1} - \kappa^M}{\kappa^{M+2} - \kappa^{M+1}} = \frac{1}{\kappa} = 10^{-0.4(s-2)}, \tag{4.21}$$

from which we can infer the following implications

$$\begin{aligned}
s &= 2 \implies m_{c1} = m_{c2} \\
s &< 2 \implies m_{c1} = 10^k m_{c2} > m_{c2} \quad \left(k = \frac{2-s}{2.5} > 0\right) \\
s &> 2 \implies m_{c1} = 10^{-l} m_{c2} < m_{c2} \quad \left(l = \frac{s-2}{2.5} > 0\right)
\end{aligned}$$

We can see from the preceding results that while the number of "brighter meteors" is always less than the number of "fainter ones" $(s > 1)$ their mass contribution is greater if $1 < s < 2$. For $s > 2$ the "fainter meteors" mass contribution and the number are both greater than the ones of "brighter meteors". We will employ the law (4.7) in one of further sections for construction of range distribution formula.

4.5.1 Determination of mass distribution index

Mass distribution index s can be determined from radar observations. The method frequently used in radioastronomy of meteors is based on a relation we will now derive to be aware of restricted conditions under which it is valid. These conditions are two. Firstly, we assume the reflection point of a meteor path coincides with the point of maximum ionization (McIntosh and Šimek [33]). Secondly, meteoroids do not decelerate during their passage of the Earth's atmosphere. Hence, we can make use of the expression (2.53) for $\alpha_{\max}$, which we substitute into (3.32) to evaluate the duration of a radar echo at the point of maximum ionization. We neglect the second term $\frac{r_0^2}{4D}$ of (3.32) due to its small value in comparison to the first one in the process. We also employ

the relation (3.13). Then the relation between the duration T_{max} of a radar echo at the point of maximum ionization and mass m_∞ is

$$T_{max} = \left(\frac{\lambda}{2\pi}\right)^2 \frac{r_e H \beta(v_\infty) \cos^2 z_R}{9 D_r \varrho_r \mu_a K H^2 \sigma v_\infty^2} m_\infty^{4/3}. \tag{4.22}$$

We express m_∞ from (4.22) and substitute it into (4.8), which is the relation expressing cumulative number of meteors N_c as a function of mass m_∞. Calculation the logarithm gives us the desired dependence of N_c on the duration T_{max} at the point of maximum ionization provided the meteoroids do not decelerate:

$$\log N_c = K_s - \frac{3}{4}(s-1) \log T_{max}. \tag{4.23}$$

All parameters connected with the real meteoroids are included in the constant K_s. Obviously, K_s depends on $\frac{1}{s-1}$ but it does not play important role in computation s from the slope of the curve (4.23). We take the value of s computed in this way as a starting one in our model (that is valid generally at all points of the ionization curve).

Fitting the $\log N_c$ vs. $\log T_{max}$ curve following (4.23),we can see that it should be linear. But in practice we find this dependence to be curved, so the number of more persistent reflections drops more rapidly than it would if it were determined only by the law of mass distribution of the meteoric bodies. This phenomenon is observed in both meteor showers and sporadic background. A lot of authors have proposed various explanation of this discrepancy, e.g. (McIntosh [34]) or (Nicholson and Pool [37]). We maintain the position that was for the first time presented in Pecina [39]. The author have demonstrated that non-equal collecting areas for meteors of various durations cause a decrease of the computed mass distribution index s and furthermore that the evaluation of the mass distribution index s cannot be segregated from that of the flux. We fully identify with these statements. Due to unequal collecting areas for meteors with various durations the mass distribution index s is usually lower than we expect. It is valid that the longer duration the larger collection area so the actual curve has steeper slope and as a consequence greater value.

Chapter 5

Range distribution model

5.1 Definition of range distribution

By means of observations we gain the data the characteristics of which are described in section (4.4). When we sort out observed radar echoes into chosen range intervals according to the other characteristics (i.e. an observed time interval, a selected interval of durations), we can get a column chart similar to the diagram (5.1). Thus, the range distribution is the dependence of the echo rates on ranges from the radar.

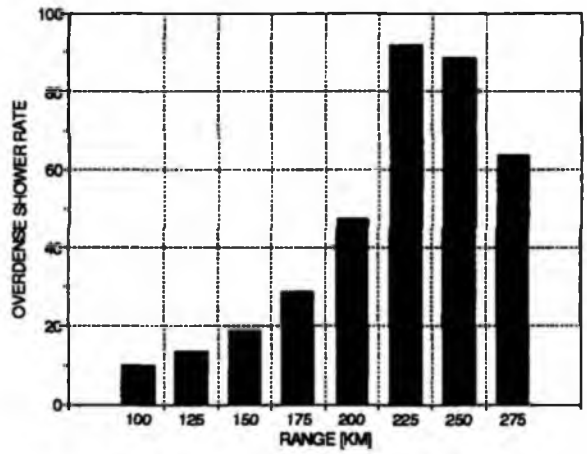

Figure 5.1: This example of the typical range distribution was made from radar meteors recorded during observations of Geminid meteor shower, between 23 and 3 UT, on the 13th and 14th of December, in 2000. The histogram comprises overdense echoes with durations greater than 0.4 s. The vertical axis shows shower rates in particular 25-km-wide range intervals, which are represented by their initial points on the horizontal axis.

The range distribution mirrors the fact that ionized meteor trails associated with a particular meteor shower occur inside a restricted height interval. The interval depends on the radiant po-

sition, on the masses and speeds of meteoroids contributing to the range distribution and on the other physical quantities, which we can describe by means of the ablation coefficient σ and the shape-density parameter K (e.g. Ceplecha et.al. [15]). Since during the observations of meteor showers we register simultaneously a lot of meteors with various masses, their mass distribution described by the mass distribution index s together with the shower flux density Θ_{m_0} have an influence upon the shape of their range distribution curve. We have developed the model reflecting all these facts that allows us to compute several important quantities typical for particular meteor showers. Derivation of the range distribution model is included in the next sections.

5.2 Range distribution model: principal formula

In this section we draw our attention to the derivation of the principal formula of our model. As a consequence of the fact that the range distribution is a result of the contribution of meteors having various masses, our theoretical model has to be based on the generalization of the well-known mass distribution power law (4.7) we will modify for our purpose. The law was derived from observations over a large part of the sky. Assuming that it is valid inside any element of the echo plane and also in any sufficiently short time interval we will alter (4.7) in the following way. Apparently, the larger collecting area and the longer time interval the greater number of meteors we should observe. That results in a more general mass distribution law in the Belkovich's form (Belkovich [6])

$$d^3N = c_n\, m^{-s}\, dm\, dS\, dt. \tag{5.1}$$

Here dt is the time interval, $dS = RdRd\vartheta$ is the element of the collecting area within the echo plane. (Section (4.1) gives a detailed account of coordinates R and ϑ.)

To specify the normalizing factor c_n, we employ the definition of the shower flux density. Let us remember that Θ_{m_0} is a number of meteors crossing the unit surface of the echo plane per time unit having masses in excess of m_o. Mass m_o is an optional constant that will be discussed later. The definition together with the law (5.1) leads to the following relation connecting the shower flux density Θ_{m_0} with the normalizing factor c_n:

$$\Theta_{m_0} = \int_{m_0}^{+\infty} \frac{d^3N}{dS\,dt}\, dm = c_n \int_{m_0}^{+\infty} m^{-s}\, dm = \frac{c_n}{s-1}\, m_0^{1-s}. \tag{5.2}$$

Eliminating c_n between equations (5.1) and (5.2) yields the important generalized mass distribution power law

$$d^3N = (s-1)\,\Theta_{m_0}\, m_0^{s-1}\, m^{-s}\, dm\, dS\, dt. \tag{5.3}$$

Obviously, $m \geq m_0$ has to be valid. Since mass of a meteoroid decreases during its passage through the Earth's atmosphere and the rate of mass loss is different for meteoroids of various sizes, shapes and chemical composition, the mass m in (5.3) should represent m_∞ of the meteoroid, i. e. its mass before entering the Earth's atmosphere. Moreover, since the quantity m_∞ is not directly observable

KNIHOVNA MAT.-FYZ. FAKULTY
Knihovna Fr. Zavišky (fyz. odd.)
Ke Karlovu 3
121 16 Praha 2

we have to transform it to include only observable one. Generally, we have two possibilities based on the data, which are at our disposal from observations (see section 4.4). We can choose either a duration of an overdense echo or amplitude of an underdense echo. Both quantities are connected with linear electron density α_e and therefore with mass m_∞. There are two reasons for decision to exclude underdense echoes from our work. Firstly, their amplitudes connected with α_e (physical meaning is given by the equation (3.28)) depend on the positions of the specular points within the radar pattern. Because our observations belong only to single-station ones, we are not able to determine these positions. Secondly, the specular points can be situated at any point of the ionization curve in reality. This fact could cause troubles during computation of mass of meteoroids. The whole ionization curve of meteoroids with small mass can lie under the critical linear electron density. But the ionization curve of meteoroids with bigger mass has two parts, underdense and overdense ones and the specular point can be involved in underdense part. Fig. 5.2 includes two ionization curves computed from (2.50) for the sake of simplicity. So, we would count this radar echo as an underdense one, but in reality it would be an overdense echo. For this reason we decided to make use of overdense meteors to avoid just described problem. Their duration are handy because it does not depend on the position within the antenna pattern. To make the picture complete there is no possibility to use duration T_U of underdense echoes because this quantity is not related to physical characteristics of meteors. Eventuality to employ amplitudes of overdense echoes is also impracticable because we have no physical theory connecting the linear electron densities of overdense echoes with their amplitudes.

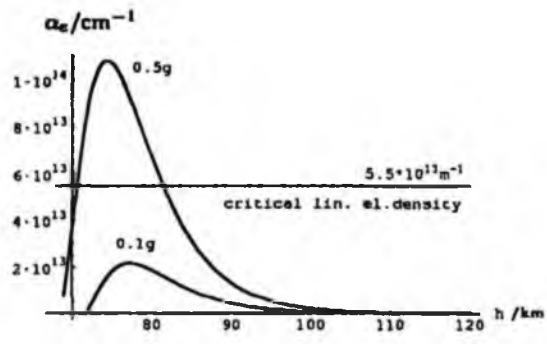

Figure 5.2: The course of the ionization curves for two values of m_∞, 0.1 g and 0.5 g. In the case of smaller mass any point of the ionization curve does not exceed the critical linear electron density. On the contrary, the second ionization curve ($m_\infty = 0.5$ g) has two parts, the overdense and underdense one. Both curves were computed after (2.50) for $v_\infty = 36$ km s^{-1}, $\sigma = 0.01$ s^2 km^{-2} and $K = 1$ cm^2 g$^{-2/3}$, $z_R = 45°$, $H = 5.409$ km, $\varrho_o = 56.803$ kg m^{-3} and $\mu_a = 6.69414 \times 10^{-26}$ kg. The used model of ionization probability β was in accord with (2.47).

To proceed further, we rewrite (5.3) as

$$d^3N = (s-1)\,\Theta_{m_0}\, m_0^{s-1}\, m_\infty^{-s}\, dm_\infty\, dS\, dt. \tag{5.4}$$

In the above equation d^3N stands for an incremental rate with respect to mass. Since it is better to deal with cumulative rates due to greater rates in practice, our theoretical range distribution model is based on the cumulative quantity. To answer this purpose, we carry out the integration in (5.4) with respect to mass from a certain value of m_∞ to $+\infty$. We obtain

$$d^2N_c = \Theta_{m_0}\,(m_0/m_\infty)^{s-1}\, dS\, dt. \tag{5.5}$$

Here d^2N_c is the cumulative number of meteors having masses in excess of m_∞ registered during the time element dt and within the element of the echo plane dS. (5.5) is our principal formula in the differential form. We get its integral form by integration of (5.5) with respect to time t and collecting area $S_{\rm col}$:

$$N_c = \Theta_{m_0} \int_{t_1}^{t_2} dt \int_{S_{\rm col}} (m_o/m_\infty)^{(s-1)}\, dS = \Theta_{m_0} \int_{t_1}^{t_2} dt \int_{R_1}^{R_2} dR\, R \int_{\vartheta_1(R)}^{\vartheta_2(R)} \left(m_o^{1/3}/m_\infty^{1/3}\right)^{3(s-1)} d\vartheta. \tag{5.6}$$

We would like to stress here that m_o does not depend on the position of the train reflecting point within the collecting area and is, therefore, constant with respect to the the integration. The explicit functional dependence of $m_\infty^{-1/3}$ on the integration variables can be inferred from the physical theory outlined in the previous sections. We need to express this quantity as a function of observed duration T_D. When combining together the equations (2.56), (3.13) and (3.32) we arrive at

$$\left(T_D + \frac{r_o^2}{4D(h)}\right) x^2 = c\,a\,\varrho(\varrho-\varrho_B)\left\{1-(1-\mu)\,\frac{b}{\cos z_R}\,[\varrho-\varrho_B-\varrho_B\ln\varrho/\varrho_B]\,x\right\}^{\frac{\mu}{1-\mu}},\quad \varrho\geq\varrho_B. \tag{5.7}$$

Here the symbols x, a, b, c stand for:

$$x = m_\infty^{-1/3} \tag{5.8}$$

$$a = K\sigma v_\infty^2\,\beta \tag{5.9}$$

$$b = K\sigma v_\infty^2\, H \tag{5.10}$$

$$c = \left(\frac{\lambda}{2\pi}\right)^2 \frac{r_e}{\mu_a\, D_r\, \rho_r} = \text{const.} \tag{5.11}$$

Also c is a constant that depends only on the used equipment via λ. Furthermore, it is important to note that the parameters a and b depend namely on the physical properties of meteoroids. It means on the shape-density parameter K, the ablation parameter σ, and on the ionization probability β. We suppose both quantities a and b to be the same for all members of a particular shower. We can also write by means of (5.9), (5.10) and (5.11) the following useful relations:

$$K\cdot\sigma = \frac{b}{H\,v_\infty^2}, \tag{5.12}$$

$$\beta = H\frac{a}{b}. \tag{5.13}$$

The physical meaning have only two last quantities and, therefore, only resulting values of these quantities will be presented instead of a and b in the section dealing with results of our effort. Thus, we have the function $x = x(a, b, \mu, \varrho_B)$ that we can insert into (5.6) and perform the integration. The unknown parameters we wish to obtain are: $\Theta_{m_0}, s, K \cdot \sigma, \mu, \beta$ and ϱ_B. Because all values of ϱ_B tended to zero when applying formula (5.6) to observed range distributions we decided to exclude it from computed parameters and put it fixed value of zero. The following four Figures, 5.3 and 5.4, demonstrate the changes of the range distribution with changing the parameters $s, K \cdot \sigma, \mu$ and β it depends on. The dependence on flux Θ_{m_0} is linear so that there is no need to draw the corresponding picture. All four curves are computed for the radiant of Geminids between 1 and 2 hours LT, for mass $m_0 = 10^{-5}$ kg, $v_\infty = 36$ km s^{-1}, $D_r = 4.2\,\mathrm{m}^2\,\mathrm{s}$ (height of 93 km), $H = 5.409$ km and $\varrho_o = 56.803$ kg m^{-3}.

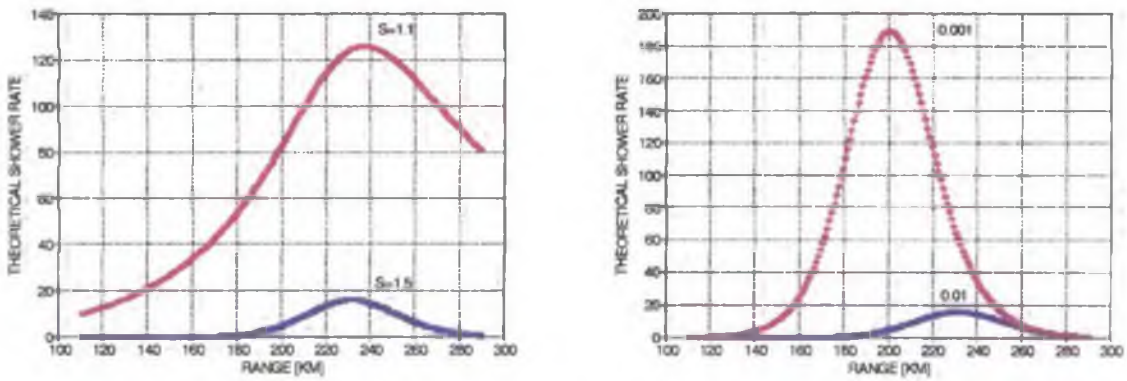

Figure 5.3: The left picture shows theoretical range distribution as a function of mass distribution index s. Decreasing s causes increasing echo rates. The position of maximum is preserved. The right picture presents theoretical range distribution as a function of product $K \cdot \sigma$. Obviously, the higher the value of this product the more distant and less powerful the maximum is. The relevant curves are marked with the corresponding value of the product.

The formula (5.6) expresses the fact that we collect meteors crossing the collecting area of the echo plane S_{col} during the time interval (t_1, t_2). In other words, we integrate over time interval during which the observation was carried out and over the surface from where the radar is able to register radar echoes. We can see that the number of meteors within the range interval (R_1, R_2) depends on mass distribution index s and is directly proportional to Θ_{m_0}.

The limits of the integration are the following:

t_1, t_2 are time limits of observational interval (optional),

R_1, R_2 are limits of particular range interval (optional),

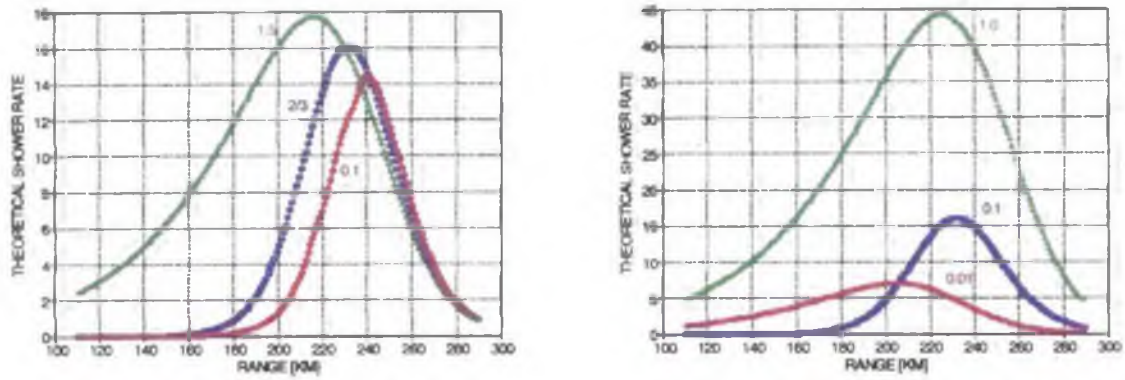

Figure 5.4: The left picture shows theoretical range distribution as a function of Levin's μ. Range extension of the distribution depends on the value of μ. The higher this value the wider extent of the distribution. The relevant curves are marked with the corresponding value of μ. The right picture presents theoretical range distribution as a function of β. Obviously, the lower this value the less strong the maximum is.

ϑ_1, ϑ_2 are bounds of angular interval within the collecting area S_{col} depending on the range from radar and on the radiant position as we shall immediately see.

To visualize the dependence of (5.6) on time via $\cos z_R$ we have generated a few theoretical range distributions computed for various radiant positions. These distributions have been computed for Geminid radiant and are depicted in the Figure 5.5. It is clear that the higher radiant elevation the greater rates of echoes. Moreover, it can be seen that the maximum of the range distribution moves to the more distant ranges with increasing radiant elevation. The Geminid radiant culminates around 2.5h LT.

We have to establish the way how to get the angular limits. The angles can be computed with the assistance of the radar equation valid for echoes of overdense trails (3.33) and relations (3.32), (3.13), (3.35). The conditions for their computation follows from the fact that receiving power P_R has to be greater or equal than limiting power P_{min}.

$$P_T \frac{\lambda^2}{27\pi^2} \sqrt{D_r \rho_r} \sqrt{T_D + c_1\, v(h)^{2a}\, \varrho(h)^{1-2a}}\, \frac{G^2(\vartheta)}{R^3 \sqrt{\varrho(h)}} = P_{\mathrm{min}}, \tag{5.14}$$

The dependence of (5.14) on height h are included in two members, in the air density $\varrho(h)$ and in the term $c_1\, v(h)^{2a}\, \varrho(h)^{1-2a}$. The second member is usually very small in comparison to T_D so that it does not play an important role in computation. In spite of this we take it into account. The boundaries ϑ_1, ϑ_2 are limiting values of the region inside which $P_R \geq P_{\mathrm{min}}$ (in the case of the Ondřejov meteor radar $P_{\mathrm{min}} = 2 \cdot 10^{-13}$ W). The relation between height h, ϑ and R is given by a formula (4.5).

The computation is based on the least - square fit of the theoretical rates computed according to (5.6) to an observed range distributions. The mathematical method is described in the next

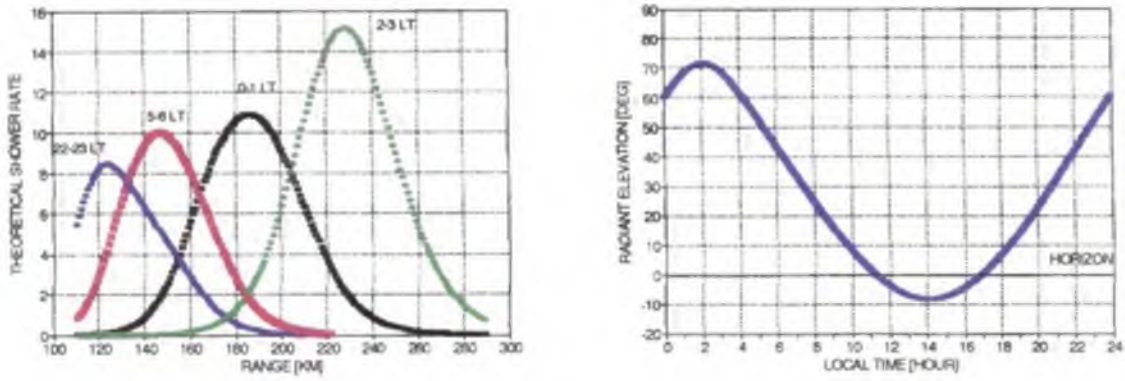

Figure 5.5: The left picture shows theoretical range distribution as a function of time. All four curves are marked with relevant limits of time interval t_1 and t_2 in LT and were computed for mass $m_0 = 10^{-5}$ kg, $v_\infty = 36$ km s^{-1}, $K \cdot \sigma = 0.01$ s^2 km^{-2}, $s = 1.5$, $\mu = 2/3$, $\beta = 0.100$, $D_r = 4.2\,\mathrm{m^2\,s}$ (height of 93 km), $H = 5.409$ km and $\varrho_o = 56.803$ kg m^{-3}. We present on the right picture just for comparison the time course of the elevation of the Geminid radiant.

section.

5.3 Mathematical methods of getting parameters

We get the parameters $\Theta_{m_0}, s, a, b, \mu$ and ϱ_B from the least - square fit of the theoretical rates computed according to our principal formula (5.6) to an observed range distribution:

$$\sum_{i=1}^{n} [N_i^O - N_i^C(\Theta_{m_0}, s, a, b, \mu, \varrho_B)]^2 = \min. \tag{5.15}$$

N_i^O is a number of meteors observed in a particular range interval and $N_i^C(\Theta_{m_0}, s, a(K,\sigma), b(K,\sigma))$ is a computed theoretical number of echoes. The symbol n stands for a total number of range intervals. Since N_i^C depends on all parameters except Θ_{m_0} in a nonlinear way we have to search for them iteratively. In computations like these, methods that take advantage of partial derivatives of N_i^C with respect to wanted parameters prove useful. Let us give some indication of the iterative process. If we have to solve a task to look for unknown parameters p_j from the condition

$$Q(p_j) = \sum_{i=1}^{n} w_i [y_i - f_i(p_j)]^2 = \min, \tag{5.16}$$

with w_i as weights, y_i measured quantities and $f_i(p_j)$ their mathematical model that depend on p_j in a nonlinear way. We approximate the function $Q(p_j)$ by its Taylor expansion around the parameters found in k-iteration:

$$Q(p_j^{k+1}) = Q(p_j^k) + \sum_{\alpha=1}^{m} \frac{\partial Q}{\partial p_\alpha}(p_j^k)\,(p_\alpha^{k+1} - p_\alpha^k) + \frac{1}{2}\sum_{\alpha,\beta=1}^{m} \frac{\partial^2 Q}{\partial p_\alpha \partial p_\beta}(p_j^k)\,(p_\alpha^{k+1} - p_\alpha^k)(p_\beta^{k+1} - p_\beta^k), \tag{5.17}$$

where m is a number of parameters the model depends on. At minimum of (5.17) the condition

$$\frac{\partial Q}{\partial p_i^{k+1}} = 0$$

should be satisfied. After taking derivative of (5.17) we get the equation:

$$\frac{\partial Q}{\partial p_i}(p_j^k) + \sum_{\alpha=1}^{m} \frac{\partial^2 Q}{\partial p_i \partial p_\alpha}(p_j^k)\,(p_\alpha^{k+1} - p_\alpha^k) = 0. \tag{5.18}$$

It is obvious that $\partial^2 Q/\partial p_i \partial p_\alpha$ are elements of the square matrix having dimension m. After multiplication of (5.18) by a matrix inverse to $\partial^2 Q/\partial p_i \partial p_\alpha$ we get the iterative recipe of the Gauss-Newton method (e. g. Meloun and Militký [36]):

$$p_\gamma^{k+1} = p_\gamma^k - \sum_{\delta=1}^{m} \left(\frac{\partial^2 Q}{\partial p_\gamma \partial p_\delta} \right)^{-1} \frac{\partial Q}{\partial p_\delta}, \qquad \gamma = 1, \ldots, m. \tag{5.19}$$

The good initial estimate of searched parameters are necessary in order the Gauss-Newton method could work. This fact causes generally troubles when inverting the matrix $A_{\gamma\delta} \equiv \partial^2 Q/\partial p_\gamma \partial p_\delta$. To overcome these troubles Levenberg and Marquardt [51] proposed to replace the matrix $A_{\gamma\delta}$ by another matrix $A_{\gamma\delta} + \lambda_{LM}\,\mathrm{diag}A_{\gamma\delta}$, where $\mathrm{diag}A_{\gamma\delta}$ is a diagonal matrix with elements coinciding with those of original $A_{\gamma\delta}$ and λ_{LM} is a parameter the authors recommend to chose in a rather artificial way. The sense of this proposition lies in the fact that the addition allows performing the inversion of the new matrix and the parameter λ_{LM} controls the length of an iteration step. The larger this parameter the shorter the step. This idea inspired Pecina [42] in further extension of this method. The length of iteration step should depend on quantitative expression of the fitting process. This is given by the magnitude of Q according to (5.16). The greater Q the shorter should be the iteration length. This leads to proposition to replace $A_{\gamma\delta}$ by $A_{\gamma\delta} + \lambda_P\, Q\,\mathrm{diag}A_{\gamma\delta}$. Inserting this matrix into (5.19) and considering (5.16) a function of p_j represented by the right hand side of (5.19) the one dimensional minimization of Q with respect to λ_P yields the desired expression for λ_P. This is rather ponderous and will be given somewhat later when expressing the derivatives of Q as a function of derivatives of $f(p_j)$ from (5.16).

From (5.16) follows that

$$\frac{\partial Q}{\partial p_j} = -2 \sum_{i=1}^{n} w_i\,[y_i - f_i(p_l)]\,\frac{\partial f_i}{\partial p_j},$$

and

$$\frac{\partial^2 Q}{\partial p_j \partial p_m} = 2 \sum_{i=1}^{n} w_i \frac{\partial f_i}{\partial p_j} \frac{\partial f_i}{\partial p_m} - 2 \sum_{i=1}^{n} w_i\,[y_i - f_i(p_l)]\,\frac{\partial^2 f_i}{\partial p_j \partial p_m} \approx 2 \sum_{i=1}^{n} w_i \frac{\partial f_i}{\partial p_j} \frac{\partial f_i}{\partial p_m}.$$

The second term in the middle part of the previous line is usually neglected because it causes the worse iteration behaviour during computations namely when the set of parameters is far from their values giving minimum of (5.16). In order to simplify further expressions we define the vectors P_j, G_k and M_l together with matrix S_{jk} by putting

$$P_j = \sum_{i=1}^{n} w_i\,[y_i - f_i]\,\frac{\partial f_i}{\partial p_j}, \quad S_{jk} = \sum_{i=1}^{n} w_i \frac{\partial f_i}{\partial p_j} \frac{\partial f_i}{\partial p_k}, \quad G_k = \sum_{\alpha=1}^{m} S_{k\alpha}^{-1} P_\alpha, \quad M_l = \sum_{\beta=1}^{m} S_{l\beta}\,\delta_{l\beta}\,G_\beta, \tag{5.20}$$

where δ_{ij} stands for the Kronecker symbol. When comparing the definition of P_j and S_{jk} with partial derivatives of Q we can see that

$$\frac{\partial Q}{\partial p_\alpha} = -2\,P_\alpha, \quad \frac{\partial^2 Q}{\partial p_\alpha \partial p_\beta} = 2\,S_{\alpha\beta}, \implies \left(\frac{\partial^2 Q}{\partial p_\alpha \partial p_\beta}\right)^{-1} = \frac{1}{2}\,S^{-1}_{\alpha\beta}.$$

Inserting for these derivatives into (5.19) we already get the recipe for computation of p_j:

$$p_j^{k+1} = p_j^k + G_j. \tag{5.21}$$

This is explicit expression for the Gauss-Newton method. The corresponding formula of modified Levenberg-Marquardt method due to Pecina [42] can be written as

$$p_j^{k+1} = p_j^k + \sum_{k=1}^{m} \left(S_{jk} + \frac{\sum_{\alpha=1}^{m} M_\alpha G_\alpha}{\sum_{\beta,\gamma=1}^{m} S^{-1}_{\beta\gamma}\, M_\beta\, M_\gamma} \operatorname{diag} S_{jk} \right)^{-1} P_k. \tag{5.22}$$

We have used this recipe in all further computations. These begin with chosen initial estimate. The subsequent values of parameters are computed using (5.22). The computations are carried out until the subsequent sets of parameters differ by more than the prescribed constant.

To complete this chapter we have to add explicit expressions for N_i^C from (5.15). This is given by (5.6). When substituting there for $m_\infty^{-1/3} \equiv x$ from (5.7) we receive the desired expression

$$N_i^C = \Theta_{m_0} \int_{t_1}^{t_2} dt \int_{S_{col}} (m_0^{1/3}\, x)^{3(s-1)} dS. \tag{5.23}$$

The derivative of N_i^C with respect to Θ_{m_0} is easy to write:

$$\frac{\partial N_i^C}{\partial \Theta_{m_0}} = \int_{t_1}^{t_2} dt \int_{S_{col}} (m_0^{1/3}\, x)^{3(s-1)} dS. \tag{5.24}$$

Also the derivative with respect to s can easily be performed. The results reads

$$\frac{\partial N_i^C}{\partial s} = 3\,\Theta_{m_0} \int_{t_1}^{t_2} dt \int_{S_{col}} (m_0^{1/3}\, x)^{3(s-1)} \ln (m_0^{1/3}\, x)\, dS. \tag{5.25}$$

The derivatives with respect to remaining parameters can be written as

$$\frac{\partial N_i^C}{\partial p} = 3\,(s-1) \int_{t_1}^{t_2} dt \int_{S_{col}} (m_0^{1/3}\, x)^{3(s-1)}\, \frac{1}{x}\, \frac{\partial x}{\partial p}\, dS, \tag{5.26}$$

where p stands for one of the parameters a, b, μ, ϱ_B. The particular derivatives can be evaluated from (5.7) when defining the auxiliary quantity $\xi = b\,[\varrho - \varrho_B - \varrho_B \ln(\varrho/\varrho_B)] \,/\, \cos z_R$:

$$\frac{1}{x}\frac{\partial x}{\partial a} = \frac{1}{2a}\,\frac{1-(1-\mu)\,\xi\,x}{1-(1-3\mu/2)\,\xi\,x} \tag{5.27}$$

$$\frac{1}{x}\frac{\partial x}{\partial b} = -\frac{1}{b}\,\frac{\mu\,\xi\,x}{1-(1-3\mu/2)\,\xi\,x} \tag{5.28}$$

$$\frac{1}{x}\frac{\partial x}{\partial \mu} = \frac{1}{2(1-\mu)^2}\,\frac{\mu(1-\mu)\,\xi\,x + \{1-(1-\mu)\,\xi\,x\}\,\ln\{1-(1-\mu)\,\xi\,x\}}{1-(1-3\mu/2)\,\xi\,x} \tag{5.29}$$

$$\frac{1}{x}\frac{\partial x}{\partial \varrho_B} = \frac{1}{2(\varrho-\varrho_B)}\,\frac{\mu\,\frac{b(\varrho-\varrho_B)\,\ln(\varrho/\varrho_B)}{\cos z_R}\,x - 1 + (1-\mu\,\xi\,x)}{1-(1-3\mu/2)\,\xi\,x}. \tag{5.30}$$

Chapter 6

Results

6.1 Input data

Before moving on to the results we have gained we will devote this section to the input data. In the section (4.4) there are the data overview we have at our disposal from observations. As was mentioned above, the Ondřejov meteor radar has been under operation since 1958 and observations have mainly concentrated on four meteor showers. They are: Quadrantids, Perseids, Leonids and Geminids. From that time the unique four long-term series of data have been managed to accumulate. At this moment the Perseid series includes 31 years, the Leonid one 26 years, the Quadrantid one 46 years and the Geminid one 38 years of observations. We have tried to use the method of range distribution to every year of each series. Besides, we have also applied our method to two daytime showers that belong to the Taurid complex, ζ Perseids and β Taurids. Their observations were performed from 2003 to 2005 during the study of the Taurid complex. This study was supported by grant GA ČR 205/03/1405. The first results related to an application of the simplified method in the case of these two daily showers have already been published in Pecinová and Pecina [48]. We have applied our method also to γ Draconids meteor shower observed during its last increased activity in 1998.

Despite the huge volume of data it was not easy at all to choose the suitable range distribution for computations belonging to the particular year. To make the previous statement clearer we have to mention a few fact about data processing. Because our observations are only single-station ones the methods of observations do not permit to determine the direction in which a meteoroid plunges into the Earth's atmosphere. Hence, we do not know whether it belongs to the observed shower or to the background. To determine the shower activity we have to map the level of background activity. For that reason an activity before and after shower activity has to be observed and after that we are able to construct a shower activity curve. Obviously, the data serve mainly for statistics. When we have looked for a range distribution suitable for computations by our method we have met a lot of obstacles. We can divide them into two categories. First one relates to the

technical problems such as interruptions of observations due to power failure, very high noise level, human errors, problems with equipment and so on. Because of these technical faults it was not possible to determine the shower activity level and consequently to construct the relevant range distribution. Even in some years observations were not performed at all due to reparations of the radar, its modernization or the other technical problems. The second category includes problems with echo rates. It is clear that we need rather stronger activity in order the range distribution could be well-defined and the range distribution method could be applied. But, there were very low or zero shower activity in some years, e.g. Quadrantids 1963, Perseids 1972. Thus, the majority of range distributions we have used were obtained during the maximum shower activity and during the larger time intervals, e.g. 2 hours. Furthermore, it was mentioned above that the Ondřejov meteor radar is able to observe unambiguously from 100 km to 600 km with the blocking gap between 300 and 380 km. Rich experience with observations and proceeding data indicates that absolute majority of echoes occur within the interval $< 100, 300 >$ km. The shower rates in greater distances ($< 380, 600 >$ km) from the radar vary from one shower to another and does not exceed approximately 10%. This fact relates to the radar equation for overdense echoes (3.33) because the strength of signal decreases with the third power of range from the radar. For that reason we have restricted themselves to range limits from 100 to 300 km. Moreover, the position of maximum of the range distribution changes with time due to time dependence of the shower radiant position as we have shown in Fig. 5.5. In view of this fact at some position of the shower radiant the maximum of the range distribution overstepped the range limits $< 100, 300 >$ km and was so bad determined that again we were not able to get anything. It was the case of faster meteor showers such as Leonids. But on the other hand, we have managed to construct two or more range distributions in one year under the favorite conditions.

To sum up, searching for the well-defined range distributions of overdense echoes was sometimes like looking for a needle in a haystack. We have proceeded as follows. Firstly, we have usually divided shower rates into 20-km-wide or 25-km-wide intervals from 100 km to 300 km and then we interpolated them to get rates into 5-km-wide intervals with the assistance of the interpolating procedure SINOD (single interpolation in one dimension) published by Steffen [54]. The distributions gained in this way have served as an input to our computations.

The process of computation is the following. Primarily, we have defined normalized rates as observed rates within particular range group divided by the rate at the maximum range. Then these rates do not depend on Θ_{m_0} as it can easily be recognized from (5.6). They are functions of s, $K.\sigma$, μ, β and ρ_B. Numerical computations have revealed that the normalized rates depend mainly on s and $K \cdot \sigma$. They depend in somewhat weaker way on μ and β. Therefore, the process of computation was divided into several substeps. During the first one only s and $K \cdot \sigma$ were computed while the remaining ones were kept constant. The starting value of the mass distribution index s we take to be around the value computed from the $\log N$ vs. $\log T_D$ fit. The starting value of $K \cdot \sigma$ was 0.01 corresponding to $K = 1$ and $\sigma = 0.01$. The starting value of μ was set to 2/3

and the corresponding value of β was set to the value of this quantity following from the formula of Kashcheev et al. [26]. After getting the s and $K \cdot \sigma$ values the next parameter from the above mentioned set is added and so on. Eventually all these parameters are evaluated. In the second (and last) stage the Θ_{m_0} is calculated from (5.23) where the original (not normalized) rates are used. The relevant mathematical method for getting parameters is described in section (5.3).

Constants and starting values of computation common to all of five showers are the following:

- the average mass of meteoroid atoms: $\mu_a = 40 \times \mu_H$ where $\mu_H = 0.1673534056 \times 10^{-26}$ kg is the mass of the hydrogen atom (e. g. Ceplecha et al. [15]),
- the constants ρ_o and H result from the least-square fit of dependence (2.1) to the real atmosphere represented by CIRA [17],
- $D_r = 4.2\,\mathrm{m^2\,s^{-1}}$ at the height of 93 km (e. g. Belkovich [6]),
- the mass distribution index s we take to be around the value computed from the $\log N$ vs. $\log T_D$ fit (4.23),
- the possible value of duration of underdense radar echo was examined in the subsection (3.3.1). It is clear from this calculation that at hights higher than 93 km the value 0.17 s cannot be reached. At the lower heights the value of ambipolar diffusion coefficient can drop to about one half of the value adopted in the subsection (3.3.1) so that the duration of underdense echo can be as high as 0.34 s. To be on the safe side we have adopted the lowest value of the overdense echo duration to be 0.4 s.
- the limiting mass $m_o = 10^{-5}$ kg was chosen in the following way. The highest electron density occurs at the maximum of the ionization curve. The relation between the maximum electron line density and the corresponding mass is given by (2.53). The lowest possible mass results for $\cos z_R = 1$. Thus, $m_\infty = 9\mu_a H \alpha_{max}/4\beta$. The higher the mass of a meteoroid the higher the electron line density and vice versa. Moreover, the reflection at other point than at that of maximum ionization requires higher value of meteoroid producing mass to yield the same signal strength as at the maximum ionization. The electron line density of overdense trail relates to the duration of echo, T_D via (3.32) which yields for the limiting mass the formula $m_o = 9\pi^2\mu_a H D T_D/\beta\lambda^2 r_e$ where we have neglected the term $r_o^2/4D$. The lowest possible mass results for the highest ionization probability which corresponds to Leonids having highest shower velocity known so far. While formula of Kashcheev et al. [26] yields $\beta = 0.3815$ the corresponding formula of Verniani and Hawkins [59] provides us with $\beta = 0.2541$. It is clear that we have to use the former value. Hence, $m_o = 0.8 \times 10^{-5}$kg at the height of 93 km. This value holds true at the point of maximum ionization. At other points which do not coincide with the maximum one the mass must be even higher. Since the reflection

just at the point of maximum ionization is rather exceptional we can relate the limiting mass to $m_o \simeq 1 \times 10^{-5}$ kg without introducing substantial error into our considerations. If we want to estimate the corresponding magnitude we have to find the maximum light intensity of the light curve. The atmospheric density at the light maximum is given by (2.51). When introducing (2.37) into (2.41) for $\dot{m}$ we obtain the light curve with Levin's μ. On substituting there (2.51) we get the maximum intensity I_{max} in the form

$$I_{max} = \frac{\tau(v_\infty)\, v_\infty^3 \cos z_R}{2H}\, m_\infty\, \mu^{\frac{\mu}{1-\mu}}.$$

The absolute magnitude corresponds to $\cos z_R = 1$. Eventually we use (4.12) and the desired relation is:

$$M = -2.5 \log \left[\frac{\tau(v_\infty)\, v_\infty^3}{2H}\, m_\infty\, \mu^{\frac{\mu}{1-\mu}} \right]. \tag{6.1}$$

Obviously, the absolute magnitude value depends on luminous efficiency τ. The interested reader can get its value e.g. in Ceplecha [13] and compute the absolute magnitude for various masses m_∞ and velocities v_∞.

- the ranges of observed meteors are reduced with the precision of 2 km.

- The physical theory employed so far considered $\mu = 2/3$ as standard. As we have mentioned in the subsection entitled Use of Levin's proposition the case of variable μ different from the above assumption can partially allow for effects such as fragmentation and can substantially improve the ability of our model to fit observed range distribution. This is clearly visible from Figure 6.1 where are shown the observed distribution together with result of the 1st step ($\mu = 2/3$) and the 2nd one i. e. variable μ. A look at this picture justifies our decision to include variable μ into our model.

- We usually observe an activity of a particular shower during a few days (symmetrically around its expected maximum) so that we do not need to take into account the daily motion of its radiant due to wide antenna beam. On the other hand during observations of a shower background the particular shower radiant is corrected for its daily motion. It is necessary to say that we neglect the daily motion of radiants in our computations. The radiant positions listed in further text are the same we used in observations as well as in computations.

6.2 Obtained results

To summarize, we have tried to compute five unknown parameters: $\Theta_{m_0}, s, K\cdot\sigma, \mu, and \beta$. The computation is based on the least-squares fit of the theoretical rates computed according to (5.6) to an observed range distributions. The mathematical method of computations is described in the section (5.3). Unfortunately it is impossible in our model to split K from σ and we can compute only their product. However, the multiplication restricts the extend of their possible values. Since

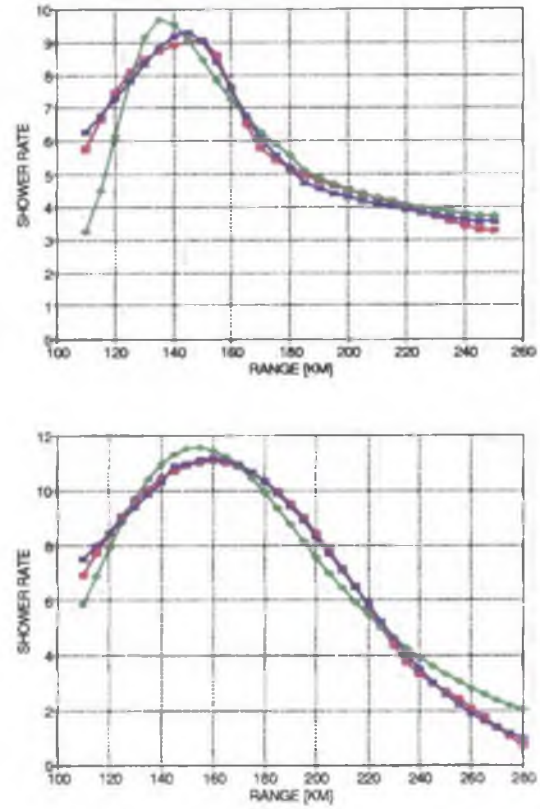

Figure 6.1: The example showing the difference between the observed range distribution (red) and the ones following from the application of the method of this work. The green distribution has resulted from the computation under the assumption $\mu = 2/3$, while the blue one has resulted from computation when μ has been variable. The left picture presents case of Leonids 1998, November 17 with $\mu = 1.80$ while the right picture presents range distribution of Quadrantids 1987, January 4 with $\mu = 1.82$. See also the tables relevant for particular shower in the further course of the work.

the shape density parameter depends on density of a meteoroid we try to estimate the value of σ for various kind of meteoroid substance provided a spherical shape of a meteoroid body in the process. The results corresponding to each meteor shower are placed into relevant next subsections. We have also calculated the weighted means of obtained parameters but we need to always keep in mind that Θ_{m_0} and s are quantities dependent on solar longitude and on year of an observation. Their means can only serve for getting the whole picture namely in the case of Leonids.

6.2.1 Quadrantids

The Quadrantid meteor shower, being active in the beginning of January, belongs together with Geminids and Perseids to most prominent showers. This stream has very sharp and narrow maximum between January 3 - 4 with the maximum activity appearing around $L_\odot \simeq 283°.2$ where the relating equinox is J2000. The period of activity as deduced from visual observations is 4 - 6 hours wide. Our long-term radar observations have revealed that the period of activity of radar meteors can be wide several days, usually from January 1 to 6. We cannot observe this shower between 6 - 10 hours of local time because of the proximity of radiant to local zenith and, consequently, very low elevations of the reflecting points for which our antenna is insensitive. The Quadrantids move in a short-period orbit with a period of revolution of about 5 years. The parent body was not known for quite long period. Hasegawa [19] has suggested the comet C/1491 to be likely the Quadrantid parent. McIntosh [32] has studied the orbit of 96P/Machholtz and has found an orbital similarity between the comet and Quadrantids. At the end of nineties Williams and Collander-Brown [63] has discussed a possible connection of the asteroid 5496 (1973 NA) with the stream and recently Jenniskens [20] has proposed the asteroid 2003 EH1 to be the parental body. He has also concluded that the object is an intermittently active comet. Quite recently Porubčan and Kornoš [50] have studied the orbital history of the Quadrantid meteor stream on the basis of the updated version of the IAU MDC photographic meteor catalogue. They have found that two of filaments of the stream have followed the orbital evolution of 2003 EH1 asteroid. The remaining filaments have probably their origin in other bodies mentioned above. As a consequence, it is probable that the activity of Quadrantid shower is due to more bodies contributing to the stream having thus filamentary structure with particular filaments causing activity in different years. We have accepted $\alpha = 230°$, $\delta = +49°$ and $v_\infty = 43$ km s^{-1} for this shower.

The Quadrantid meteor shower has been studied by the radar for many years. Our series of this shower consists of 36 years at present. We have managed to perform computations of 45 range distributions across 32 years. The Table 6.1 collect our results on Quadrantids. Since we assume the meteoroids contributing to the shower activity in various years are the same with respect to their physical properties, our results collected in the Table 6.1 can further be used to get quantities representing the shower as a whole. We have used the weighted means of all cases included in the Table 6.1 with the weights being inverse of the standard deviations from it. We have got the following results: $s = 1.77 \pm 0.02$, $K \cdot \sigma = 0.042 \pm 0.001$, $\mu = 1.55 \pm 0.02$ and $\beta = 0.107 \pm 0.007$.

Now our results can be compared with results of other authors. The IMO calender for 2005 brings the population index $\zeta = 2.10$ for Quadrantids. Using the appropriate relation between ζ and s mentioned above we get the recomputed value $s = 1.81$ which is quite close to our resulting value. The calendar does not bring any other information which could be compared with our other quantities. Our result is well comparable with the corresponding one published by Pecina [39]. Šimek [55] studied dynamics and evolution of the structure of five meteors streams including Quadrantids. He used radar data collected at Ondřejov. His investigation lead to $s = 1.61 \pm 0.03$ which is lower than our result. This is due to the fact that he employed the Kaiser's formula for the calculation of s which does not include the correction for different collecting areas. The value of μ greater than 2/3 reflects other than isotropic ablation of Quadrantid meteoroids, probably due to fragmentation. Similar result has been reached for Leonids as well as Perseids as we will see in the further course of the work. The resulting β is lower than the value following from extrapolation of Jones [23] (he has claimed his formula being valid only for velocities up to 35 km s^{-1}), and greater than values given both by Kashcheev et al. [26] and Verniani and Hawkins [59].

As was mentioned above, we are not able to split mutually K and σ in our model. To our best knowledge there is not any value of either K or σ still published. However, the multiplication restricts the extent of their possible values. Since the shape-density parameter depends on density of a meteoroid (see (2.7)) we have tried to estimate the value of σ for various kind of meteor substance. We assumed a spherical shape of a meteoroid particle. The result expressing the range of the ablation parameter from most fragile cometary material to material of Geminid type is in the Table 6.4.

6.2.2 Perseids

The Perseid shower occurs quite regularly every year in August with its maximum activity around $L_\odot \simeq 140°$. Its display comprises several weeks from July 17 up to August 24. This shower belongs to well known showers of clearly cometary origin with 109P/Swift-Tuttle as parent body. For this shower we have accepted $\alpha = 44°$, $\delta = +58°$ and $v_\infty = 61$ km s^{-1}. The Perseid series consists of 31 years at present but we could work with 13 of them only. The results are in Table 6.5 that lists 18 range distributions.

Also as in the case of Quadrantids we made use of the data collected in the Table 6.5 to get the weighted means of quantities which could represent the shower as a whole. These means read: $s = 1.45 \pm 0.01$, $K \cdot \sigma = 0.044 \pm 0.003$, $\mu = 1.06 \pm 0.03$ and $\beta = 0.205 \pm 0.001$. The IMO population index is 2.60 which results in the mass distribution index value $s = 2.04$. This is substantially higher than our result. We cannot explain this discrepancy at present. The Šimek [55] result reads $s = 1.61 \pm 0.02$. There is clearly visible increase of activity of the shower expressed in increase of the flux in the period 1988 - 1993 with the peak at its end which was attributed to the activity of a new Perseid filament recognized by Roggemans [52]. Its activity was also studied by Šimek and Pecina [56] using Ondřejov radar data. Our finding conforms the behaviour reported

by these authors. Even though μ is much lower than for Quadrantids it is still higher than usually assumed value 2/3. This again implies probable fragmentation process during ablation of Perseid meteoroids. The resulting value of β lies between the corresponding value following from Verniani and Hawkins formula and the one following from Kashcheev et al. [26] expression.

Also proceeding as in case of Quadrantids provides us with the Table 6.7.

6.2.3 Leonids

The Leonid shower occurs in November every year with maximum activity around $L_\odot \simeq 234°$. However, this regular display is rather weak. It comprises several days from November 14 up to November 21. Also this shower belongs to well known showers of clearly cometary origin with 55P/Tempel-Tuttle as parent body. In addition to the weak activity, strong storms exist that repeat every 33 - 34 years. The occurrence of these storms is due to dense core of meteoric material ejected from the comet during its historical approaches to the Sun. Their concentration seems to be confined behind the comet. It implies that these storms can occur only after the perihelion passage of the comet and not prior to it. This is also actually observed. Last storms in the last century occurred in 1965 - 1966 and 1998 - 2002. Their observations revealed an evident filamentary structure of the stream. For this shower we have accepted $\alpha = 153°$, $\delta = +22°$ and $v_\infty = 71$ km s^{-1}.

The Leonid series consists of 26 years at present, Table 6.8 lists 11 cases from 7 years including the data from the comet return in 1965 and 1966. However, we could have not investigate the data from the very activity maximum in 1966 due to a huge amount of meteors recorded at that time causing that the film was overexposed and, consequently, the individual meteors could not have been mutually distinguished. So we had to use data from periods when the record was readable. Investigation of Leonids activity within these years using radar was described by Šimek and Pecina [57]. They reported higher activity in 1966 and lower in 1965. We can compare our Θ_{m_0} values with corresponding ones at mutually similar solar longitudes. In 1965 our $\Theta_{m_0} = (4.67 \pm 0.32) \cdot 10^{-12}$ m^{-2}s^{-1} compares very well with $\Theta_{m_0} \simeq 4.25 \cdot 10^{-12}$ m^{-2}s^{-1} of Šimek and Pecina [57]. Also our data from 1966, i. e. $\Theta_{m_0} = (1.19 \pm 0.09) \cdot 10^{-12}$ m^{-2}s^{-1} and $\Theta_{m_0} = (2.05 \pm 0.13) \cdot 10^{-12}$ m^{-2}s^{-1} compare well with $\Theta_{m_0} \simeq 1.0 \cdot 10^{-12}$ m^{-2}s^{-1} and $\Theta_{m_0} \simeq 2.0 \cdot 10^{-12}$ m^{-2}s^{-1}. The above authors presented also the mass distribution index s as a function of solar longitude. Comparing our resulting s with the ones of Šimek and Pecina [57] brings the fact that ours are lower than those of these authors in both years. While our data have provided us with $s = 1.21 \pm 0.05$(1965) and $s = 1.24 \pm 0.09$, $s = 1.12 \pm 0.01$(1966), those from above mentioned paper are: $s = 1.46$ (1965) and $s = 1.56$, $s = 1.78$. We would like to make a note that while in 1965 our values relate to observed maximum, in 1966 both our values were gained prior to observed maximum ($L_\odot = 235°.182$) and after it.

We have also made computations with the data from the last return in 1998 - 2002. On the whole the activity within these years was much lower than the activity in sixties. The results on

activity and mass distribution in 1998 and 1999 were published by Šimek and Pecina [58]. Their flux in 1998 at the same solar longitude $L_\odot = 234°.448$ was $\Theta_{m_0} \simeq 1.0 \cdot 10^{-12}$ m^{-2} s^{-1} while our one $\Theta_{m_0} = (1.10 \pm 0.03) \cdot 10^{-12}$ m^{-2} s^{-1}. At the longitude $L_\odot = 234°.531$ their value reached $\Theta_{m_0} \simeq 1.5 \cdot 10^{-12}$ m^{-2} s^{-1} while our one $\Theta_{m_0} = (1.67 \pm 0.18) \cdot 10^{-12}$ m^{-2} s^{-1} and at $L_\odot = 234°.699$ $\Theta_{m_0} \simeq 1.5 \cdot 10^{-12}$ m^{-2} s^{-1} and $\Theta_{m_0} = (2.05 \pm 0.15) \cdot 10^{-12}$ m^{-2} s^{-1}. It can easily be seen that our fluxes are in a good agreement with those values of Šimek and Pecina [58]. Also the resultant values of the mass distribution indices can be compared. Our values listed in Table 6.8 are for 1998 and 1999: $s = 1.44 \pm 0.04$, $s = 1.20 \pm 0.06$, $s = 1.26 \pm 0.04$, $s = 1.48 \pm 0.09$ while the respective values of Šimek and Pecina [58] are: $s = 1.22 \pm 0.01$, $s = 1.16 \pm 0.01$, $s = 1.27 \pm 0.01$ and $s = 1.44 \pm 0.02$. Again, our values are somewhat higher indicating use of Kaiser's formula for getting mass distribution indices by the above mentioned authors. We need to remark the fact that our computed values from 1998 related to $L_\odot = 234°.531$ and $L_\odot = 234°.699$ were gained at the maximum activity period. Our value from 1999 were gained from the shower activity behind its maximum ($L_\odot = 235°.285$).

The relevant results of observations within the period 2000 - 2002 concerning activity and mass distribution have been published by Pecina and Pecinová [45]. We can compare the mass distribution indices. Our one describing the activity on November 18, 2000 has value $s = 1.31 \pm 0.08$ while the corresponding index of Pecina and Pecinová is $s = 1.21 \pm 0.05$, the first one in Table 6.8 of 2001 is $s = 1.30 \pm 0.05$ and compares with $s = 1.19 \pm 0.06$, the 2nd one $s = 1.36 \pm 0.13$ with $s = 1.26 \pm 0.07$ and the last one $s = 1.28 \pm 0.05$ compares with $s = 1.26 \pm 0.07$. It is clearly visible that our values from Table 6.8 are generally higher than indices Pecina and Pecinová [45] arrived at. This fact can again be ascribed to the difference between Kaiser's method which does not consider various collecting areas for echoes having different durations and method. We would like to mention again that our value from 2000 corresponds to one of smaller peak of shower activity. In 2001 the first value covers the period just after the primary maximum, the second one can be connected to the secondary peak. In 2002 the relevant range distribution comprises a bit broader period than only the main maximum ($L_\odot = 236°.610$).

As in the previous cases we made use of the data from Table 6.8 to calculate the weighted means of shower representing quantities. We have got: $s = 1.26 \pm 0.02$, $K \cdot \sigma = 0.082 \pm 0.003$, $\mu = 1.55 \pm 0.29$ and $\beta = 0.343 \pm 0.002$. The IMO value of the population index is 2.5 which leads to $s = 1.99$. However, it is not clear from the calendar whether this value relates to the storm observed after the last comet return or to the activity observed outside the storms. Comparing our numbers with Šimek [55] result $s = 1.36 \pm 0.03$ we can see that our one is lower. We agree with him that the mass distribution index of Leonids is lower than of other cometary showers, i.e. Quadrantids and Perseids. The possible span of values of the ablation parameter, σ, for Leonid meteoroids, is presented in Table 6.9. The interval of σ lies at higher values than at the other showers in question implying higher ablation ability of Leonid meteoroids. Spurný at al. [53] arrived at the value $\sigma = 0.1$ s^2 km^{-2} on the basis of their observations in 1998 and 1999. Our

value is close to that mentioned above. Also the high value of μ witnesses of the fragmentation of Leonid particles. The resulting ionization probability lies again between the values yielded by Verniani and Hawkins [59] and Kashcheev et al. [26] values.

6.2.4 Geminids

The Geminid shower presents an example of annual shower display with stable activity lasting from December 7 to December 17. Its radar activity maximum occurs between $261°.25 \leq L_{\odot} \leq 262°.15$ depending on the duration category (Pecina and Šimek [46]). No any parent body was known for Geminids until the discovery of 3200 Phaeton which is generally accepted at present to be associated with the stream (Whipple [62]). We have used the following radiant position and velocity for Geminid meteors: $\alpha = 112°$, $\delta = +32°$ and $v_{\infty} = 36$ km s^{-1}.

The Geminid series consists of 38 years at present. In the Table 6.10 there are included 50 cases from 34 years. Our results were used to get the following shower representing quantities: $s = 1.55 \pm 0.01$, $K \cdot \sigma = 0.021 \pm 0.001$, $\mu = 0.66 \pm 0.01$ and $\beta = 0.081 \pm 0.001$. As far as the mass distribution index is concerned it is lower than the one following from the IMO population index 2.60 corresponding to $s = 2.04$. The cause of the discrepancy is not known at present. Pecina and Šimek [46] analyzed the behaviour of the stream during the period 1958 - 1997. Their weighted mean value $s = 1.48 \pm 0.02$ is lower than our one resulting from the range distribution analysis. Also Šimek's [55] value $s = 1.48 \pm 0.03$ is lower than our one. This is due to the usage of Kaiser's formula for computing mass distribution index by preceding authors. The product $K \cdot \sigma$ we have arrived at cannot be used for calculation of the possible interval of σ since Geminids were considered as one possible material type. As far as bulk density of Geminid meteoroids is concerned the generally adopted value was not found. For example, Babadzhanov [2] reached $\delta = 2.9 \pm 0.6$ g cm^{-3} while Bellot Rubio et al. [7] published $\delta = 1.94 \pm 0.7$g cm^{-3}. Ceplecha and McCrosky [14] on the basis of observations of Geminid fireballs arrived at higher value that lies between 3 and 4 g cm^{-3}. Adopting $\delta = 2.5$ g cm^{-3} for them we obtain $\sigma = 0.03\,s^2\,\mathrm{km}^{-2}$. This value is smaller than those of the other (cometary) showers indicating the fact that Geminid meteoroid properties differ from showers with a comet origin. We have received substantially lower value of μ in comparison with corresponding values valid for other showers. This fact can be due to lower fragmentation rate involved in ablation process of the Geminid meteoroids we observed. Our ionization probability is somewhat lower than that of Jones ending at velocity of 35 km s^{-1}. On the other hand, it is greater than the Verniani and Hawkins [59] as well as Kashcheev et al. [26] values. We would like to compare also our results on Θ_{m_0} and s correspond to those of Pecina and Šimek [46] but it is practically impossible thanks to the different methods that were used. Values of above mentioned authors were computed as a function of solar longitude within small intervals with data from all considered years falling into that interval, i. e. some process of smoothing data was applied. Also the sporadic background was determined as some mean background from all years involved into analysis. As a consequence their shower rates can differ from ours substantially.

Our present results are based on data from the particular year only and time interval of a few hours when the contemporary background was determined. Let us make a note only that our values of flux indicate strong variability one year to another from 1.17 $\times 10^{-12}\,\mathrm{m}^{-2}\,\mathrm{s}^{-1}$ (1994) to 7.11 $\times 10^{-12}\,\mathrm{m}^{-2}\,\mathrm{s}^{-1}$ (1960) (which is however rather exceptional value). The weighted mean is $\Theta_{m_0} = (3.49 \pm 0.11) \times 10^{-12}\,\mathrm{m}^{-2}\,\mathrm{s}^{-1}$. After comparison we can conclude that our fluxes are approximately 1.5 times greater than those of preceding authors. We have not found any marked trend in our flux data results.

6.2.5 Taurids

We have also investigated the daytime showers ζ Perseids and β Taurids belonging to the well-known Taurid complex stream. We have observed these showers in 2003 as well as in 2004 and 2005. Nevertheless, the data from 2004 did show any remarkable activity both in case of ζ Perseid and β Taurid showers. For this purpose we could not calculate any range distribution for that year. As far as the data from 2005 are concerned they have not been proceeded up to the present time. So, we need to focus on 2003 year only. We have used the following radiant position and velocity for β Taurid meteors: $\alpha = 87°$, $\delta = +19°$ and $v_\infty = 32$ km s^{-1}. The values of the radiant position and velocity for ζ Perseid meteors are: $\alpha = 62°$, $\delta = +23°$ and $v_\infty = 29$ km s^{-1}.

The shower rates we registered in 2003 were rather low as one can see from the work by Pecina et al. [47]. As a consequence, the range distributions were not very well defined so that we had to restrict our computations to only one day in both cases, on which the quality of the data was the highest. Moreover, all radar echoes of both daytime showers were recorded between 100 km and 300 km and the duration of overdense echoes did not exceed 10 s.

As far as ζ Perseids are concerned we made use of the data registered on June 8 between 3 and 7 UT. We have published preliminary results of the range distribution method yet in Pecinová and Pecina [48] computed under the assumption of $\mu = 2/3$. They are: $\Theta_{m_0} = (15.10 \pm 0.98) \cdot 10^{-12}$ m^{-2} s^{-1}, $s = 2.08 \pm 0.22$, $K \cdot \sigma = (0.92 \pm 0.24) \cdot 10^{-2}$ s^2 $\mathrm{kg}^{-2/3}$ and $\beta = 0.059 \pm 0.008$. The extension of the approach to the construction of the range distribution embodied by the method of this work leads to the result listed in the Table 6.13. After comparison the quantities the simplified ($\mu = 2/3$) method with the one presented in this work we can see that the former method leads to rather precisious values. It is understandable because application of our method with changeable μ corresponds to the observations in a better way. Under the terms of their errors the quantities in question are in accordance with the exception of ionization probability β. Furthermore, we can see that the mass distribution index following from the $\log_{10} N$ vs. $\log_{10} T_D$ fit: $s = 2.45 \pm 0.10$ has almost the same value as the one in Table 6.13.

The possible values of σ, based on data from Table 6.13, computed for various types of meteoroid material are presented in Table 6.14.

In the case of β Taurids we focused on the data recorded on June 25 between 4 and 7 UT. Also in this case we have published preliminary results of the range distribution method yet in Pecinová

and Pecina [48] computed under the assumption of $\mu = 2/3$. They are: $\Theta_{m_0} = (3.53 \pm 0.35) \cdot 10^{-12}$ $m^{-2}\ s^{-1}$, $s = 2.53 \pm 0.55$, $K \cdot \sigma = (0.73 \pm 0.11) \cdot 10^{-2}\ s^2\ kg^{-2/3}$ and $\beta = 0.080 \pm 0.011$. The more sophisticated range distribution method presented in this work leads to the result presented in the Table 6.13. Comparison between the quantities gained by the simplified ($\mu = 2/3$) and present method supports the contention mentioned above in the case of ζ Perseids. Moreover, the mass distribution index s in both cases has almost the same value that is substantially higher than the one following from the $\log_{10} N$ vs. $\log_{10} T_D$ fit: $s = 1.15 \pm 0.36$.

The possible values of σ computed for various types of meteoroid material are presented in Table 6.16.

To conclude, it can easily be seen from Tables 6.16 and 6.14 that for both daytime showers the ranges of σ do not differ a lot.

6.2.6 γ Draconids

The γ Draconid (or Giacobinid) shower activity was at Ondřejov in 1998, too. Since this shower is known to be formed by meteoroids having the lowest bulk density from all streams ever observed, which is lower than 1 g cm^{-3} (e. g. Ceplecha et al. [15], it is interesting also for the application of our range distribution method. We have used the following radiant position and velocity for γ Draconid meteors: $\alpha = 262°$, $\delta = +54°$ and $v_\infty = 23$ km s^{-1}. Its activity in 1998 was confined on approximately 2 hours interval at 12 UT on October 8. We were able to construct the corresponding range distribution and apply our method on it. The results are listed in Table 6.17. We can compare our values of Θ_{m_0} and s with the ones published by Watanabe et al. [61]. Their quantities are based on HD TV observation. They arrived at the population index $\zeta = 2.1 \pm 0.7$ which corresponds with $s = 1.81 \pm 0.36$. This value is in good agreement with our value 1.88 ± 0.17. They published $\Theta_{m_0} = 16 \times 10^{-12}\, m^{-2} s^{-1}$ while our value is $2.3 \times 10^{-12}\, m^{-2} s^{-1}$. However, they related their value to 7th magnitude whereas our magnitude computed by using (6.1) and μ from Table 6.17 is +4.5. Conversion between these two values is not easy to perform due to lack of information but we think that they roughly correspond.

With the value of the product $K \cdot \sigma$ from Table 6.17 we obtain Table 6.18 including the possible values of σ for the shower meteoroids.

We can see that the ablation parameter reaches the highest value in comparison with the others we have computed. So, we can conclude that results published in Ceplecha et al. [15] are confirmed also by application of our method.

KNIHOVNA MAT.-FYZ. FAKULTY
Knihovna Fr. Zbvišky (fyz. odd.)
Ke Karlovu 3
121 16 Praha 2

Table 6.1: Results of application of equation (5.6) to the Quadrantid shower meteors. The first column contains the year when the meteors were observed, the second the day of observation, the third the beginning hour of observation, bh, while the next the corresponding end hour, eh. The column headed by ri contains the range interval inside which the meteors were collected, in kilometers. The quantity $L_\odot$ is solar longitude of the centre of observation interval related to the equinox of J2000. The flux Θ_{m_0} is expressed in units of $10^{-12}\,\mathrm{m}^{-2}\,\mathrm{s}^{-1}$ for $m_0 = 10^{-5}$ kg. The remaining quantities were defined in previous sections.

Year	Day	bh	eh	ri	$L_\odot$	Θ_{m_0}	s	$K \cdot \sigma$	μ	β
1961	3	0	2	113 - 288	282°931	3.75 ± 0.48	1.80 ± 0.09	0.024 ± 0.004	1.54 ± 0.10	0.100 ± 0.032
1962	3	10	12	113 - 288	283°093	2.44 ± 0.20	1.74 ±0.09	0.047 ± 0.009	1.43 ± 0.13	0.102 ± 0.043
1964	3	2	6	113 - 288	282°270	5.37 ± 0.12	1.86 ±0.08	0.061 ± 0.007	1.71 ± 0.13	0.098 ± 0.033
1965	3	10	12	113 - 288	289°331	7.36 ± 0.29	1.84 ±0.09	0.036 ± 0.004	1.38 ± 0.12	0.105 ± 0.042
1966	3	8	10	113 - 238	282°983	3.67 ± 0.38	1.91 ±0.09	0.058 ± 0.007	1.40 ± 0.20	0.111 ± 0.041
1967	4	10	12	113 - 288	283°821	4.10 ± 0.11	1.88 ±0.09	0.047 ± 0.008	1.69 ± 0.20	0.110 ± 0.039
1968	4	2	4	113 - 288	283°227	6.54 ± 0.10	1.82 ±0.09	0.035 ± 0.007	1.70 ± 0.16	0.100 ± 0.042
1969	3	4	5	113 - 288	283°007	4.09 ± 0.13	1.67 ±0.11	0.018 ± 0.006	1.40 ± 0.14	0.110 ± 0.040
1975	4	4	6	113 - 288	283°511	2.75 ± 0.09	1.74 ±0.12	0.049 ± 0.004	1.61 ± 0.22	0.100 ± 0.039
1976	4	0	4	113 - 288	283°130	1.92 ± 0.08	1.80 ±0.10	0.055 ± 0.007	1.33 ± 0.17	0.111 ± 0.043
1977	3	2	6	113 - 213	282°953	3.89 ± 0.25	1.72 ±0.14	0.028 ± 0.005	1.27 ± 0.12	0.120 ± 0.052
1978	3	2	4	113 - 288	282°647	4.06 ± 0.26	1.76 ±0.18	0.042 ± 0.009	1.62 ± 0.03	0.098 ± 0.039
1980	4	1	5	113 - 288	283°140	3.61 ± 0.13	1.61 ±0.09	0.055 ± 0.009	1.42 ± 0.18	0.108 ± 0.040
1982	3	1	5	113 - 288	282°626	3.53 ± 0.19	1.87 ±0.08	0.061 ± 0.008	1.69 ± 0.29	0.111 ± 0.041
1982	4	1	5	113 - 288	283°646	3.76 ± 0.22	1.76 ±0.09	0.038 ± 0.006	1.48 ± 0.16	0.111 ± 0.039
1983	4	3	5	113 - 238	283°422	4.63 ± 0.16	1.72 ±0.09	0.041 ± 0.003	1.76 ± 0.13	0.100 ± 0.040

Table 6.2: The first continuation of Table 6.1.

Year	Day	bh	eh	ri	$L_{\odot}$	Θ_{m_0}	s	$K \cdot \sigma$	μ	β
1985	3	9	15	113 - 263	283°240	6.90 ± 0.30	1.86 ±0.13	0.034 ± 0.006	1.32 ± 0.12	0.107 ± 0.040
1986	3	13	15	113 - 288	283°060	2.90 ± 0.17	1.81 ±0.10	0.047 ± 0.009	1.38 ± 0.21	0.102 ± 0.020
1987	3	12	14	113 - 288	282°757	1.73 ± 0.10	1.78 ± 0.10	0.030 ± 0.002	1.75 ± 0.13	0.110 ± 0.040
1987	4	4	6	113 - 288	283°437	4.11 ± 0.25	1.69 ±0.09	0.055 ± 0.006	1.82 ± 0.17	0.105 ± 0.036
1988	4	3	5	113 - 288	283°132	4.21 ± 0.16	1.80 ±0.09	0.031 ± 0.004	1.37 ± 0.20	0.110 ± 0.035
1991	4	3	5	113 - 238	283°366	5.82 ± 0.16	1.80 ±0.09	0.039 ± 0.006	1.56 ± 0.14	0.107 ± 0.036
1992	4	3	5	113 - 288	283°110	6.98 ± 0.31	1.81 ±0.08	0.039 ± 0.009	1.40 ± 0.15	0.104 ± 0.042
1992	4	1	5	113 - 288	283°067	6.62 ± 0.03	1.71 ±0.08	0.051 ± 0.009	1.50 ± 0.13	0.110 ± 0.040
1994	3	1	5	113 - 238	282°545	5.08 ± 0.17	1.75 ±0.11	0.05 ± 0.01	1.377 ± 0.145	0.099 ± 0.041
1994	4	1	5	113 - 288	283°564	5.66 ± 0.13	1.79 ±0.10	0.040 ± 0.006	1.57 ± 0.18	0.102 ± 0.040
1995	4	4	6	113 - 288	283°390	5.39 ± 0.25	1.66 ±0.09	0.035 ± 0.006	1.47 ± 0.11	0.131 ± 0.045
1995	4	10	12	163 - 288	283°645	5.28 ± 0.19	1.70 ±0.09	0.043 ± 0.007	1.73 ± 0.10	0.111 ± 0.042
1996	4	3	5	113 - 288	283°083	3.41 ± 0.12	1.77 ±0.09	0.040 ± 0.005	1.42 ± 0.12	0.120 ± 0.051
1996	4	1	5	113 - 288	283°041	4.08 ± 0.10	1.68 ±0.09	0.047 ± 0.004	1.68 ± 0.17	0.105 ± 0.040
1997	3	3	5	113 - 213	282°820	6.11 ± 0.48	1.73 ±0.08	0.064 ± 0.010	1.78 ± 0.20	0.113 ± 0.042
1997	3	1	5	113 - 213	282°778	9.19 ± 0.82	1.79 ±0.10	0.067 ± 0.009	1.35 ± 0.15	0.108 ± 0.029
1998	3	2	6	112 - 289	282°558	23.48 ± 0.19	1.81 ±0.09	0.050 ± 0.009	1.35 ± 0.10	0.111 ± 0.040
1998	3	10	12	163 - 288	282°855	3.45 ± 0.18	1.55 ±0.08	0.042 ± 0.007	1.26 ± 0.20	0.120 ± 0.040
1999	4	2	6	112 - 289	283°311	5.31 ± 0.21	1.72 ±0.07	0.032 ± 0.005	1.27 ± 0.18	0.115 ± 0.040

Table 6.3: The second continuation of Table 6.1.

Year	Day	bh	eh	ri	$L_\odot$	Θ_{m_0}	s	$K \cdot \sigma$	μ	β
1999	4	2	4	112 - 289	283°269	3.47 ± 0.10	1.87 ±0.10	0.052 ± 0.009	1.10 ± 0.13	0.101 ± 0.035
2000	4	2	4	112 - 289	283°012	4.81 ± 0.18	1.70 ±0.08	0.031 ± 0.006	1.52 ± 0.15	0.109 ± 0.044
2000	4	10	12	112 - 289	283°351	4.99 ± 0.30	1.78 ±0.07	0.042 ± 0.009	1.49 ± 0.21	0.105 ± 0.035
2001	3	0	4	112 - 214	282°710	2.99 ± 0.08	1.69 ±0.09	0.041 ± 0.007	1.80 ± 0.14	0.102 ± 0.044
2001	3	10	14	187 - 289	283°135	3.80 ± 0.10	1.82 ±0.08	0.036 ± 0.008	1.90 ± 0.10	0.110 ± 0.045
2001	3	10	12	112 - 289	283°092	3.59 ± 0.14	1.93 ±0.09	0.043 ± 0.005	1.73 ± 0.14	0.103 ± 0.043
2002	3	12	14	112 - 288	282°913	1.17 ± 0.15	1.91 ±0.14	0.058 ± 0.005	1.72 ± 0.15	0.090 ± 0.035
2004	4	1	5	112 - 289	282°986	3.01 ± 0.16	1.73 ±0.10	0.041 ± 0.004	1.52 ± 0.20	0.111 ± 0.044
2005	3	10	12	112 - 289	282°568	2.39 ± 0.20	1.76 ±0.14	0.051 ± 0.007	1.66 ± 0.12	0.107 ± 0.036
2005	3	10	14	190 - 289	283°109	2.87 ± 0.11	1.88 ±0.09	0.034 ± 0.005	1.89 ± 0.13	0.111 ± 0.041

Table 6.4: The possible values of the ablation parameter, σ, for various bulk density of the Quadrantid meteoroids.

δ [g cm^{-3}]	0.5	1.0	1.5	2.0	2.5	3.0
	0.022	0.035	0.045	0.055	0.064	0.072

Table 6.5: Results of application of equation (5.6) to the Perseid shower meteors. The first column contains the year when the meteors were observed, the second the day of observation, the third the beginning hour of observation, bh, while the next the corresponding end hour, eh. The column headed by ri contains the range interval inside which the meteors were collected, in kilometers. The quantity $L_\odot$ is solar longitude of the centre of observation interval related to the equinox of J2000. The flux Θ_{m_0} is expressed in units of $10^{-12}\,\mathrm{m}^{-2}\,\mathrm{s}^{-1}$ for $m_0 = 10^{-5}$ kg. The remaining quantities were defined in previous sections.

Year	Day	bh	eh	ri	$L_\odot$	Θ_{m_0}	s	$K \cdot \sigma$	μ	β
1980	12	10	10	110 - 291	140°.111	2.72 ± 0.30	1.45 ± 0.08	0.054 ± 0.004	1.01 ± 0.22	0.216 ± 0.078
1981	11	22	4	112 - 289	139°.463	3.34 ± 0.37	1.60 ±0.06	0.060 ± 0.007	1.50 ± 0.21	0.197 ± 0.061
1981	12	0	2	112 - 289	139°.463	4.00 ± 0.24	1.40 ±0.12	0.014 ± 0.004	0.97 ± 0.10	0.212 ± 0.083
1982	12	22	24	112 - 289	140°.100	3.72 ± 0.15	1.43 ±0.18	0.034 ± 0.009	0.99 ± 0.13	0.184 ± 0.069
1982	12	22	4	112 - 289	140°.180	3.59 ± 0.34	1.52 ±0.19	0.067 ± 0.011	1.10 ± 0.19	0.208 ± 0.087
1983	12	22	24	112 - 289	139°.856	3.79 ± 0.28	1.30 ±0.17	0.059 ± 0.009	1.20 ± 0.21	0.202 ± 0.072
1983	13	0	2	112 - 289	139°.936	3.90 ± 0.19	1.33 ±0.20	0.048 ± 0.010	1.09 ± 0.22	0.209 ± 0.080
1985	13	2	4	112 - 289	140°.483	3.99 ± 0.18	1.47 ±0.21	0.06 ± 0.010	1.442 ± 0.18	0.202 ± 0.073
1985	13	12	14	112 - 289	140°.883	3.96 ± 0.21	1.31 ±0.10	0.05 ± 0.008	0.984 ± 0.12	0.208 ± 0.070
1986	13	0	2	112 - 189	140°.640	3.39 ± 0.17	1.38 ±0.09	0.059 ± 0.007	0.90 ± 0.10	0.212 ± 0.082
1989	12	8	12	112 - 289	139°.780	3.64 ± 0.13	1.53 ±0.14	0.056 ± 0.008	1.00 ± 0.20	0.199 ± 0.089
1991	13	0	2	112 - 289	139°.890	3.84 ± 0.32	1.46 ±0.14	0.035 ± 0.009	0.859 ± 0.203	0.192 ± 0.077
1992	11	22	2	110 - 191	139°.599	4.15 ± 0.37	1.56 ±0.12	0.054 ± 0.005	1.24 ± 0.22	0.212 ± 0.072
1993	12	12	16	112 - 200	139°.913	4.23 ± 0.36	1.41 ±0.10	0.087 ± 0.007	1.13 ± 0.18	0.21 ± 0.082
1995	14	4	10	112 - 289	141°.311	3.53 ± 0.41	1.50 ±0.06	0.016 ± 0.010	0.82 ± 0.11	0.212 ± 0.074
1996	12	0	6	112 - 241	139°.695	3.16 ± 0.33	1.47 ±0.05	0.015 ± 0.004	1.18 ± 0.22	0.199 ± 0.068

Table 6.6: The continuation of Table 6.5.

Year	Day	bh	eh	ri	$L_\odot$	Θ_{m_0}	s	$K \cdot \sigma$	μ	β
2000	12	6	10	112 - 189	139°873	3.25 ± 0.34	1.37 ±0.13	0.023 ± 0.004	0.99 ± 0.24	0.202 ± 0.077
2000	12	6	10	212 - 289	139°873	3.26 ± 0.28	1.41 ±0.15	0.060 ± 0.020	1.37 ± 0.27	0.212 ± 0.069

Table 6.7: The possible values of the ablation parameter, σ, for various bulk density of the Perseid meteoroids.

δ [g cm^{-3}]	0.5	1.0	1.5	2.0	2.5	3.0
	0.023	0.036	0.048	0.058	0.067	0.076

Table 6.8: Results of application of equation (5.6) to the Leonid shower meteors. The first column contains the year when the meteors were observed, the second the day of observation, the third the beginning hour of observation, bh, while the next the corresponding end hour, eh. The column headed by ri contains the range interval inside which the meteors were collected, in kilometers. The quantity $L_\odot$ is solar longitude of the centre of observation interval related to the equinox of J2000. The flux Θ_{m_0} is expressed in units of $10^{-12}\,\mathrm{m}^{-2}\,\mathrm{s}^{-1}$ for $m_0 = 10^{-5}$ kg. The remaining quantities were defined in previous sections.

Year	Day	bh	eh	ri	$L_\odot$	Θ_{m_0}	s	$K \cdot \sigma$	μ	β
1965	17	4	8	113 - 288	235°.123	4.67 ± 0.32	1.21 ± 0.05	0.121 ± 0.056	1.51 ± 0.21	0.346 ± 0.100
1966	17	0	4	113 - 288	234°.700	1.19 ± 0.09	1.24 ±0.09	0.097 ± 0.009	1.43 ± 0.16	0.347 ± 0.121
1966	17	4	8	113 - 203	234°.868	2.05 ± 0.13	1.12 ±0.01	0.082 ± 0.014	1.37 ± 0.30	0.332 ± 0.110
1998	17	0	2	110 - 251	234°.448	1.10 ± 0.03	1.44 ±0.04	0.095 ± 0.013	1.80 ± 0.19	0.342 ± 0.113
1998	17	3	4	110 - 211	234°.531	1.67 ± 0.18	1.20 ±0.06	0.05 ± 0.006	1.38 ± 0.15	0.349 ± 0.100
1998	17	7	8	110 - 291	234°.699	2.05 ± 0.15	1.26 ±0.04	0.079 ± 0.008	1.88 ± 0.14	0.332 ± 0.123
1999	18	4	6	170 - 291	235°.369	5.02 ± 0.37	1.48 ±0.09	0.094 ± 0.028	1.70 ± 0.29	0.338 ± 0.099
2000	18	1	3	113 - 288	235°.988	3.31 ± 0.35	1.31 ±0.08	0.084 ± 0.011	1.44 ± 0.10	0.332 ± 0.104
2001	18	12	13	110 - 191	236°.155	11.19 ± 0.62	1.30 ±0.05	0.098 ± 0.010	1.34 ± 0.16	0.359 ± 0.118
2001	19	1	4	110 - 171	236°.786	8.06 ± 0.30	1.36 ±0.13	0.079 ± 0.008	1.62 ± 0.03	0.352 ± 0.127
2002	19	1.5	4.5	110 - 291	236°.526	6.14 ± 0.17	1.28 ±0.05	0.087 ± 0.030	1.38 ± 0.44	0.342 ± 0.110

Table 6.9: The possible values of the ablation parameter, σ, for various bulk density of the Leonid meteoroids.

$\delta\,[\mathrm{g\,cm^{-3}}]$	0.5	1.0	1.5	2.0	2.5	3.0
	0.043	0.068	0.089	0.108	0.125	0.141

Table 6.10: Results of application of equation (5.6) to the Geminid shower meteors. The first column contains the year when the meteors were observed, the second the day of observation, the third the beginning hour of observation, bh, while the next the corresponding end hour, eh. The column headed by ri contains the range interval inside which the meteors were collected, in kilometers. The quantity $L_\odot$ is solar longitude of the centre of observation interval related to the equinox of J2000. The flux Θ_{m_0} is expressed in units of $10^{-12}\,\mathrm{m}^{-2}\,\mathrm{s}^{-1}$ for $m_0 = 10^{-5}$ kg. The remaining quantities were defined in previous sections.

Year	Day	bh	eh	ri	$L_\odot$	Θ_{m_0}	s	$K \cdot \sigma$	μ	β
1959	13	2	6	113 - 288	260°.916	2.49 ± 0.48	1.77 ± 0.15	0.019 ± 0.002	0.56 ± 0.17	0.074 ± 0.029
1960	13	2	6	187 - 288	261°.667	7.11 ± 0.45	1.55 ±0.09	0.009 ± 0.001	0.43 ± 0.16	0.087 ± 0.032
1961	14	0	4	113 - 288	262°.342	4.49 ± 0.18	1.62 ±0.08	0.011 ± 0.002	0.70 ± 0.08	0.080 ± 0.032
1962	12	0	4	240 - 288	260°.044	5.26 ± 0.10	1.45 ±0.04	0.021 ± 0.004	0.678 ± 0.098	0.085 ± 0.028
1963	12	20	24	113 - 288	260°.629	5.02 ± 0.26	1.56 ±0.06	0.031 ± 0.004	0.63 ± 0.07	0.078 ± 0.022
1964	11	20	24	113 - 238	260°.375	3.37 ± 0.33	1.50 ±0.10	0.013 ± 0.004	0.78 ± 0.10	0.082 ± 0.036
1965	12	20	24	113 - 213	261°.126	4.25 ± 0.29	1.46 ±0.04	0.021 ± 0.007	0.69 ± 0.14	0.083 ± 0.030
1965	13	20	24	113 - 288	262°.142	3.99 ± 0.19	1.44 ±0.05	0.025 ± 0.003	0.56 ± 0.10	0.078 ± 0.023
1966	14	0	2	188 - 288	262°.061	2.67 ± 0.25	1.48 ±0.04	0.019 ± 0.005	0.50 ± 0.13	0.081 ± 0.031
1967	13	0	4	113 - 288	260°.776	4.87 ± 0.43	1.48 ±0.14	0.028 ± 0.005	0.60 ± 0.10	0.082 ± 0.029
1968	13	0	4	113 - 288	261°.531	3.72 ± 0.24	1.59 ±0.04	0.022 ± 0.003	0.67 ± 0.09	0.075 ± 0.030
1969	12	0	4	113 - 288	260°.259	4.31 ± 0.18	1.63 ±0.09	0.028 ± 0.004	0.70 ± 0.09	0.084 ± 0.028
1969	12	4	8	113 - 263	260°.429	5.35 ± 0.32	1.55 ±0.10	0.022 ± 0.004	0.81 ± 0.14	0.077 ± 0.030
1969	14	0	4	113 - 288	262°.292	5.42 ± 0.37	1.53 ±0.11	0.017 ± 0.005	0.67 ± 0.09	0.079 ± 0.029
1973	12	0	4	113 - 288	260°.225	6.04 ± 0.36	1.50 ±0.12	0.018 ± 0.005	0.68 ± 0.09	0.082 ± 0.027
1974	14	0	4	113 - 288	261°.998	4.36 ± 0.63	1.65 ±0.09	0.018 ± 0.002	0.68 ± 0.09	0.079 ± 0.030

Table 6.11: The first continuation of Table 6.10.

Year	Day	bh	eh	ri	$L_\odot$	Θ_{m_0}	s	$K \cdot \sigma$	μ	β
1975	13	0	4	113 - 288	260°725	4.14 ± 0.17	1.52 ±0.06	0.015 ± 0.004	0.70 ± 0.09	0.082 ± 0.029
1975	14	0	4	113 - 288	261°741	3.84 ± 0.23	1.61 ± 0.07	0.021 ± 0.003	0.79 ± 0.11	0.076 ± 0.023
1976	13	0	4	113 - 288	261°477	3.52 ± 0.39	1.55 ±0.09	0.019 ± 0.004	0.70 ± 0.10	0.082 ± 0.028
1977	12	0	4	113 - 288	260°204	2.49 ± 0.13	1.62 ±0.10	0.021 ± 0.002	0.71 ± 0.09	0.083 ± 0.030
1977	13	0	4	163 - 288	261°221	3.06 ± 0.14	1.40 ±0.07	0.026 ± 0.003	0.65 ± 0.12	0.088 ± 0.036
1978	12	2	4	113 - 288	259°984	3.60 ± 0.20	1.50 ±0.07	0.023 ± 0.002	0.67 ± 0.08	0.081 ± 0.027
1978	14	2	4	113 - 288	262°017	2.90 ± 0.19	1.54 ±0.07	0.023 ± 0.003	0.66 ± 0.10	0.082 ± 0.028
1980	12	2	4	113 - 288	260°484	3.59 ± 0.15	1.58 ±0.08	0.022 ± 0.003	0.64 ± 0.12	0.080 ± 0.028
1980	13	2	4	113 - 288	261°501	4.05 ± 0.29	1.58 ±0.07	0.026 ± 0.003	0.71 ± 0.09	0.084 ± 0.031
1981	10	4	6	113 - 288	258°273	4.56 ± 0.18	1.52 ±0.08	0.019 ± 0.003	0.70 ± 0.11	0.078 ± 0.022
1981	12	2	4	113 - 288	260°222	2.49 ± 0.22	1.60 ±0.08	0.022 ± 0.007	0.68 ± 0.12	0.082 ± 0.035
1981	14	2	4	113 - 288	262°253	3.19 ± 0.22	1.58 ±0.08	0.024 ± 0.004	0.70 ± 0.13	0.087 ± 0.031
1982	13	0	6	113 - 288	260°849	3.04 ± 0.19	1.68 ±0.09	0.031 ± 0.004	0.82 ± 0.11	0.082 ± 0.025
1982	14	0	6	113 - 288	261°991	2.33 ± 0.52	1.52 ±0.07	0.028 ± 0.004	0.68 ± 0.12	0.083 ± 0.027
1984	10	4	6	113 - 288	258°500	3.96 ± 0.37	1.52 ±0.07	0.020 ± 0.002	0.70 ± 0.09	0.080 ± 0.022
1985	13	0	4	113 - 288	261°165	2.60 ± 0.27	1.56 ±0.09	0.017 ± 0.003	0.62 ± 0.09	0.079 ± 0.021
1986	13	0	4	113 - 288	260°903	2.55 ± 0.29	1.66 ±0.09	0.024 ± 0.008	0.61 ± 0.11	0.081 ± 0.028
1986	14	0	2	113 - 288	261°878	3.34 ± 0.10	1.52 ±0.06	0.024 ± 0.004	0.63 ± 0.11	0.086 ± 0.031
1987	15	0	4	113 - 288	262°674	4.14 ± 0.19	1.62 ±0.09	0.026 ± 0.004	0.67 ± 0.11	0.083 ± 0.031

Table 6.12: The second continuation of Table 6.10.

Year	Day	bh	eh	ri	$L_{\odot}$	Θ_{m_0}	s	$K \cdot \sigma$	μ	β
1989	13	0	4	113 - 288	261°139	3.42 ± 0.24	1.69 ±0.07	0.027 ± 0.003	0.70 ± 0.11	0.085 ± 0.031
1989	14	0	4	113 - 288	262°155	2.92 ± 0.23	1.58 ±0.07	0.021 ± 0.003	0.64 ± 0.12	0.081 ± 0.031
1990	13	0	4	113 - 288	260°876	2.46 ± 0.17	1.43 ±0.09	0.019 ± 0.002	0.69 ± 0.15	0.080 ± 0.027
1991	14	0	4	113 - 288	261°638	3.72 ± 0.26	1.46 ±0.07	0.021 ± 0.003	0.66 ± 0.08	0.085 ± 0.027
1992	12	0	4	113 - 288	260°358	1.57 ± 0.08	1.56 ±0.09	0.030 ± 0.004	0.54 ± 0.10	0.084 ± 0.030
1994	12	1	5	113 - 288	259°883	1.17 ± 0.22	1.41 ±0.09	0.029 ± 0.004	0.71 ± 0.11	0.083 ± 0.032
1995	13	0	4	113 - 288	260°589	2.25 ± 0.24	1.57 ±0.10	0.034 ± 0.004	0.68 ± 0.10	0.083 ± 0.033
1995	14	0	4	113 - 288	261°606	4.13 ± 0.42	1.67 ±0.10	0.023 ± 0.004	0.78 ± 0.12	0.080 ± 0.026
1996	12	2	4	113 - 263	260°374	2.41 ± 0.19	1.51 ±0.11	0.024 ± 0.003	0.54 ± 0.10	0.082 ± 0.034
1997	13	0	4	113 - 288	261°085	4.22 ± 0.13	1.53 ±0.08	0.02 ± 0.003	0.62 ± 0.12	0.081 ± 0.026
2000	12	0	4	112 - 289	260°303	3.02 ± 0.48	1.66 ±0.08	0.019 ± 0.002	0.71 ± 0.10	0.084 ± 0.026
2000	13	0	4	112 - 289	261°320	4.07 ± 0.36	1.71 ±0.15	0.025 ± 0.003	0.68 ± 0.12	0.088 ± 0.033
2000	14	0	4	112 - 289	262°336	4.14 ± 0.37	1.62 ±0.05	0.023 ± 0.003	0.66 ± 0.10	0.080 ± 0.029
2000	13	1	5	113 - 288	261°362	3.05 ± 0.53	1.43 ±0.08	0.020 ± 0.002	0.49 ± 0.15	0.088 ± 0.035
2001	13	1	5	113 - 288	261°102	2.40 ± 0.17	1.54 ±0.12	0.017 ± 0.002	0.57 ± 0.11	0.083 ± 0.030

Table 6.13: Results of application of equation (5.6) to the ζ Perseid shower meteors. The first column contains the year when the meteors were observed, the second the day of observation, the third the beginning hour of observation, bh, while the next the corresponding end hour, eh. The column headed by ri contains the range interval inside which the meteors were collected, in kilometers. The quantity $L_\odot$ is solar longitude of the centre of observation interval related to the equinox of J2000. The flux Θ_{m_0} is expressed in units of $10^{-12}\,\mathrm{m}^{-2}\,\mathrm{s}^{-1}$ for $m_0 = 10^{-5}$ kg. The remaining quantities were defined in previous sections.

Year	Day	bh	eh	ri	$L_\odot$	Θ_{m_0}	s	$K \cdot \sigma$	μ	β
2003	8	4	8	110 - 291	76°.982	14.73 ± 0.83	2.46 ± 0.16	0.019 ± 0.003	1.92 ± 0.04	0.047 ± 0.006

Table 6.14: The possible values of the ablation parameter, σ, for various bulk density of the ζ Perseid meteoroids.

$\delta\,[\mathrm{g\,cm}^{-3}]$	0.5	1.0	1.5	2.0	2.5	3.0
	0.010	0.016	0.021	0.025	0.029	0.033

Table 6.15: Results of application of equation (5.6) to the β Taurid shower meteors. The first column contains the year when the meteors were observed, the second the day of observation, the third the beginning hour of observation, bh, while the next the corresponding end hour, eh. The column headed by ri contains the range interval inside which the meteors were collected, in kilometers. The quantity $L_\odot$ is solar longitude of the centre of observation interval related to the equinox of J2000. The flux Θ_{m_0} is expressed in units of $10^{-12}\,\mathrm{m}^{-2}\,\mathrm{s}^{-1}$ for $m_0 = 10^{-5}$ kg. The remaining quantities were defined in previous sections.

Year	Day	bh	eh	ri	$L_\odot$	Θ_{m_0}	s	$K \cdot \sigma$	μ	β
2003	25	5	8	110 - 291	93°.233	4.32 ± 0.37	2.38 ± 0.11	0.012 ± 0.003	1.82 ± 0.02	0.071 ± 0.007

Table 6.16: The possible values of the ablation parameter, σ, for various bulk density of the β Taurid meteoroids.

$\delta\,[\mathrm{g\,cm}^{-3}]$	0.5	1.0	1.5	2.0	2.5	3.0
	0.007	0.010	0.013	0.016	0.019	0.021

Table 6.17: Results of application of equation (5.6) to the γ Draconid shower meteors. The first column contains the year when the meteors were observed, the second the day of observation, the third the beginning hour of observation, bh, while the next the corresponding end hour, eh. The column headed by ri contains the range interval inside which the meteors were collected, in kilometers. The quantity $L_\odot$ is solar longitude of the centre of observation interval related to the equinox of J2000. The flux Θ_{m_0} is expressed in units of $10^{-12}\,\mathrm{m}^{-2}\,\mathrm{s}^{-1}$ for $m_0 = 10^{-5}$ kg. The remaining quantities were defined in previous sections.

Year	Day	bh	eh	ri	$L_\odot$	Θ_{m_0}	s	$K \cdot \sigma$	μ	β
1998	8	12	14	160 - 270	195°028	2.30 ± 0.39	1.88 ±0.17	0.375 ± 0.052	1.94 ± 0.11	0.029 ± 0.006

Table 6.18: The possible values of the ablation parameter, σ, for various bulk density of the γ Draconid meteoroids. In this case we have tried to estimate σ even for low value of $\delta = 0.2\mathrm{g\,cm}^{-3}$.

$\delta\,[\mathrm{g\,cm}^{-3}]$	0.2	0.5	1.0	1.5	2.0	2.5	3.0
	0.106	0.196	0.311	0.407	0.493	0.572	0.646

Chapter 7

Summary and Conclusion

We have developed a theory that makes use of the range distributions of shower meteors which have observed by the Ondřejov meteor radar. Our approach to the construction of this theory is based on the simple physical theory of meteors with neglection of the deceleration of meteors contributing to the range distribution, which is justifiable. This distribution is a function of a few very important physical parameters characterizing the meteoroids of a particular shower such as the shape-density coefficient, K, and the ablation parameter, σ. Also the ionization probability, β, considered as a function of meteoroid velocity, is one of quantities our theoretical distribution depends on. The physical theory we have employed allows only the product $K \cdot \sigma$ to enter the final formulae. Since observed meteoroids of all showers are known to suffer from fragmentation during their atmospheric flights we needed to include this effect in our theory as well. It proved to be rather tough proposition because to be able to consider the influence of fragmentation on the ionization curve, we have to know at what point of the curve the fragmentation takes place and its intensity. However, this is a piece of information which is not at our disposal. Moreover, to obtain the ionization curve taking into account fragmentation we would have to sum up the signals of the parent body as well as of all fragments which is not possible to carry out in practice. On the other hand, it is clear that the influence of fragmentation manifests itself as shorter both light and ionization curves with their peaks being higher than the ones of nonfragmenting meteoroids. However, very similar effect can be seen from the theory bearing in mind the Levin's proposition about the variation of the meteoroid cross section, which is characterized by new parameter, μ. Its classical value is 2/3. We have allowed it to vary within much broader interval, $\mu > 0$. To conclude, our theory allows us to compute two parameters related to the structure of meteor showers (and depending on solar longitude), Θ_{m_0} and s, and three quantities, $K \cdot \sigma$, μ and β, describing physical properties of meteoroids.

Our principal formula of the range distribution (5.6) gives the number of meteors the radar in use can register within the collecting area of the echo plane. The older approach of Pecina [38] to the determination of the domain of integration was based on the assumption that this is given by

the point of maximum ionization. We have developed more sophisticated approach in which we have abandoned that wrong assumption and our range distribution model relies only on the radar equation of overdense echoes.

We have used our theory to study the physical properties of meteoroids of the Quadrantid, Perseid, Leonid and Geminid showers we have been observing quite regularly for a long time and meteoroids of the ζ Perseid, β Taurid and γ Draconid (Giacobinid) that we have been monitoring rather irregularly during some campaigns. For that reason the subsection dealing with the daytime showers, ζ Perseids and β Taurids, includes only one year, 2003 and also the data of γ Draconids cover only one year 1998 when the shower activity had increased for about two hours while sections devoted to four main showers are much richer. The resulting values of parameters of our interest calculated as weighted means with standard deviations as weights, are summarized in the Table 7.1.

Table 7.1: Weighted values of parameters of interest for showers we have used in our analysis. The flux Θ_{m_0} is in units of $10^{-12}\,\mathrm{m}^{-2}\,\mathrm{s}^{-1}$ and velocity v_∞ in units of km s^{-1}.

Shower	Θ_{m_0}	s	$K \cdot \sigma$	μ	β	v_∞
Quadrantids	4.56 ± 0.30	1.77 ± 0.02	0.042 ± 0.001	1.55 ± 0.02	0.107 ± 0.007	43
Perseids	3.66 ± 0.06	1.45 ± 0.01	0.044 ± 0.003	1.06 ± 0.03	0.205 ± 0.001	61
Giacobinids	2.30 ± 0.39	1.88 ± 0.17	0.375 ± 0.052	1.94 ± 0.11	0.029 ± 0.006	23
Leonids	3.67 ± 0.21	1.26 ± 0.02	0.082 ± 0.003	1.55 ± 0.29	0.343 ± 0.002	71
Geminids	3.49 ± 0.11	1.55 ± 0.01	0.021 ± 0.001	0.66 ± 0.01	0.082 ± 0.001	36
β Taurids	4.32 ± 0.37	2.38 ± 0.11	0.012 ± 0.003	1.82 ± 0.02	0.071 ± 0.007	32
ζ Perseids	14.73 ± 0.83	2.46 ± 0.16	0.019 ± 0.003	1.92 ± 0.04	0.047 ± 0.006	29

Since we cannot split K from σ we estimate the possible interval of σ assuming various bulk density of meteoroids to get value of the ablation parameter. The Table 7.2 list this quantity for the showers included into Table 7.1. The possible values of meteoroid densities can be found e.g. in Babadzhanov [2] or in Bellot Rubio et al. [7].

In the light of results summarized in the above tables we can conclude the following facts:

- we have managed to apply our model to 127 range distributions of 7 different showers.
- Flux does not vary a lot from one shower to another. In another words, all investigated showers possess approximately the same value of flux Θ_{m_0}. It implies that their space density has to differ. Let us denote the space density of a shower as n, which relates to the flux, Θ_{m_0}, via $\Theta_{m_0} = n\,v$, where v is the velocity the shower meteoroids have as if they were not captured by the Earth, i. e. their heliocentric velocity. It means that n differs roughly in the ratio of velocities of particular shower.

Table 7.2: The possible values of the ablation parameter, σ, for various bulk density of the meteoroids of showers from Table 7.1. Geminids are assumed to have the bulk density $\delta = 2.5\,\mathrm{g\,cm^{-3}}$.

Shower / $\delta\,[\mathrm{g\,cm^{-3}}]$	0.2	0.5	1.0	1.5	2.0	2.5	3.0
Quadrantids		0.022	0.035	0.045	0.055	0.064	0.072
Perseids		0.023	0.036	0.048	0.058	0.067	0.076
Giacobinids	0.106	0.196	0.311	0.407	0.493	0.572	0.646
Leonids		0.043	0.068	0.089	0.108	0.125	0.141
Geminids						0.032	
β Taurids		0.007	0.010	0.013	0.016	0.019	0.021
ζ Perseids		0.010	0.016	0.021	0.025	0.029	0.033

- In agreement with values of s the shower with highest percentage of brighter meteors within its population is the Leonid one. Contrary to this, the showers with highest percentage of fainter meteors are the ζ Perseids and β Taurids.

- The highest ablation ability is inherent to the γ Draconid meteoroids. We have thus confirmed results known from photographic observations also in the case of radar meteors owing to our range distribution method. The value of ablation parameter we have arrived at is in good agreement with the value $\sigma = 0.2$ published by Ceplecha et al. [15]. The lowest value we have obtained is that of β Taurids, ζ Perseids and Geminids being about twice lower than that of other showers of cometary origin with the exception of Leonids and Giacobinids. In case of Geminids this indicates different physical properties of their meteoroids in comparison with properties of cometary ones. The higher value of σ of Leonids as compared with the corresponding values of Quadrantids and Perseids indicates probably the younger age of the meteoroids of Leonid storms from 1965 - 1966 and 1998 - 2002 in comparison with older age of Quadrantids and Perseids. As far as the daytime showers are concerned we have got a span of σ rather low. The small values of σ may indicate membership of daytime showers meteoroids to the asteroidal component of Taurid complex rather than to the cometary one as it was proposed by Babadzhanov [1].

- The values of μ much higher than the conventional 2/3 have been found at all cometary showers as well as for the daytime ones. The highest value has been found for γ Draconids as we expected. However, rather unexpectable high values of μ have been obtained also for both daytime showers. It would point out on the cometary origin of these meteoroids which is in stark contrast to small values of σ. At this moment we are not able to interpret this fact. The lowest one has been determined for Geminids which is almost conventional. This finding indicates again the physical properties of Geminid meteoroids different from the ones of cometary showers.

- We have obtained also the ionization probabilities for 7 various values of meteor velocities as represented by the corresponding velocities of studied showers. The result is depicted in the Figure 7.1 where also the curves following from the Verniani and Hawkins [59] formula together with the one of Kashcheev et al. [26] and Jones [23] are drawn. We can easily see that at low velocities only ζ Perseids and β Taurids conform to the Jones formula. Our β value of Giacobinids is higher than that of Jones while the corresponding ionization probabilities of Geminids and Quadrantids are lower. All showers with $v_\infty \leq 43\text{km s}^{-1}$ have provided us with β higher than that the Kashcheev et al. formula. The values of Perseids and Leonids lie between the ones of Verniani and Hawkins and Kashcheev et al.

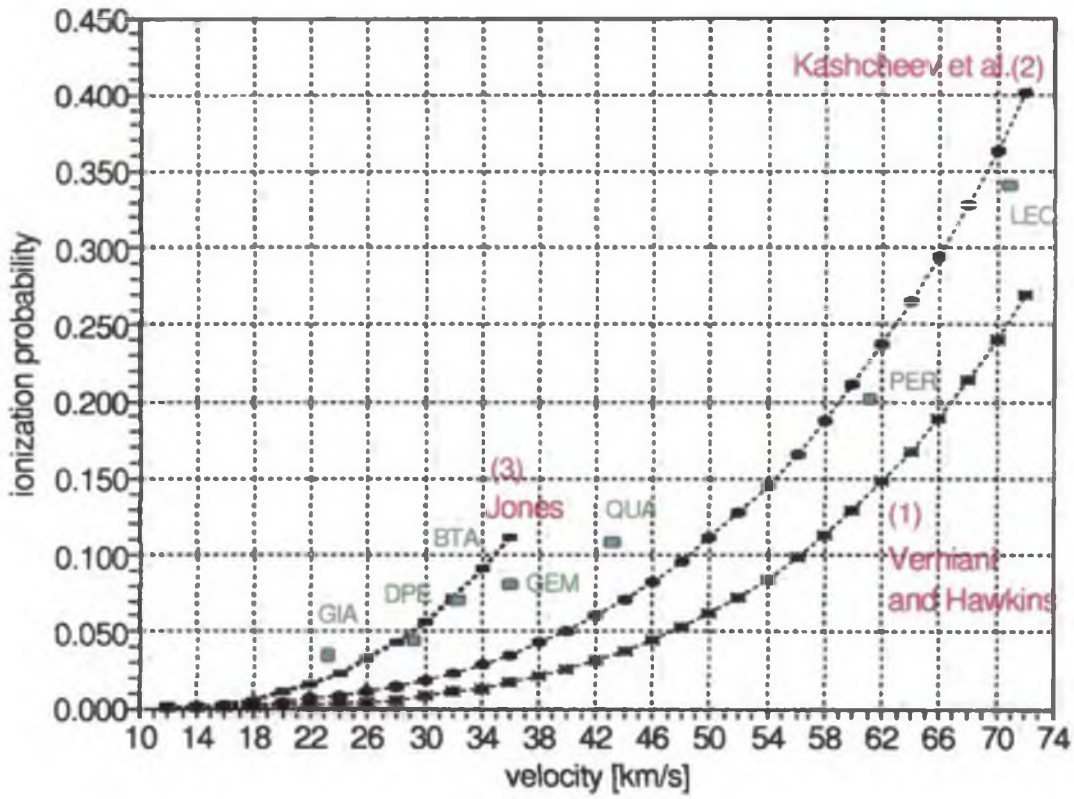

Figure 7.1: The ionization probability β as a function of velocity v_∞ of the particular shower. The curves (1), (2) and (3) are drawn by the Verniani and Hawkins [59], the Kashcheev et al. [26] and the Jones [23] formulae.

The theory we have developed can be used to infer some physical parameters of shower meteors based on the radar observations. We hope that the range distribution model will become a handy tool enriching meteor astronomy.

Bibliography

[1] Babadzhanov P. B.: Search for meteor showers associated with Near-Earth Asteroids, I. Taurid Complex, Astronomy and Astrophysics 373, p. 329, 2001

[2] Babadzhanov P. B.: Fragmentation and densities of meteoroids, Astronomy and Astrophysics 384, p. 317, 2002

[3] Baggaley W. J.: Mon. Not. R. astr. Soc. 147, p. 231, 1970

[4] Baggaley W. J.: Mon. Not. R. astr. Soc. 159, p. 203, 1972

[5] Bateman H., Erdelyi A.: Tables of integral transforms, Volume II, Nauka Moscow, 1970 (in russian)

[6] Belkovich, Statistical theory of meteor radiolocation, Publishing House of the Kazaň univ., 1971 (in russian)

[7] Bellot Rubio L. R., Martínez Gonzáles M. J., Ruiz Herrera L., Licandro J., Martínez Delgado D., Rodríguez Gill P. and Serra-Ricart M.: Modeling the photometric and dynamical behavior of Super-Schmidt meteors in the Earth's atmosphere, Astronomy and Astrophysics 389, p. 680, 2002

[8] Bibarsov R. Sh.: Comets and meteors 21, p. 32 , 1972 (in russian)

[9] Bronshten V.A.: Physics of Meteoric phenomena, Kluver Academic publisher, Dordrecht, Boston, Lancaster, 1983

[10] Campbell-Brown M., Jones J.: Determining the initial radius of meteor trains: fragmentation, Mon. Not. R. Astron. Soc. 343, p. 775, 2003

[11] Ceplecha Z.: Bull. Astron. Inst. Czechosl. 5, p. 60, 1954

[12] Ceplecha Z.: Bull. Astron. Inst. Czechosl. 26, p. 242, 1975

[13] Ceplecha Z.: Bull. Astron. Inst. Czechosl. 39, p. 221, 1988

[14] Ceplecha Z., McCrosky R. E.: Gross-fragmentation of meteoroids and bulk density of Geminids from photographic fireball records, in Asteroids, Comets, Meteors, ed. A. W. Harris & E. Bowell, Lunar and Planetary Institute, Houston, p. 109, 1992

[15] Ceplecha Z., Elford W. G., Revelle O.D., Hawkes R.L., Porubčan V., Šimek M.: Meteor phenomena and bodies, Space Science Reviews 84, p. 321, 1998

[16] Chen F. F.: Introduction into plasma physics, Academia, Prague, 1984 (in Czech)

[17] CIRA (COSPAR International Reference Atmosphere), Akademie Verlag, Berlin, 1972

[18] Greenhow J. S., Neufeld E. L.: J. Atmosph. Terr. Phys. 6, p. 133, 1955

[19] Hasegawa, I.: Pub. Astron. Soc. Japan 31, p. 257, 1979

[20] Jenniskens, P.: IAU Circ. No. 8252, 2003

[21] Jones J., McIntosh B. A., Šimek M.: Ozone and the duration of overdense radio meteors, J. Atmosph. Terr. Phys. 52, p. 253, 1990

[22] Jones W.: Mon. Not. R. astr. Soc. 275, p. 812, 1995

[23] Jones W.: Theoretical and observational determinations of the ionization coefficient of meteors, Mon. Not. R. astr. Soc. 228, p. 995, 1997

[24] Kaiser, T. R.: in Meteors, ed. T. R. Kaiser Pergamon Press, London, 1955

[25] Kaiser, T. R.: The determination of the incident flux of radio-meteors, Mon. Not. R. astr. Soc. 123, p. 265, 1961

[26] Kashcheev B. L., Lebedinets V. N., Lagutin M. F.: Results of IGY Research, Research of Meteors, No.2, 1967 (in russian)

[27] Kolmakov V. M.: Initial radius of meteor trails, Comets and meteors 32, 1982 (in russian)

[28] Landau L. D., Lifšic E.M. : Elektrodynamics of continuous media, Nauka Moscow, 1982 (in russian)

[29] Levin B. Yu.: The physical theory of meteors and meteoric matter in the solar system, Izdatel'stvo Akad. Nauk SSSR, 1965 (in russian)

[30] Manning L. A.: J. Geophys. Res. 63, p. 181, 1958

[31] Massey H. S., Sida D. W.: Phil. Mag. 46, p. 190, 1955

[32] McIntosh B. A.: Icarus 35, p. 299, 1990

[33] McIntosh B. A., Šimek M.: Canad. J. Phys. 47, p. 7, 1969

[34] McIntosh, B. A., Šimek M.:Bull. Astron. Inst. Czechosl. 25, p. 180, 1974

[35] McKinley D. W. R.: Meteor Science and Engineering, McGraw Hill, New York, 1961

[36] Meloun M., Militký J.: Statistical analysis of experimental data, Academia, Praha, 2005 (in Czech)

[37] Nicholson T. F., Poole L. M. G.: Planet Space Sci. 22, p. 1669, 1972

[38] Pecina P.: The determination of incident flux of meteor matter using radar, PhD. theses, Astronomical Institute of Academy of Sciences of Czechoslovakia, 1980 (in Czech)

[39] Pecina, P.: On the determination of the mass distribution index from radar observations, Bull. Astron. Inst.Czechosl. 35, p. 183, 1984

[40] Pecina P.: Bull. Astron. Inst. Czechosl. 39, p. 193, 1988

[41] Pecina P.: On the variable meteor parameters, in Proceedings of the Meteoroids 2001 Conference, Swedish Institute of Space Physics, Kiruna, Sweden, p. 271, 2001

[42] Pecina, P.: personal communication, 2004

[43] Pecina, P.: personal communication, 2005

[44] Pecina, P., Ceplecha, Z.: New aspects in single-body meteor physics, Bull. Astron. Inst. Czechosl. 34, p. 102, 1983

[45] Pecina P., Pecinová D.: Ondřejov radar observations of Leonid shower activity in 2000-2002, Astronomy and Astrophysics 426, p. 1111, 2004

[46] Pecina P., Šimek M.: Analysis of the Geminid meteor stream, 1958 - 1997, from radar observations, Astronomy and Astrophysics 344, p. 991, 1999

[47] Pecina P., Porubčan V., Pecinová P., Toth J.: Radar observations of Taurid complex meteor showers in 2003: activity and mass distribution, in Proceedings of the international conference Meteoroids 2004, Earth, Moon and Planets, in press

[48] Pecinová D., Pecina P.: Radar meteors range distribution and some parameters of meteoroids: application to *zeta* Perseids and β Taurids showers, in Proceedings of the international conference Meteoroids 2004, Earth, Moon and Planets, in press

[49] Plavcová Z., Šimek M.: Meteor radar of the Ondřejov observatory, Bull. Astron. Inst. Czechosl. 11, p. 228, 1960

[50] Porubčan V., Kornoš L.: The Quadrantid meteor stream and 2003 EH1, Contrib. Astron. Obs. Skalnaté Pleso 35, p. 5, 2005

[51] Press W. H., Teukolsky S. A., Vetterling W. T., Flannery B. P.: Numerical Recipes in Fortran, The Art of Scientific Computing, Second Edition, Cambridge University Press, 1992

[52] Roggemans P.: The Perseid meteor stream in 1988: a double maximum!, WGN 20, p. 127, 1989

[53] Spurný P., Betlem H., van't Leven J., Jenniskens P.: Meteoritics and Planetary Science 35, p. 243, 2000

[54] Steffen M.:A simple method for monotonic interpolation in one dimension, Astronomy and Astrophysics 239, p. 443, 1990

[55] Šimek M.: Dynamics and evolution of the structure of five meteor streams, Bull. Astron. Inst. Czechosl. 38, p. 80, 1987

[56] Šimek M., Pecina P.: Activity of the new filament in the Perseid meteor stream, in Physics, Chemistry, and Dynamics of Interplanetary Dust, eds. B. A. S. Gustafson and M. S. Hanner, pp. 109-112, Astr. Soc. Pacific, San Francisco, 1996

[57] Šimek M., Pecina P.: Leonid meteor stream from Ondřejov radar observations in 1965 - 1967, Astronomy and Astrophysics 357, p. 777, 2000

[58] Šimek M., Pecina P.: Radar observation of the Leonids in 1998 and 1999, Astronomy and Astrophysics 365, p. 622, 2001

[59] Verniani F., Hawkins, G. S.: On the Ionizing Efficiency of Meteors., Astrophys. J. 140, p. 1590, 1964

[60] Voloshchuk J. I., Kashcheev B. L., Kruchinenko V. G.: Meteors and meteor matter, Naukova Dumka, Kyjev, 1989 (in russian)

[61] Watanabe J., Abe S., Takanashi M., Hashimoto T., Iiyama O., Ishibashi Y., Morishige K., Yokogawa S.: HD TV Observation of the Strong Activity of the Giacobinid Meteor Shower in 1998, Geoph. Res. Let. 26, No. 8, p. 1117, 1999

[62] Whipple F. L.: IAU Circ. No. 3881, 1983

[63] Williams I. P., Collander-Brown S. J.: Mon. Not. R. astr. Soc. 294, p. 127, 1998